DEFECTS IN NOVEL SUPERFLUIDS: SUPERSOLID HELIUM AND COLD GASES

By

KINJAL DASBISWAS

A THESIS PRESENTED TO THE GRADUATE SCHOOL
OF THE UNIVERSITY OF FLORIDA IN PARTIAL FULFILLMENT
OF THE REQUIREMENTS FOR THE DEGREE OF
DOCTOR OF PHILOSOPHY

UNIVERSITY OF FLORIDA

2012

To my parents, both physicians, who have always supported and nurtured my ambitions to be a physicist

ACKNOWLEDGMENTS

I am grateful to my adviser, Professor Alan T. Dorsey, for the pivotal role he has played as a mentor in my PhD He introduced me to many topics in condensed matter physics, particularly the novel topic of supersolid helium. I have learned a number of techniques through working with him, but equally importantly, he has taught me to choose my problems carefully and to present my results in a coherent manner.

I would like to thank Professors Peter J. Hirschfeld, Amlan Biswas, H.-P. Cheng and Susan B. Sinnott for useful discussions and for serving on my committee. I would also like to acknowledge Professors Y. -S. Lee and Pradeep Kumar for their valuable inputs about the supersolid problem, Professors D. L. Maslov, Richard Woodard, S. L. Shabanov, and K. A. Muttalib for their inspiring teaching, and the Max Planck Institute in Dresden for giving me the opportunity to attend a summer school on Bose-Einstein condensates. I am indebted to some of my graduate student colleagues for stimulating discussions and for ensuring a collegial environment in the department. I am grateful to K. Nichola and P. Marlin for their generous assistance with the administrative aspects of my graduate program.

I would like to acknowledge the National Science Foundation for the support they have extended to my research, and also the Graduate School and Department of Physics at the University of Florida, who have provided me with an alumni fellowship and other forms of support.

Finally I would like to express my gratitude to friends and family, who supported me in these five years. I am especially indebted to my parents who have invested much effort and affection in my upbringing and education.

TABLE OF CONTENTS

LIST OF TABLES

LIST OF FIGURES

Abstract of Thesis Presented to the Graduate School
of the University of Florida in Partial Fulfillment of the
Requirements for the Degree of Doctor of Philosophy

DEFECTS IN NOVEL SUPERFLUIDS:
SUPERSOLID HELIUM AND COLD GASES

By

Kinjal Dasbiswas

August 2012

Chair: Alan T. Dorsey
Major: Physics

We investigate the role played by various topological defects, especially crystal dislocations and superfluid vortices, in some novel superfluids - such as the putative supersolid phase in solid helium-4 (^{4}He) and in dilute Bose-Einstein condensates (BEC) in traps.

The first part of this work addresses recent experimental findings in solid helium, such as the period shift in resonant oscillators that has been interpreted to be a signature of superfluidity *coexisting* with crystalline order in solid helium. We use Landau's phenomenological theory for phase transitions to establish that crystal defects such as dislocation lines and grain boundaries can induce local superfluid order and show that a network of dislocation lines can give rise to bulk superfluid order within a crystal. Our findings are also relevant to other phase transitions in the presence of crystal defects.

The second part concerns the stability and dynamics of a single vortex in a rotating trap of a Bose-Einstein condensate (BEC) and the possibility of the macroscopic quantum tunneling of such a vortex from a metastable minimum at the trap center. The complete dynamics of such a vortex is derived by integrating out the phonon modes from a hydrodynamic action, and estimates for the tunneling rate are obtained using a variety of semiclassical methods. This is analogous to the problem of tunneling of a charged particle through a potential barrier in the presence of a very high magnetic field,

the Magnus force on the vortex being analogous to the Lorentz force on a charge. We conclude that the vortex action has a complicated nonlocal form and further, that the Magnus-dominated dynamics of the vortex tends to suppress tunneling.

CHAPTER 1
INTRODUCTION

1.1 Superfluids: Helium and Dilute BEC

The history of the modern study of the properties of materials at very low temperatures dates back to the development of technology to liquefy helium and the consequent discovery of superconductivity just over a century ago. The phenomena seen at low temperatures are often novel and at odds with intuition because quantum effects become more important as the thermal vibrations of atoms in matter are reduced. Theoretically, many of these phenomena are understood to be consequences of Bose-Einstein condensation, an outcome of the laws of quantum statistics, where all particles following Bose statistics inhabit the same ground state when cooled down to absolute zero. Aside from the fundamental insights into the laws of quantum mechanics it provides, the study of matter at very low temperatures has also yielded practical applications of social significance: for example the use of superconductors to create the large magnetic fields needed for the diagnostic medical procedure of MRI.

Kamerlingh Onnes first liquefied helium-4 in 1908. Soon after(1911), he discovered superconductivity in mercury when measuring the abrupt disappearance of resistance in mercury at 4.19 K [1]. Kamerlingh Onnes and Keesom collected many hints of a phase transition in helium in the Leiden laboratory, including the remarkable anomaly in the heat capacity with a famous λ shape at a temperature of $T_\lambda \sim 2.17$ K. In many ways, helium was the ideal candidate for observing quantum phenomena at low temperatures in liquids because it remains liquid till very close to absolute zero (unlike other materials that freeze into solid). This is because of its small mass that favors quantum fluctuations, and because unlike the even lighter hydrogen that tends to form molecules, it is chemically inert and has weaker interactions. Keesom distinguished the high and low temperature phases as liquid helium I and II, respectively. John F. Allen and Don Misener first showed the inviscid nature of helium II in 1937 when they examined its flow

through very small capillaries [2]. Similar results were found simultaneously by Pyotr Kapitza, leading him to suggest that helium II was in fact a superfluid [3].

A phenomenological "two-fluid" model for helium II was developed soon after by Tisza[4], Landau[5], and others based on the notion that part of liquid helium below T_λ turned superfluid, but the other part remained "normal", i.e. was dissipative (had finite viscosity) and could transport entropy like ordinary fluids. This could be intuitively understood from Landau's theory of Bose and Fermi liquids (which was also developed at about this time), and the attendant idea that low energy excitations from the ground state of a weakly interacting bosonic system could be characterized as "quasiparticles" with definite momentum and energy. The superfluid component of "two-fluid" helium II could then be identified with the ground state of the Bose liquid while the normal component corresponded to the quasiparticles. Landau identified the quasiparticles of a Bose liquid as being of two types: quantized sound waves or phonons, whose energy ϵ depends linearly on momentum p as $\epsilon = cp$, where c is the speed of sound, and "rotons" or quanta of rotational motion with the spectrum $\epsilon(p) = \Delta + (p - p_0)^2/2m$. This phenomenological model proved to fit the excitation spectrum obtained from neutron scattering experiments on helium II [6] very well but a clearer and more microscopic understanding of these quasiparticles was not obtained until 1956, when Feynman developed a variational *Ansatz* to describe the atomic interactions in liquid helium [7]. Well before that, Landau had made several remarkable predictions based on his two-fluid hydrodynamics, which to this day remain the "smoking gun" signatures of the superfluid phase:

- There is a certain critical velocity v_c of a superfluid, such that it loses its superfluidity if made to flow faster than that. This is so because flows faster than $v_c = \epsilon(p)/p$ excite quasiparticles in the liquid that destroy the superfluid phase.
- It is possible to set the normal and superfluid parts into oscillations that are out of phase with each other. (This mode of oscillation had been suggested earlier by Tisza and came to be known as "second sound".)

- When a container of the liquid is rotated, only the normal part of the liquid rotates along with it. The superfluid component decouples from the rotation and so there is an apparent decrease in the moment of inertia as the liquid is cooled down past its λ- point.

The last of these was verified soon after by Andronikashvili [8] using a "torsional oscillator" setup shown in Fig. 1-1, that has special bearing on some of the ideas to be introduced later in this dissertation. A stack of concentric disks was suspended in liquid helium by a torsion rod that could be twisted to oscillate the stack. If the spacing between disks was small enough, the normal component of the fluid was dragged with the oscillating disks. As liquid helium is cooled below its λ-point, the superfluid component stops rotating. This decoupling leads to a change in the moment of inertia of the oscillator, and a consequent measurable shift in the resonant frequency of oscillations. Additionally, the Q-factor of the oscillator provides an estimate of the dissipation involved.

It was however Fritz London in 1938 [9] who first realized that the phenomenon of Bose-Einstein condensation underlay the curious properties of superfluid helium. Although accepted unhesitatingly now, the idea of a Bose-Einstein condensation historically took time to get established as a real effect, and its connection with superfluidity was certainly not immediately apparent. Einstein had first realized the possibility of a macroscopic fraction of atoms condensing to their ground state at low temperatures [10], based on the statistics worked out by S. N. Bose in 1924 [11]. His argument for condensation in a noninteracting gas of atoms obeying Bose statistics is deceptively simple. The mean occupation number of a single particle state ν in such a system is given by the Bose distribution function

$$f(\epsilon_\nu) = \frac{1}{e^{(\epsilon_\nu - \mu)\beta} - 1},$$

where $\beta \equiv 1/k_B T$, and μ is the chemical potential that ensures that the number of particles in the system is fixed.

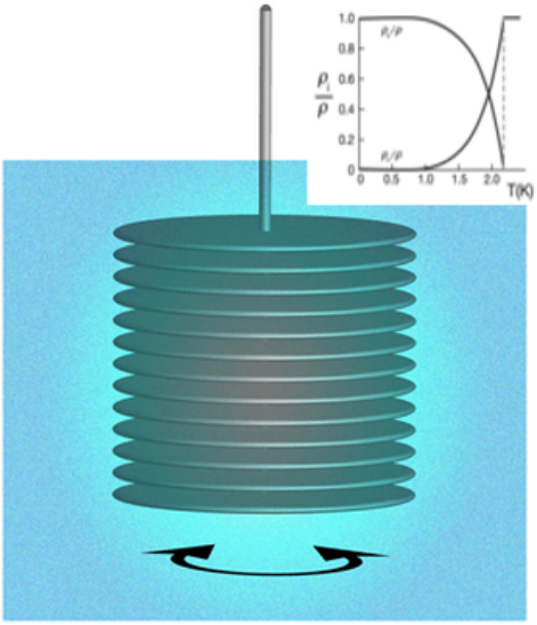

Figure 1-1. A schematic of the torsional oscillator setup used by Andronikashvili in 1946 (Keesom is also credited with a similar experiment) to demonstrate the decoupling of the superfluid from rotation. A stack of concentric disks was suspended in liquid helium by a torsion rod that could be twisted to set the stack into oscillations. The normal component of the fluid is dragged along with the oscillating disks, but the superfluid part does not rotate. The resulting estimates of the density of the normal and superfluid components as the temperature is varied, is shown in the inset. Illustration by Alan Stonebraker and reprinted with permission from Iacopo Carusotto, Physics **3**, 5 (2010), ©APS, 2010.

The density of states for a noninteracting, free gas in 3D is

$$g(\epsilon) = \frac{Vm^{\frac{3}{2}}}{2^{\frac{1}{2}}\pi^2\hbar^3}\epsilon^{\frac{1}{2}}.$$

It is an interesting mathematical property of the Bose function above that in three or higher dimensions [1] there is an upper bound on the number of atoms that can be accommodated in the excited states at a given temperature. To see this, we write the

[1] The argument sketched here is for free Bose gas in a box. On including the confining potential from a harmonic trap, it is possible to get condensation in 1 or 2D.

expression for the total number of atoms in the excited states for a 3D Bose gas, and scale out the temperature dependence of the resulting integral as

$$N_{ex} = \int_0^\infty d\epsilon g(\epsilon) f(\epsilon) = c(k_B T)^{\frac{3}{2}}.$$

The constant c is given by (in 3D)

$$c = \frac{V m^{\frac{3}{2}}}{2^{\frac{1}{2}} \pi^2 \hbar^3} \Gamma(3/2) \zeta(3/2),$$

where Γ and ζ are the Gamma function and Riemann zeta function respectively. The latter is finite at $3/2$ and so we have a finite number of atoms in the excited states. This suggests that the remaining atoms, if any, have to be accommodated in the ground state, which could then be macroscopically occupied. The critical temperature for this condensation is then the point where the number of particles that could be accommodated in the excited states equals the total number of particles:

$$c(k_B T)^{\frac{3}{2}} \sim N.$$

This straightforward result was however historically held to be a pathological artifact of the theory of noninteracting bosons, which would be absent when interactions were taken into account. London estimated the critical temperature for a gas of helium atoms, and found it to be 3.3 K, remarkably close to the $T_\lambda = 2.17$ K measured in liquid helium. He then suggested that a Bose condensation was responsible for the λ-transition and that the critical temperature was reduced as a result of the interactions. This condensate description helped explain many experimental facts known about helium II. If exactly one state was macroscopically occupied, then the entire system could be characterized by the wavefunction of that single state $\psi(\mathbf{r}, t) = |\psi_0(\mathbf{r}, t)| exp[i\theta(\mathbf{r}, t)]$. We then define the superfluid velocity as

$$\mathbf{v}_s \equiv (\hbar/m)\nabla\theta. \tag{1–1}$$

This shows that the superfluid velocity is irrotational. Also there is no information associated with the single state, and so the superfluid fraction carries no entropy, as postulated in the two-fluid model.

We should point out here that the theory of Bose-Einstein condensation is unresolved in several ways. There is no rigorous proof for the macroscopic occupation of a single state in a general interacting system of bosons at $T = 0$. The only proof available, the one provided originally by Einstein, is for noninteracting systems. There is nothing to assure us that interactions do not deplete the condensate phase, or that they do not lead to condensation in multiple states. The situation is even less clear for nonequilibrium systems. Helium, being a strongly interacting liquid, is far from the ideal Bose gas assumed by Einstein - although evidence for macroscopic occupation of the ground state was found through neutron scattering experiments. The search for Bose condensation in other systems, particularly those with weak interactions, was therefore an important missing link in the history of low temperature physics.

A new era began when a Bose-Einstein condensate (BEC) of dilute, atomic gases was first prepared in 1995 using laser cooling in magneto-optical traps, by the groups of Wiemann and Cornell at JILA, Boulder [12], and Ketterle at MIT [13]. They capitalized on a series of advances in experimental techniques involving the use of lasers followed by magnetic evaporative cooling. The challenge lay in trapping a large enough number of atoms to achieve equilibrium and have an observable condensate, and in cooling them down to the degeneracy temperature. The initial experiments were performed on weakly interacting vapors of alkali atoms such as rubidium, sodium and lithium. Since then, condensation has been achieved in fermions, molecules and particles with long-range dipolar interactions. A major advantage of working with such weakly interacting atomic BEC in traps lies in the precise control we have over such systems. The strength of the interactions between these atoms can be tuned with Feshbach resonances [103]. These atoms can be arranged into “artificial lattices” by applying

an optically generated periodic potential [14]. This analogy between atoms in optical lattices and electrons in ionic lattices can be used to carry out a program of "quantum simulation", where many important naturally occuring systems in condensed matter can be mimicked by trapped ultracold atoms tailored in the laboratory.

The physics of dilute BECs differs in several important respects from that of helium. The most important distinction lies in the role of interactions. The inter-particle separation in a dilute BEC is typically much larger than the scattering length characterizing its inter-particle interaction. Helium atoms on the other hand are closely packed and interact strongly, the interatomic separation being of the same order as the length scale of the van der Waals forces among them. An estimate of the density of atoms in BEC and liquid helium would put matters into perspective. The typical density of a BEC at the center of the trap is around 10^{15} cm^{-3}, while that of liquid helium is around 10^{22} cm^{-3}. The pronounced role of interactions in helium means that some of the condensate is depleted even near $T = 0$ and it poses a theoretically more challenging problem. For example, BECs can be quite accurately described by a Hartree Fock description in terms of the single-particle states, while any such attempt for helium is likely to fail because of the strong correlations. The critical temperature for condensate formation depends on the density as $T_c \sim n^{2/3}$, and so one needs to cool dilute Bose gases to nanoKelvins to achieve condensation, whereas helium undergoes a superfluid transition at 2.17K. An additional feature of the BECs realized by laser cooling is the important role of the confining trap potential. This external potential is usually harmonic and spatially confines the condensate while also rendering it non-uniform . The relevant theoretical framework for a uniform dilute gas was worked out in the 1950s and 60s but the presence of the external harmonic potential can give rise to new and interesting features, such as new collective modes or stability issues. The boundary conditions and surface properties have to be modified according to the trap. Another qualitative distinction can be made between the two systems: helium has been the ideal candidate

for observation of superflow, but the condensation itself is not so apparent. Dilute BECs on the other hand are manifestly condensates, whose condensate fraction can be easily measured in "time-of-flight" experiments, but superflow is harder to achieve in these confined systems.

1.2 Topological Defects: Dislocations, Vortices, etc.

Defects are ubiquitous in condensed matter systems and play an important role in determining many aspects of their properties. For example, vacancies and interstitials catalyze diffusion of particles in solids, dislocations determine the strength of crystalline materials, and vortex motion controls the resistivity of superconductors. Many material properties of practical interest depend on defects. Vortices assume particular significance in 2D systems where they can mediate phase transitions through their thermal unbinding [17, 18]. Our work has two main themes: the effect of dislocations on the superfluid phase transition and the behavior of vortices in superfluid systems.

We find for example that within the scope of a Landau theory for the superfluid phase transition, dislocations could enhance a superfluid phase transition[48, 78]. Two dimensional defects like grain boundaries are also capable of sustaining Kosterlitz-Thouless transitions. We are particularly interested in providing a plausible dislocation-based model for the observed supersolidity of solid ^{4}He [15, 16], which we argue could essentially be superfluid order existing along defect structures in the crystal.

A particularly important class of defects are "topological" defects, which occur in systems with some broken symmetry, and are characterized by a "core" region where order is locally destroyed, and a far field behavior where elastic variables describing the ordered state slowly change. An example would be the superconducting order parameter in the presence of a vortex. The topological defect is impossible to get rid of by local alterations of the order parameter field, and resemble electric charges in that their effect can be determined by observation of their effect on any surface enclosing them.

A dislocation is a one-dimensional topological defect in the regular crystalline arrangement of atoms in a solid. The simplest way to visualize a dislocation is through the Volterra construction. Imagine the perfect crystal being divided into two halves by a slip plane and then displacing one half relative to the other by some vector. This so-called Burger's vector **b** is characteristic of a dislocation line and is an integral multiple of the lattice parameter. If the Burger's vector is perpendicular to the direction

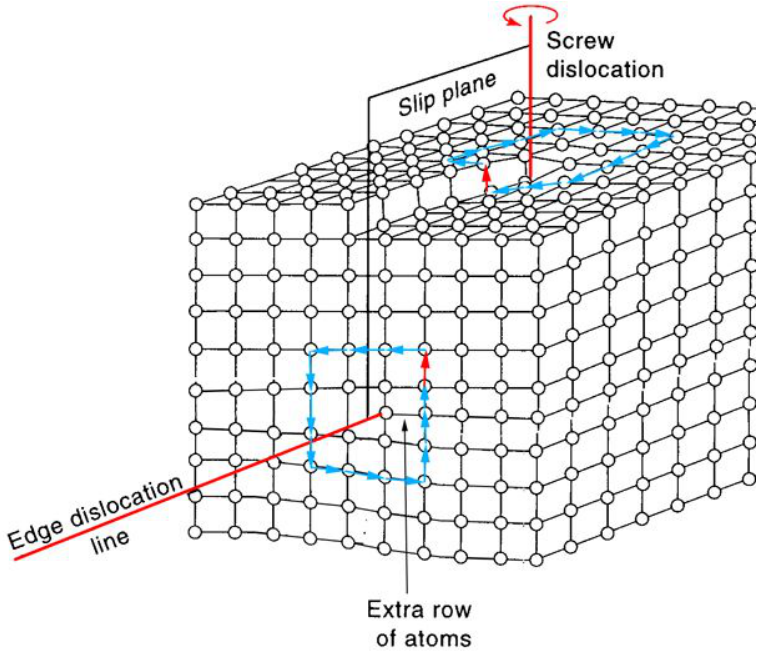

Figure 1-2. Cartoon showing both the basic types of dislocations. The Burger's vector **b** is shown by the red arrow. Reprinted with permission from http://courses.eas.ualberta.ca/eas421, accessed on April 2010.

of the dislocation line ($\mathbf{b} \perp \mathbf{t}$), the resulting structure is an edge dislocation. This can be created by forcing in an extra half plane of atoms with its edge lying along the dislocation line. The other type ($\mathbf{b} \parallel \mathbf{t}$) is a screw dislocation. A real dislocation is usually a combination of these two basic types.

Vortices are easily visualized in fluids, where they imply a core region with some singular behavior, around which the fluid rotates. Usually this rotational velocity falls away as $1/r$, where r is the radial distance from the core. This can be contrasted with rigid rotation where the velocity profile increases as r. Quantum vortices occur in a wide

variety of physical systems - from superconductors, superfluid helium, and BEC in traps to magnetic thin films, and extremely dense quantum plasmas such as found in neutron stars. They are often known to have a dramatic impact on the physical properties of the system where they are present. The motion of vortices in superconductors can suppress superconductivity by inducing potential gradients and so practical applications involving superconductivity often require these vortices to be pinned by impurities.

A quantum vortex is a point singularity in the phase field $\theta(\mathbf{x})$ of the order parameter in some system with continuously broken symmetry (such as an XY model). It satisfies the following basic topological constraint:

$$\oint d\theta = 2\pi e_v, \tag{1–2}$$

where the integral is taken around any loop enclosing the vortex, and e_v is an integer called the “charge” or “winding number” of the vortex. This is called the Feynman-Onsager identity in the context of superfluid helium, which along with superconductors, were the first systems for which the idea of a quantized vortex was posited. The density of the order parameter goes to zero at the vortex core to prevent a singularity in the energy. The energy of the vortex has two parts, a core energy E_c corresponding to the vanishing of the order parameter at the center of the vortex, and an elastic energy E_{el} associated with the slow spatial variation of the phase field far away from the vortex core. The actual phase configuration far away from the vortex core is determined by the minimization of the elastic energy and the topological constraint or quantization condition mentioned above. The exact dynamics of a vortex and its inertia are as yet somewhat controversial topics, as we will discuss later in this thesis, but are important to understand because of their relevance to material properties.

1.3 The Supersolid Conundrum

A solid can withstand shear, i.e. it is deformed but does not flow when subject to a shearing stress. A crystalline solid particularly, is characterized by a regular array

of atoms that are localized in their respective positions. Bose condensation, on the other hand, implies a large number of identical, delocalized particles. Coexistence of superfluidity and crystalline character may therefore seem paradoxical. Indeed, Penrose and Onsager [19], who were arguably the first to consider the possibility of a supersolid (in 1956), concluded that Bose condensation was not possible in a *commensurate* crystal [2] . However, in 1969 it was posited by Andreev and Lifshitz [20], and independently by Thouless [21] and Chester [22], that zero-point vacancies present in the ground state of a quantum crystal like solid ^{4}He can delocalize and cause mass transport. These vacancies would undergo Bose-Einstein condensation below a certain temperature, thus giving rise to superfluid-like behavior.

Recent studies in 2004 by Kim and Chan [23, 24] found some evidence for this phenomenon in so-called "torsional oscillator" experiments, where a sample of solid ^{4}He is placed in a container that is torsionally rotated by some external driving mechanism [see Fig. (1-3)]. At a temperature of around 100 mK, they observe a shift in the resonant period of the oscillator as shown in Fig. (1-4). This was attributed to the decoupling of a certain fraction (nonclassical rotation inertia or "NCRI") of the mass of solid ^{4}He from the rotation. The period T of oscillations is related to the moment of inertia I and elastic constant K as $T = 2\pi\sqrt{I/K}$, and so a reduction of inertia would lead to a decreased resonant period. This is exactly what was observed. This nonclassical fraction is seen to go up with decreasing temperature, and down with increasing velocity, suggesting a superfluid component.

Subsequent experiments have confirmed that anomalies exist not only in the rotational response of solid ^{4}He, but also in its elastic and thermodynamic response at similar temperatures. However, the interpretation of these results is more complicated

[2] This implies a "perfect" crystal without any vacancies, in which each unit cell contains an integer number of atoms.

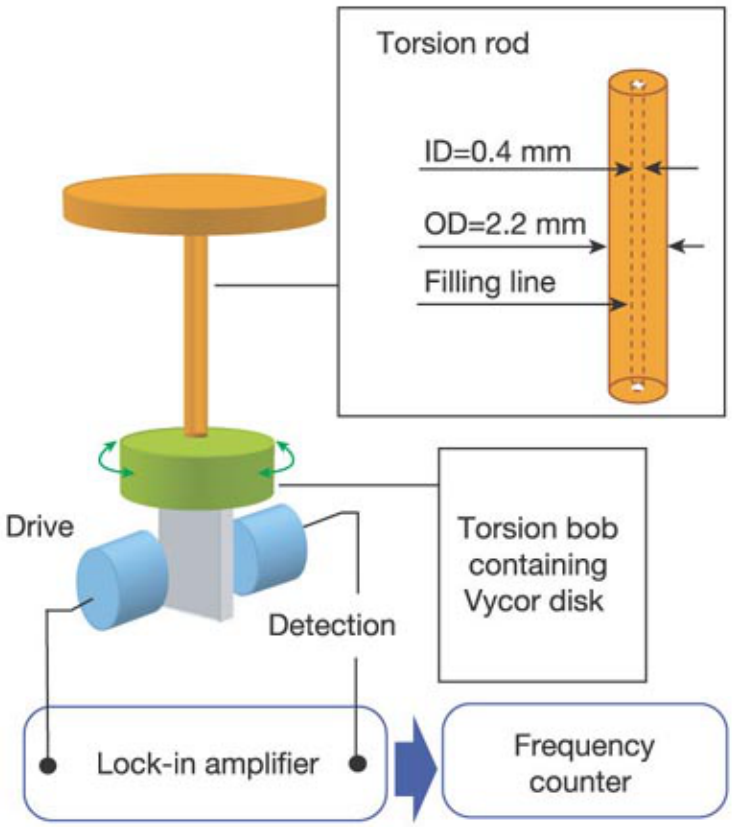

Figure 1-3. The torsional oscillator setup used by Kim and Chan in their 2004 experiment. Reprinted with permission from Ref. [23] [E. Kim and M. H. W Chan, Nature **427**, 225 (2004)], ©Macmillan Publishers Ltd: Nature, 2004.

than was imagined. It has come to be accepted that crystalline defects such as grain boundaries, dislocations and impurities play a major role in these effects. Rittner and Reppy [25, 26] find that the NCRI increases with disorder, and is suppressed on annealing the sample. Lin *et al.* [27] report a peak in the specific heat at around the same temperature where NCRI sets in, but the features of the peak strongly depend on sample quality and ^{3}He impurity concentration. A striking onset of “shear hardening” [28] has been found by Day and Beamish where the sample seems to stiffen as temperature is reduced, the temperature dependence of the shear modulus being very similar to that of the NCRI [see Fig. (1-5)]. Such stiffening has been attributed to the pinning of dislocations by ^{3}He atoms [28], or alternatively by quantum “roughening” of the dislocation lines [29], the latter mechanism being independent of ^{3}He concentration.

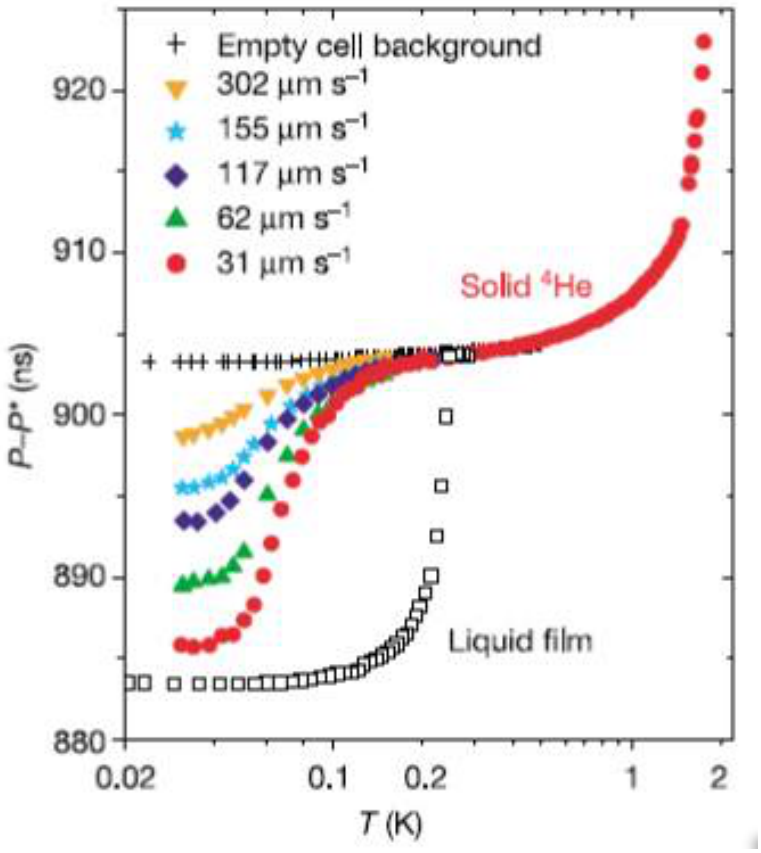

Figure 1-4. Period shifts in a torsion oscillator experiment. The shifts are seen to go down with increasing rim velocity, and are not present for the empty cell. Reprinted with permission from Ref. [23] [E. Kim and M. H. W Chan, Nature **427**, 225 (2004)], ©Macmillan Publishers Ltd: Nature, 2004.

The simple vacancy based model of supersolidity has been ruled out by quantum Monte Carlo studies [30], which find too large an energy cost associated with vacancy formation in a pure crystalline sample of solid ^{4}He. Sasaki *et al.* [31] demonstrate mass flow through grain boundaries. All this taken together motivates our quest for a dislocation-based model for supersolidity, where we build on previous work by Dorsey *et al.* [32] and Toner [78] based on the Landau theory for phase transitions, to show how a network of dislocations could induce superfluid order within solid ^{4}He.

While there is no question that the disorder enhances the “supersolid” phenomenon, there is some debate about whether supersolidity is an intrinsic property of ^{4}He crystals as originally supposed, or if it is solely brought about by defects present in

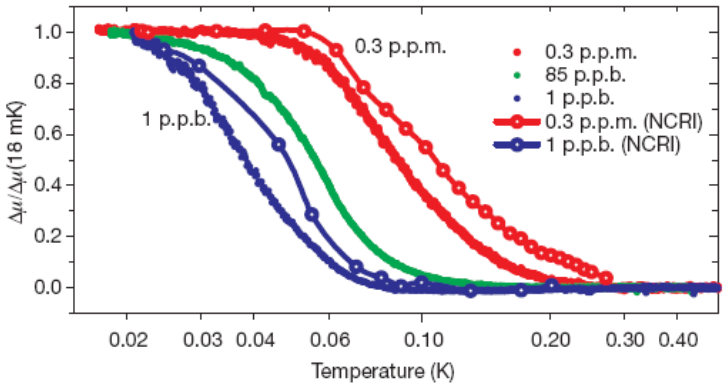

Figure 1-5. Shear hardening in solid ^{4}He, shown for different ^{3}He concentrations . Reprinted with permission from Ref. [28] [J. Day and J. Beamish, Nature **450**, 853 (2007).], ©APS, 2007.

such samples. There are many experiments to suggest that superflow really takes place. There was a suggestion that the shift in the resonant peak in the torsional oscillator experiments could entirely be due to the stiffening of the shear modulus seen by Beamish. Recent studies [34] with a very hard-walled container where stiffening of ^{4}He would not affect the elastic modulus of the overall system have ruled this out. Significantly, no such shift in period is observed in torsional oscillator experiments on solid ^{3}He [34], making a strong case for the presence of a Bose condensate. Our model is however more general and would serve to explain the enhancement of the effect brought about by dislocations, even if this were to be an intrinsic effect.

1.4 Vortices in Rotating Bose-Einstein Condensates

The rotation of a quantum fluid strikingly illustrates the constraints set by quantum mechanics on the velocity field of a quantum macroscopic object. Vortices in superfluid helium were first theoretically predicted by Feynman and Onsager, and were soon experimentally detected by Vinen, Packard and others [35]. Ever since BECs were realized in 1995, the effort to create and detect vortices in them was on. There is one practical difficulty which had to be surmounted in this quest. Unlike liquid helium in a

rotating container where the roughness in the walls is believed to nucleate vortices, ag BEC is in a magneto-optical trap where such a mechanism is not available.

Two basic experimental approaches have been used to create and study vortices in a BEC. The first, carried out in JILA in 1999 [36], uses a mixture of two hyperfine components of ^{87} Rb, spinning one up with respect to the other by applying an external electromagnetic beam. The second was performed in ENS, Paris in 2000 [37], and is analogous to the rotating-bucket method of conventional low-temperature physics. Here the axisymmetric magnetic trap in which the atoms are confined is deformed by an off-center laser beam, which effectively "stirs" and rotates the trap by applying a dipolar force on each condensate atom.

The vortices in a dilute BEC are typically larger than in helium and their size can be controlled by varying the density or species of the trapped atoms. They are also easier to observe once created. This is typically done in the "time-of-flight" experiments, where the BEC trap is rotated while also being cooled down below its condensation temperature, and once the vortices are thought to have formed, the trapping potential is released. The condensate expands in the absence of a trap and the vortex size also increases to several μm. The condensate is probed by optical means, i.e. by shining a laser beam that is tuned to the excitation frequency of the Rb atoms, such that the actual density can be probed. The vortices then show up as "holes" in the condensate density. These experiments were able to confirm certain theoretical predictions made about vortices in BEC [38, 39], such as the existence of a critical velocity of trap rotation, Ω_c, above which a vortex is stabilized.

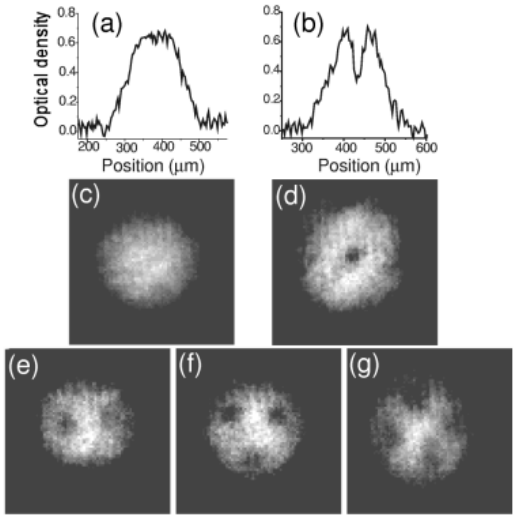

Figure 1-6. Transverse absorption images of a Bose-Einstein condensate stirred with a laser beam. For all five images, the condensate number is $N \sim 10^5$, and the temperature is below 80 nK. The rotation frequency $\Omega/(2\pi)$ is respectively (c) 145 Hz, (d) 152 Hz, (e) 169 Hz, (f) 163 Hz, (g) 168 Hz. In (a) and (b) we plot the variation of the optical thickness of the cloud along the horizontal transverse axis for the images (c) (0 vortex) and (d) (1 vortex). Reprinted with permission from Ref. [37] [K. W. Madison, F. Chevy, W. Wohlleben, and J. Dalibard, Phys. Rev. Lett. **84**, 806 (2000)], ©APS, 2000.

CHAPTER 2
DISLOCATION-INDUCED SUPERFLUIDITY

There is no completely satisfactory microscopic model for the existence of superfluidity in a crystal which can explain the various anomalous effects discovered recently in solid helium [23]. However, if a real thermodynamic phase transition takes place in solid helium at around these temperatures, it could be described by Landau's theory for second order phase transitions [40]. Landau assumed that an ordered phase could be characterized by a finite function called the "order parameter", $\psi(\mathbf{x})$, which would be zero when the order is lost, i.e. in the disordered phase. Near the transition temperature, one could expand the free energy of the system in terms of this order parameter, in a way that respects the inherent symmetries of the system. For the prototypical second order phase transition, e.g. the ferromagnetic or superconducting transition, this would be written as

$$F = \int d^3x \left[\frac{1}{2} c |\partial\psi|^2 + \frac{1}{2} a(T) |\psi|^2 + \frac{1}{4} u |\psi|^4 \right].$$

Here $a(T)$ is a smooth function of temperature, $a = a_0(T - T_0)/T_0$ where T_0 is the critical temperature below which order first appears. The quantity $\xi \equiv \hbar/\sqrt{2ma(T)}$ is the coherence length, a length scale over which "order" prevails in the system. Near T_0, the coherence length diverges as $\xi \sim 1/\sqrt{(T - T_0)}$. However the conclusions of this theory, such as the "critical exponent" of $\nu = -1/2$ found here, and the critical temperature T_0, are modified by the effect of fluctuations, which become especially important near criticality. Such a phenomenological description is expected to hold very generally irrespective of the detailed interactions in the system, and is a minimal model that can come in handy in describing a complex system such as solid helium.

Parts of this chapter are reproduced from the published articles: "K. Dasbiswas, D. Goswami, C.-D. Yoo and A. T. Dorsey, Phys. Rev. B **81**, 64516 (2010)" and "D. Goswami, K. Dasbiswas, C.-D. Yoo and A. T. Dorsey, Phys. Rev. B **84**, 054523 (2011)."

Historically, such a model was applied with great success to superconductors by Landau and Ginzburg [41], and is known as the Ginzburg-Landau theory in this context. The analogous theory for neutral superfluids (often called the Ginzburg-Pitaevskii model [42], but which we generically call a "Landau theory" in this chapter) was not so successful in describing the λ-transition in liquid helium, presumably because of the large role played by fluctuations.

In this chapter, we first introduce the Landau theory for a supersolid transition by coupling the superfluid order parameter to the elastic strains of the crystal lattice. Such a phenomenological description is useful even if there is no bulk supersolid transition, and in fact we use this to predict that the superfluid transition temperature is enhanced by the presence of a dislocation line in the crystal. We introduce a formalism to describe this "dislocation-induced" one-dimensional superfluid and then provide quantitative estimates of this effect.

2.1 Landau Theory for the Supersolid Phase Transition

The transition from normal fluid to superfluid (NF-SF) in ^{4}He is a standard example of a continuous phase transition, and can be described by a Landau theory. Following Dorsey, Goldbart and Toner [32], we assume that the phase transition from normal solid to supersolid (NS-SS) is also continuous. A Landau theory of the transition can then be developed by coupling the superfluid order parameter to the elasticity of the crystalline ^{4}He lattice. The main consequences of this theory as predicted by Dorsey *et al*. are anomalies in the elastic coefficients near the transition and conversely local alterations in the transition temperature brought about by inhomogeneous strains in the lattice. One common way in which these strains can arise in real solids is through the presence of crystal defects such as vacancies, interstitials, dislocations, or grain boundaries [43]. It will be shown subsequently that edge dislocations in particular can induce superfluidity in their vicinity at temperatures higher than in the bulk.

As in the case of superfluids and other instances of ordered phases with continuously broken U(1) symmetry, we characterize the supersolid phase by an order parameter that is a complex scalar field $\psi(\mathbf{x})$. The microscopic interpretation of this order parameter is that it corresponds to the quantum wave function of the many body ground state to which all the ^{4}He atoms Bose condense at zero temperature. The universal properties of this transition can be obtained irrespective of the microscopic details of the system by considering an expression of the Landau free energy in terms of the lowest relevant powers of the order parameter and its spatial gradients, that satisfy all the symmetry properties of the system,

$$F = \int d^3x \left[\frac{1}{2} c_{ij} \partial_i \psi \partial_j \psi^* + \frac{1}{2} a(T) |\psi|^2 + \frac{1}{4} u |\psi|^4 \right]. \tag{2–1}$$

Here $a(T)$ is a smooth function of temperature, which for a regular superfluid transition (such as for NF-SF in ^{4}He) is, $a = a_0(T - T_0)/T_0$ where T_0 is the bulk critical temperature below which superfluidity first appears. The actual transition temperature can differ from this because of the effect of thermal fluctuations. The coefficients c_{ij} correspond to the anisotropy inherited from the crystal. For an isotropic superfluid or cubic crystal, $c_{ij} = c\delta_{ij}$. a_0, c and u are all phenomenological parameters (all positive) that arise from the expansion of the free energy in this Landau theory.

However, in the presence of a crystal we should take into account the phonon modes that arise because of the crystallinity of the system. These are associated with displacements of atoms $u(\mathbf{x})$ in the lattice from their mean positions because of strain fields in the crystal. As the Landau free energy above has to be invariant under rotations and translations, the displacement field $u(\mathbf{x})$ can couple to the superfluid order parameter only through the symmetric strain tensor, defined as $u_{ij} \equiv \frac{1}{2}(\partial_i u_j + \partial_j u_i + \partial_i u_k \partial_j u_k)$. To the lowest order the coupling with crystallinity affects only the term in the Landau free energy that is quadratic in the order parameter, and the coefficient $a(T)$ is now a function of spatial coordinates, $a(T) = a_0(T - T_0)/T_0 + u_{ij} a_{ij}$.

Solid ^{4}He has a hcp crystal lattice (except for a small region in its phase diagram where it is bcc), and the coupling tensors c_{ij} and a_{ij} must have that same symmetry structure. For the rest of our presentation here, we treat the isotropic case for the sake of clarity, with the conviction that our key results are more general and do not depend on the specific lattice structure. Under this simplifying assumption, the Landau free energy can be written as

$$F = \int d^3x \left[\frac{c}{2} |\nabla \psi|^2 + \frac{1}{2} a(\mathbf{x}) |\psi|^2 + \frac{1}{4} u |\psi|^4 \right], \tag{2–2}$$

where the superfluidity couples to the crystallinity through the trace of the strain tensor, $a(\mathbf{x}) = a_0(T - T_0)/T_0 + a_1 u_{ii}(\mathbf{x})$. The spatial dependence of the quadratic coefficient of the Landau free energy suggests that the critical temperature T_c may be modified by elastic strains present in the crystal.

2.2 Superfluid-Dislocation Coupling

A crystal defect structure like a dislocation line disrupts the regular arrangement of atoms in its neighborhood. This shifting of the positions of the atoms of the lattice from their minimum energy configurations induces elastic strains in the crystal. The analysis of the previous section suggests that the local critical temperature T_c for a possible superfluid transition can be modified through the coupling of the superfluid order parameter with the elastic strain field. We have arrived at essentially similar conclusions using different methods in the context of the putative supersolid state of ^{4}He [48, 78, 79]. The same idea has also been explored through approaches other than the phenomenological Landau theoretic description we pursue. Quantum Monte Carlo simulations for example find superfluidity along the core of a screw dislocation in solid ^{4}He [44]. In this section, we present the result of coupling the strain field of a single, quenched, edge dislocation to the superfluid order parameter. We postpone the discussion of more realistic situations involving multiple or mobile dislocations to Chapter 3 of this dissertation.

It is also interesting to note that similar studies on superconductors within the phenomenological Landau theory have reported an increase in the T_c in the neighborhood of an edge dislocation [45, 73]. This is somewhat counterintuitive from a microscopic point of view, as the presence of disorder and nonmagnetic defects is usually expected to inhibit pairing and to reduce the superconducting gap. However, pairing is not important in superfluid ^{4}He, which is a Bose liquid. We suggest then that the superfluid signature seen in torsional oscillator experiments can be attributed to superfluidity induced locally along dislocation lines.

Without any loss of generality, we consider a single straight edge dislocation pointing along the z-axis and passing through the origin of our coordinate system. The Burger's vector $\mathbf{b}$ is along the y-axis. This corresponds to a situation where an extra half plane of atoms has been introduced with edge lying along the x-axis. If isotropy is assumed, the quantity of interest that couples to the superfluid order parameter in Eq. (4–8) of the previous section is the trace of the strain tensor, which is physically the local fractional volume change of the crystal lattice. This has been derived in Appendix A from considerations of linear elasticity theory [50, 74] to be

$$u_{ii} = \frac{4\mu}{2\mu + \lambda} \frac{b \cos\theta}{r}, \tag{2–3}$$

where μ and λ are the Lamé elastic constants, and we have introduced the coordinates $\mathbf{x} = (\mathbf{r}, z)$, with $\mathbf{r}$ in the $x - y$ plane [(r, θ) are polar coordinates in the $x - y$ plane]. The local change in T_c is reflected in the term quadratic in the order parameter in the Landau theory,

$$a(\mathbf{x}) = a_0 \left(t_0 + B \frac{\cos\theta}{r} \right). \tag{2–4}$$

Here, a_0, b and u are phenomenological parameters (all positive); $t_0 = (T - T_0)/T_0$ is the reduced temperature, with T_0 the mean-field critical temperature for the supersolid transition in the *absence* of the dislocations ($t_0 > 0$ is the normal solid and $t_0 < 0$,

the supersolid); and B is a coupling constant (into which we have absorbed the elastic constants).

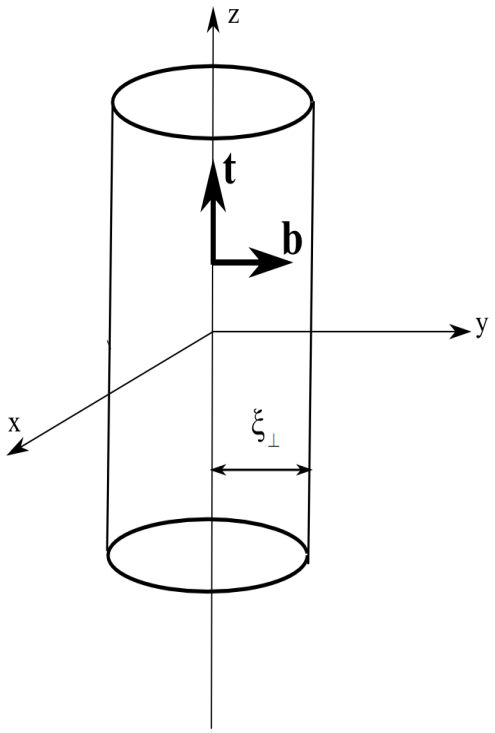

Figure 2-1. Schematic showing the dislocation axis (along z) and the tubular superfluid region that develops around it. The radius of the cylinder is determined by the length scale of the ground state wavefunction. The axis of the tube will be offset from the dislocation axis. Reprinted with permission from Ref. [48] [D. Goswami, K. Dasbiswas, C.-D. Yoo and A. T. Dorsey, Phys. Rev. B **84**, 054523 (2011)], ©APS, 2011.

To simplify the subsequent analysis, we introduce the characteristic scales of length $l = c/a_0 B$, order parameter $\chi = a_0 B/\sqrt{cu}$, and free energy $F_0 = a_0 Bc/2u$, and the dimensionless (primed) quantities $\mathbf{x}' = \mathbf{x}/l$, $\psi' = \psi/\chi$, and $\mathcal{F} = F/F_0$; in terms of the dimensionless quantities the free energy becomes

$$\mathcal{F} = \int d^3x \left\{ |\nabla\psi|^2 + [V(\mathbf{r}) - E]\,|\psi|^2 + \frac{1}{2}|\psi|^4 \right\}, \tag{2–5}$$

where $V(\mathbf{r}) = \cos\theta/r$, $E \equiv -ct_0/a_0 B^2$, and we have dropped the primes on all quantities for clarity of presentation.

2.3 Effective Landau Theory for Superfluidity along a Dislocation

So far we have set up the Landau theory for a superfluid coupled to a single dislocation in a solid. Here we argue that the effect of the dislocation must be to increase the superfluid critical temperature around itself. Before proceeding further, let us analyze the behavior in the high-temperature, normal phase. In this phase we can neglect the quartic term in the free energy; the resulting quadratic free energy is

$$\begin{aligned} \mathcal{F}_0 &= \int d^3x \left\{ |\nabla\psi|^2 + [V(\mathbf{r}) - E]\,|\psi|^2 \right\} \\ &= \int d^3x\, \psi^*(\hat{H} - E)\psi, \end{aligned} \tag{2–6}$$

where the Hermitian linear operator $\hat{H}$ is given by

$$\hat{H} = -\nabla^2 + V(\mathbf{r}). \tag{2–7}$$

We can diagonalize the free energy by introducing a complete set of orthonormal eigenfunctions $\Psi_n(\mathbf{x})$ of $\hat{H}$,

$$\hat{H}\Psi_n = E_n\Psi_n, \tag{2–8}$$

where n labels the states, and we assume that the eigenvalues E_n are ordered such that $E_0 < E_1 < \ldots$. Equation (2–8) is equivalent to a Schrödinger equation for a particle in a potential $V(\mathbf{r})$, and for the dipolar potential $V(\mathbf{r}) = \cos\theta/r$ the spectrum and eigenfunctions were obtained with extensive numerical work in Ref. [79], and is discussed in the next section. Expanding the order parameter in terms of the eigenfunctions,

$$\psi(\mathbf{x}) = \sum_n A_n\Psi_n(\mathbf{x}), \tag{2–9}$$

with expansion coefficients A_n, and substituting into the free energy, after using the orthogonality properties of the eigenfunctions we obtain

$$\mathcal{F}_0 = \sum_n (E_n - E)|A_n|^2. \tag{2–10}$$

The free energy is positive as long as $E_n > E$, for all n. Recall that $E \equiv -(c/a_0 B^2)(T - T_0)/T_0$ (with a_0 and c both positive), so high temperatures T correspond to large, negative values of E. As we decrease T, E increases, until eventually we hit a *condensation* temperature $T_{\rm cond}$ at which $E(T_{\rm cond}) = E_0$; below this temperature the quadratic free energy $\mathcal{F}_0$ becomes unstable. Rearranging a bit, we have

$$\frac{T_{\rm cond} - T_0}{T_0} = -E_0 \frac{a_0 B^2}{c}. \tag{2–11}$$

If $\hat{H}$ has negative eigenvalues–i.e., if the equivalent Schrödinger equation has bound states–then $T_{\rm cond} > T_0$, and the dislocation induces superfluidity *above* the bulk ordering temperature. As emphasized in Refs. [45, 78, 79], the dipolar potential $\cos\theta/r$, which has an attractive region irrespective of the coupling constants, *always* has a negative energy bound state. We are thus lead to the surprising and important conclusion [45, 78] that superfluidity first nucleates around the edge dislocation before appearing in the bulk of the material.

Just below the condensation temperature $T_{\rm cond}$, the nucleated order parameter has the form

$$\psi = A_0 \Psi_0(\mathbf{r}), \tag{2–12}$$

where Ψ_0 is the normalized ground state wavefunction and A_0 is an amplitude that is fixed by the nonlinear terms in the free energy [83]. Substituting Eq. (2–12) into the dimensionless free energy, Eq. (4–8), we obtain

$$\mathcal{F} = (E_0 - E)|A_0|^2 + \frac{1}{2} g |A_0|^4, \tag{2–13}$$

where the coupling constant g is given by

$$g = \int d^2 r \, \Psi_0^4(\mathrm{r}). \tag{2–14}$$

Minimizing the free energy with respect to A_0, we obtain

$$A_0 = \sqrt{(E - E_0)/g}. \tag{2–15}$$

From the extensive numerical work of Dasbiswas *et al*. [79], presented in Section 2.4 of this dissertation, we know that for the dipole potential the ground state energy is $E_0 = -0.139$ (with the energy of the first excited state $E_1 = -0.0414$), and the coupling constant $g = 0.0194$.

To recap- following the work of previous authors [45, 78] we have shown that superfluidity always nucleates *first* on edge dislocations, and we have calculated the form of the order parameter near E_0, the threshold value of E (i.e., at temperatures just below the condensation temperature). Physically, we imagine a cylindrical tube of superfluid, with a radius equal to the transverse correlation length (of order 1 in our dimensionless units), that encircles the dislocation. However, this naive mean-field picture ignores the thermal fluctuations which destroy the one-dimensional superfluidity on long length scales. What is needed is an effective one-dimensional model for the superfluid, capable of capturing nontrivial fluctuation effects. We now derive this one-dimensional model using a systematic, weakly-nonlinear analysis near the threshold E_0.

Within the mean-field Landau theory, the order parameter configurations that minimize the free energy are solutions to the Euler-Lagrange equation

$$\frac{\delta \mathcal{F}}{\delta \psi^*} = 0 = -\nabla^2 \psi + [V(\mathbf{r}) - E]\,\psi + |\psi|^2 \psi. \tag{2–16}$$

This nonlinear field equation is difficult to solve, even numerically. Instead, we resort to a *weakly nonlinear analysis* [84] near the threshold for the linear instability. Our goal is to "integrate out" the modes transverse to the dislocation and obtain an effective model for the one-dimensional superfluid nucleated along the dislocation. We then treat thermal fluctuations of this one-dimensional superfluid in the next Section.

We start by introducing a control parameter

$$\epsilon \equiv E - E_0 \tag{2–17}$$

that measures distance from the linear instability. From the analysis in the preceding Section, we see that the order parameter near threshold scales as $\epsilon^{1/2}$, which suggests a rescaling of the order parameter

$$\psi = \epsilon^{1/2}\phi, \tag{2–18}$$

with ϕ a quantity whose amplitude is $\mathcal{O}(1)$. Next, note that if we had included the plane wave behavior along the z-axis in the earlier analysis, the coefficient of $|A_n|^2$ in the quadratic free energy, Eq. (2–10), would be $-\epsilon + k^2$. This suggests that the important fluctuations along the z-axis occur at wavenumbers $k \sim \epsilon^{1/2}$, or at length scales of order $\epsilon^{-1/2}$ (i.e., long wavelength fluctuations are important close to threshold). This suggests another rescaling,

$$z = \epsilon^{-1/2}\zeta. \tag{2–19}$$

Substituting these variable changes into Eq. (2–16), and writing $E = E_0 + \epsilon$, we obtain

$$\hat{L}\phi = \epsilon\left[\partial_\zeta^2\phi + \phi - |\phi|^2\phi\right], \tag{2–20}$$

where the Hermitian linear operator $\hat{L}$ is given by

$$\hat{L} = -\nabla_\perp^2 + V(\mathbf{r}) - E_0, \tag{2–21}$$

with $\nabla_\perp^2$ the Laplacian in dimensions transverse to z. Next, we expand ϕ in powers of ϵ,

$$\phi = \phi_0 + \epsilon\phi_1 + \epsilon^2\phi_2 + \ldots. \tag{2–22}$$

Collecting terms, we obtain the following hierarchy of equations:

$$\mathcal{O}(1): \qquad \hat{L}\phi_0 = 0, \tag{2–23}$$

$$\mathcal{O}(\epsilon): \qquad \hat{L}\phi_1 = \partial_\zeta^2\phi_0 + \phi_0 - |\phi_0|^2\phi_0, \tag{2–24}$$

$$\mathcal{O}(\epsilon^2): \qquad \hat{L}\phi_2 = (1 - 3\phi_0^2)\phi_1. \tag{2–25}$$

The solution of the $\mathcal{O}(1)$ equation is the normalized ground state eigenfunction, $\Psi_0(\mathbf{r})$; there is an overall integration constant, which can be a function of ζ, which we will call $A_0(\zeta)$:

$$\phi_0 = A_0(\zeta)\Psi_0(\mathbf{r}). \tag{2–26}$$

Substitute this into the right hand side of the $\mathcal{O}(\epsilon)$ equation,

$$\hat{L}\phi_1 = \Psi_0\partial_\zeta^2 A_0 + \Psi_0 A_0 - \Psi_0^3|A_0|^2 A_0. \tag{2–27}$$

We can determine A_0 by left multiplying this equation by Ψ_0, integrating on d^2r, and using the fact that $\hat{L}$ is Hermitian, to find

$$\partial_\zeta^2 A_0 + A_0 - g|A_0|^2 A_0 = 0, \tag{2–28}$$

where g is defined in Eq. (2–14). This is the *solvability condition* for the existence of nontrivial solutions of the $\mathcal{O}(\epsilon)$ equation. In principle we could solve this equation for A_0, substitute back into the right hand side of the $\mathcal{O}(\epsilon)$, and solve the resulting inhomogeneous equation to obtain ϕ_2. In practice this is difficult for the dipole potential, so we will stop at this level of the perturbation theory. However, in Appendix B we show that for $V(\mathbf{r}) = -1/r$ (a two-dimensional Coulomb potential), the perturbation calculation can be explicitly worked out through $\mathcal{O}(\epsilon^2)$, and the results are in close agreement with detailed numerical solutions of the nonlinear field equation.

We can recast Eq. (4–20) in terms of $\zeta = \epsilon^{1/2}z$ and $A_0 = \epsilon^{-1/2}\varphi$ as

$$\partial_z^2\varphi(z) + \epsilon\varphi - g|\varphi|^2\varphi = 0, \tag{2–29}$$

which is the Euler-Lagrange equation for the free energy functional

$$\mathcal{F} = \int dz \left[\frac{1}{2}|\partial_z\varphi|^2 - \frac{1}{2}\epsilon|\varphi|^2 + \frac{g}{4}|\varphi|^4\right]. \tag{2–30}$$

Reinstating the dimensions, we obtain

$$F = \int dz \left[\frac{c}{2} |\partial_z \varphi|^2 + \frac{a}{2} |\varphi|^2 + \frac{b}{4} |\varphi|^4 \right], \tag{2–31}$$

where $a = a_0 t$, $t = (T - T_{\mathrm{cond}})/T_{\mathrm{cond}}$ is the reduced temperature measured relative to the *condensation* temperature, and $b = gu$. To recap, we have integrated out the transverse degrees of freedom (the fluctuations of which have a nonzero energy gap) and reduced the full three-dimensional problem to an effective one-dimensional model. In the next section we will study the fluctuations of this one-dimensional model, and derive an effective phase-only model for a dislocation network.

2.4 Quantitative Estimates of the Shift in Critical Temperature

2.4.1 The Quantum Dipole Problem in 2D

Here we describe the methods used to solve the linearized Ginzburg Landau equation described in the previous section. The ground state eigenvalue is of particular interest to us, since it is related to the shift in T_c in the presence of a dislocation. The eigenfunction is also used in deriving the network model in the following section. The equation to be solved is identical to a 2D Schrödinger equation for the dipolar potential,

$$-\frac{\hbar^2}{2m} \nabla^2 \psi + p \frac{\cos\theta}{r} \psi = E\psi. \tag{2–32}$$

This potential is non-central and cannot be solved analytically or by using WKB methods. It permits bound states because the potential is attractive in one half plane. The problem has a long history, especially in the context of bound and excited states for edge dislocations in semiconductors, and has been tackled using a variety of variational and other kinds of approximate methods. These early efforts, and the corresponding nondimensionalized ground state eigenvalues, are listed in Table 2-1. We solve the problem using a direct numerical approach and find a ground state eigenvalue of -0.139, which is lower than all the upper bounds established by the variational methods [57]. Some sample eigenvalues found by different methods are listed in Table 2-2.

Table 2-1. Summary of ground state energy estimates of the edge dislocation potential. Energy is given in units of $2mp^2/\hbar^2$.

References	Ground state estimate
Landauer (1954) [51]	-0.102
Emtage (1967) [52]	-0.117
Nabutovskii and Shapiro (1977) [53]	-0.1014
Slyusarev and Chishko (1984) [54]	-0.1111
Dubrovskii (1997) [55]	-0.1196
Farvacque and Francois (2001) [56]	-0.1113
Dorsey and Toner [57]	-0.1199
This work	-0.139

2.4.2 Numerical Methods Used

A detailed numerical solution of the two-dimensional Schrödinger equation with the dipole potential, Eq. (2–32), is likely to provide more accurate ground state eigenvalues in addition to determining the rest of the bound state eigenvalues and corresponding wavefunctions. We do this both by a real space diagonalization, where the Schrödinger equation is discretized on a square grid, and by expanding in the basis of the eigenfunctions of the two-dimensional Coulomb potential problem. Two special features of this dipole potential make it a numerically difficult problem: the singularity at the origin and the long range behavior of the potential. It is expected that the Coulomb wavefunctions would be better suited to capturing this long range behavior and convergence would consequently be faster. Our results show that the Coulomb basis method is more accurate for the higher bound states (which are expected to extend more in space), as the real space methods are limited by size issues. However, the real space method works better for the ground state. The Coulomb basis results have recently been further refined by Amore [58].

2.4.3 Variational Calculation

Our initial approach to determine the ground state energy has been variational because this can be carried out analytically and provides a rough estimate which can then guide our more explicit numerical solution. Given a normalized wave function

$\psi(r,\theta)$, we minimized the energy functional,

$$F[\psi,\psi^*] = \int d^2x \left(\frac{\hbar^2}{2m}|\nabla\psi|^2 + p\frac{\cos\theta}{r}|\psi|^2 \right). \tag{2–33}$$

This functional has its extrema at the solutions of the Schrödinger equation, Eq. (2–32). Note that the length and energy scales which emerge from Eq. (2–33) (or the Schrödinger equation) for this problem are $\hbar^2/2mp$ and $2mp^2/\hbar^2$. In dimensionless variables, the normalized trial wave function used in our calculation is

$$\begin{aligned} \psi(r,\theta) &= \frac{2AB}{C\sqrt{\pi}} \frac{(1-r/BC)}{\sqrt{(3-4B+2B^2)}} \exp\left(-\frac{r}{C}\right) \\ &\quad -\frac{\sqrt{1-A^2}}{C^2}\sqrt{\frac{8}{3\pi}} r\cos\theta \exp\left(-\frac{r}{C}\right), \end{aligned} \tag{2–34}$$

where A, B and C are variational parameters. We choose the trial wave function so as to account for the anisotropy of the potential. Further, the asymptotic behavior of the potential is captured by the exponentially decaying factors. The minimum expectation value of the energy occurs when $A = 0.803$, $B = -0.774$ and $C = 2.14$ with a ground state energy of -0.1199 which was found by Dorsey and Toner [57]. This value is 2.5% lower than the previous lowest variational estimate (-0.1196) obtained by Dubrovskii [55] In addition, by using this normalized trial wave function as the $\phi_0(x,y)$ we find the parameter $g = \int dxdy|\phi_0(x,y)|^4 = 0.017$.

2.4.4 Real Space Diagonalization Method

For numerical purposes the Schrödinger equation is converted to a difference equation on a square grid of spacing h, with the Laplacian approximated by its five-point finite difference form [59], resulting in a block tridiagonal matrix of size $N^2 \times N^2$, where the grid has dimensions of $N \times N$. Each diagonal element corresponds to a grid point and has values of $4/h^2 + V(x,y)$, whereas the nonzero offdiagonal elements all equal $-1/h^2$. The matrix is thus very large but sparse. We use three different numerical methods to diagonalize this matrix: the biconjugate gradient method [60], the Jacobi-Davidson algorithm [61] and Arnoldi-Lanczos algorithm [62], with the

latter two being more suited to large sparse matrices whose extreme eigenvalues are required. We use freely available open source packages (JADAMILU [63] and ARPACK [64]) both written in FORTRAN. All three approaches are projective Krylov subspace methods, which rely on repeated matrix-vector multiplications while searching for approximations to the required eigenvector in a subspace of increasing dimensions. Reference [65] provides a concise introduction to the Jacobi-Davidson method, together with comparisons to other similar methods. The implicitly restarted Arnoldi package (ARPACK) is described in great detail in Ref. [66]. Some general issues about the real space diagonalization as well as some specific features of the three methods used for it are discussed below.

The accuracy of the real space diagonalization methods is controlled by two main parameters: the grid spacing h and the total size of the grid, which is given by Nh. The finite difference approximation together with the rapid variation of the potential near the origin imply that the solution of the partial differential equation would be more accurate for a smaller grid spacing. We work with open boundary conditions, which means that a bound state wavefunction could be correctly captured only if the total size of the grid were to be greater than the natural decay length of the wavefunction. In other words, the eigenstate has to be given enough space to relax. This limits the number of bound states we can calculate accurately because a large grid size together with small grid spacings calls for a large number of grid points, thus quadratically increasing the size of the matrix to be diagonalized. Computational resources as well as the limitations of the algorithms themselves place an effective upper bound on the size of a diagonalizable matrix. We experimented to find that a $10^6 \times 10^6$ size sparse matrix was about the maximum that could be diagonalized with our computational resources.

The origin of the square grid is symmetrically offset in both x and y directions to avoid the $1/r$ singularity. We first tested the accuracy of the real space techniques for the case of the two dimensional Coulomb potential, the spectrum of which is completely

known [96]. We observe that for various lattice sizes the biconjugate method captures at most the first four states whereas the Jacobi-Davidson method returns 20 eigenstates. The eigenvalues obtained from both methods are accurate to within 2% of the exact values [96].

We have applied the biconjugate method to the edge dislocation potential for various lattice sizes, varying from 10×10 to 600×600. The number of eigenstates captured increases with the size of the lattice, as expected. The ground state energy is observed to vary from -0.134 to -0.142. We also observe that for the number of grid points exceeding $N = 2000$ we encounter a numerical instability due to the accumulation of roundoff errors. For the largest real space grid size of 600×600 ($N = 1200, h = 0.5$) we obtain seven eigenstates with a ground state energy of -0.139.

The ground state energy from the Jacobi-Davidson method, employed for the same lattice size gives -0.139, which matches well with our expectations from the variational calculation. We are able to obtain 20 bound state eigenvalues in this method using $N = 1000, h = 0.5$. It is checked that the low-lying eigenvalues are not very sensitive to values of h in this regime, so a relatively large value of 0.5 serves our purpose. As pointed out earlier, the accuracy of this method is determined by the choice of lattice parameters. The variation in the calculated ground state eigenvalue for differing lattice parameters is within 0.001, which therefore is the estimated error in the calculation of eigenvalue.

The Arnoldi-Lanczos method yields the same eigenvalues to within estimated error. It takes more time and memory resources to converge but can calculate more eigenvalues. It provides 30 bound state eigenvalues for the same set of lattice parameters as the above. Finally, after calculating the ground state wave function we find that the coupling constant $g = 0.0194$, slightly larger than the variational estimate of $g = 0.017$.

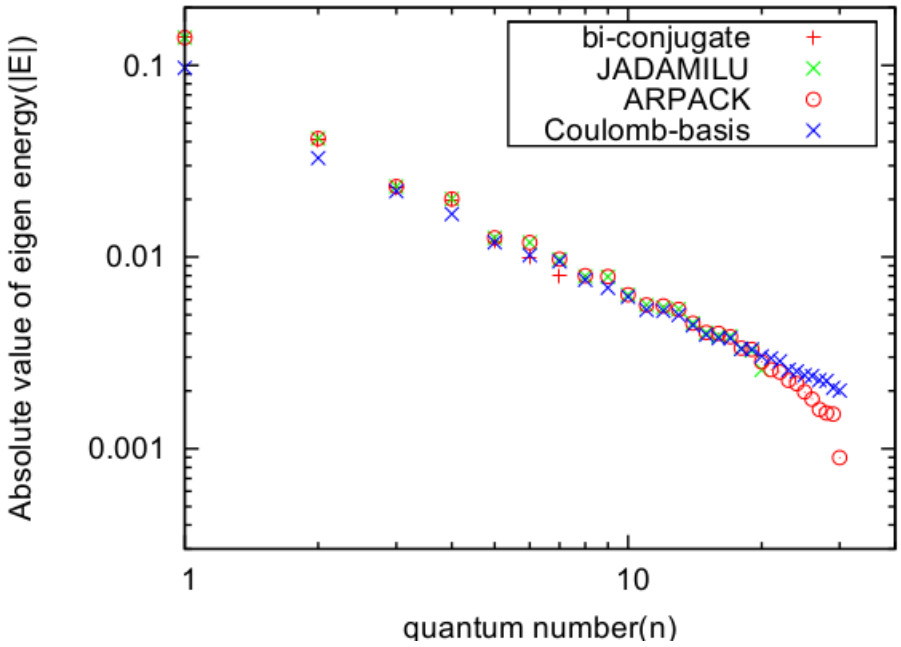

Figure 2-2. Comparison of eigenvalues of the 2D quantum dipole problem, obtained by different methods. (The plot is on a log-log scale.) Reprinted with permission from Ref. [79] [K. Dasbiswas, D. Goswami, C.-D. Yoo and A. T. Dorsey, Phys. Rev. B **81**, 64516 (2010)], ©APS, 2010.

Table 2-2. Comparison of first few energy eigenvalues obtained from different methods. Energy units: $2mp^2/\hbar^2$. n indicates quantum number of the state.

n	biconjugate	Jacobi-Davidson /Arnoldi-Lanczos	Coulomb basis
1	-0.14	-0.139	-0.0970
2	-0.041	-0.0415	-0.0328
3	-0.023	-0.0233	-0.0221
4	-0.02	-0.0201	-0.0167
5	-0.012	-0.0126	-0.0119

2.4.5 Coulomb Basis Method

We also calculate the spectrum numerically by using the linear variational method with the basis of the 2D hydrogen atom wave functions [96]. There are two advantages of this method over the real space diagonalization methods. First, the linear variational method is capable of capturing more excited states because the number of calculated bound states is not limited by the size of the real space grid but by the number of long-range basis functions. Second, the singularity at the origin of the edge dislocation

potential does not pose a problem anymore because elements of the Hamiltonian matrix become integrable.

Now we calculate the elements of the Hamiltonian matrix with a 2D edge dislocation potential. The Schrödinger equation with the 2D Coulomb potential is analytically worked out in Ref. [96]. The normalized wave functions of a 2D hydrogen atom are given by

$$\psi^{\mathsf{H}}_{n,l}(r,\theta) = \sqrt{\frac{1}{\pi}} R_{n,l}(r) \times \begin{cases} \cos(l\theta) & \text{for } 1 \le l \le n, \\ \frac{1}{\sqrt{2}} & \text{for } l = 0, \\ \sin(l\theta) & \text{for } -n \le l \le -1, \end{cases} \tag{2–35}$$

where

$$\begin{aligned} R_{n,l}(r) = {} & \frac{\beta_n}{(2|l|)!} \sqrt{\frac{(n+|l|-1)!}{(2n-1)(n-|l|-1)!}} (\beta_n r)^{|l|} \\ & \times \exp\left(-\frac{\beta_n r}{2}\right) {}_1F_1(-n+|l|+1, 2|l|+1, \beta_n r), \end{aligned} \tag{2–36}$$

with $\beta_n = 2/(2n-1)$ and ${}_1F_1$ being the confluent hypergeometric function. The elements of the Hamiltonian with the 2D dipole potential are

$$\begin{aligned} \langle \psi^{\mathsf{H}}_{n_1,l_1} | -\nabla^2 | \psi^{\mathsf{H}}_{n_2,l_2} \rangle = {} & \delta_{l_1,l_2} \int_0^\infty dr \, \left(1 - \frac{\beta^2_{n_2}}{4} r\right) \\ & \times R_{n_1,l_1}(r) R_{n_2,l_2}(r), \end{aligned} \tag{2–37}$$

$$\left\langle \psi^{\mathsf{H}}_{n_1,l_1} \left| \frac{\cos\theta}{r} \right| \psi^{\mathsf{H}}_{n_2,l_2} \right\rangle = \tilde{V} \int_0^\infty dr \, R_{n_1,l_1}(r) R_{n_2,l_2}(r), \tag{2–38}$$

where $\tilde{V} = \delta_{l_1,l_2\pm1}/2$ if both l_1 and l_2 are less or greater than 0, or $\tilde{V} = 1/\sqrt{2}$ if l_1 is 0 and l_2 positive or vice versa. The spectra are obtained for several total numbers of basis functions N_{basis}. Due to the numerical precision in calculating elements of the Hamiltonian matrix N_{basis} cannot be increased to more than 400. For $N_{\text{basis}} = 400$ we obtain about 150 bound states and the ground state energy of -0.0969. This calculated ground state energy is not reliable as it is higher than even the upper bound of -0.1199 estimated variationally earlier [57]. In order to improve the ground state energy, we

introduce an additional decaying parameter in the basis functions, and optimize the energy levels for a certain value of this parameter. With the decaying parameter we obtain the best variational estimate for the ground state energy of -0.1257 for $N_{\text{basis}} = 400$.

We show the first twenty eigenvalues obtained from different methods in Fig. 2-2 and the first five representative eigenvalues in Table 2-2. As seen earlier, the real space diagonalization methods provide a better estimate of the ground state energy whereas the Coulomb basis method is more suitable for higher excited states. The eigenvalues of both the Coulomb basis method and the real space diagonalization methods are found to match each other for excited states, and then they begin to deviate again (see Fig. 2-2). This can be understood by the fact that the extent of wave functions of the 2D edge dislocation potential does not always increase as one goes to higher excited states – the wave functions of some excited states extend less than those of lower energy. Therefore, there are intermediate bound states that are missed in the real space calculation because the size of grid used in calculation is not large enough to capture them. For example, we find four more bound states with the Coulomb basis calculation between the 18^{th} and 19^{th} excited states as calculated from the real space diagonalization method. This feature also explains the abrupt increase of the eigenvalue of the 19^{th} state calculated by using the Arnoldi-Lanczos method (ARPACK routine) in Fig. 2-2.

2.4.6 Semiclassical Analysis

It is usually insightful to consider the semiclassical solution of a quantum mechanics problem, since the higher energy eigenstates tend to approach classical behavior. A semiclassical estimate of the energy spectrum has been provided in Ref. [68]. Here the total number of eigenstates up to a value of energy E is proportional to the volume occupied by the system in the classical phase space. This is expressed by Weyl's

theorem [69] :

$$n(E) = \frac{A}{4\pi}\frac{2m|E|}{\hbar^2} + \mathcal{O}\left(\sqrt{\frac{\hbar^2}{2mp^2}|E|}\right), \tag{2–39}$$

where A is the classically accessible area in real space and $|E|$ the absolute value of energy of the state. The higher order corrections can be shown to be less important for higher excited states, which is where the semiclassical picture applies. To find A, we need the classical turning points for this potential determined by setting $E = V(r, \theta)$. Then the accessible area is the interior of a circle given by $(x - \frac{p}{2E})^2 + y^2 = (\frac{p}{2E})^2$, with area $A = \pi(p/2E)^2$. Therefore, we obtain (writing the nondimensionalized energy in our system of units as ϵ):

$$n(\epsilon) = -\frac{1}{16\epsilon}, \tag{2–40}$$

where n is the quantum number of the eigenstate and ϵ the corresponding energy. Note that the density of states $dn/d\epsilon$ scales as $1/\epsilon^2$.

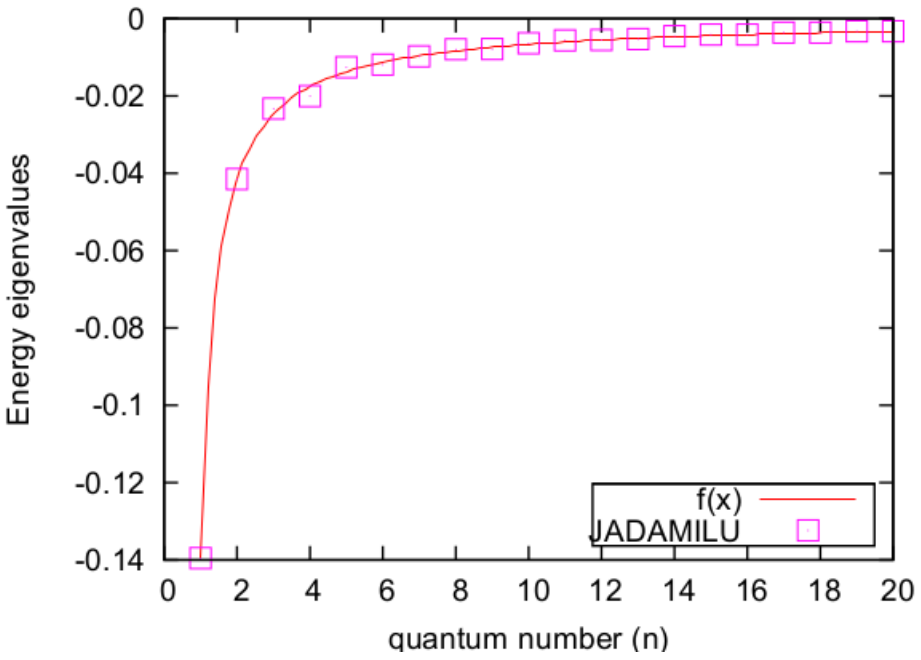

Figure 2-3. Fit for the eigenvalue spectrum of 2D quantum dipole potential obtained from JADAMILU using $f(x) = a(x - b)^c$. Fit values are -0.06, 0.61 and 0.96 for a, b and c respectively. Reprinted with permission from Ref. [79] [K. Dasbiswas, D. Goswami, C.-D. Yoo and A. T. Dorsey, Phys. Rev. B **81**, 64516 (2010).], ©APS, 2010

To check this result we fit the numerical spectrum with the following functional form:

$$\epsilon(n) = a(n-b)^c, \tag{2–41}$$

with the fitting parameters having values $a = -0.06, b = 0.5, c = -0.98$, each correct to within 5%. (Since we are dealing with bound states here, all the energy eigenvalues are negative, and the higher excited states have lower absolute eigenvalues.) We show the fit to the spectrum obtained from JADAMILU routine in Fig. 2-3. The semiclassically derived dependence is found to closely match with the fit for numerically calculated energy eigenstates, except for the $b = 0.5$ factor. In the limit of large n values i.e. higher excited states, the fit relation tends to the semiclassical result as expected.

The classical trajectories for this potential bear the signature of chaotic dynamics showing space-filling nature and strong dependence on initial conditions. However, for reasons not yet clear to us, they are not ergodic, filling up only a wedge-shaped region in real space instead of the full classically allowed circle. The quantum mechanical probability density as calculated from the eigenfunctions also exhibits such wedge-shaped regions. Some sample wavefunctions obtained from our numerical calculations have been presented. Figure. 2-4 shows the lowest five eigenstates and Fig. 2-5 shows some higher excited states. As expected, the wavefunctions are confined to the left half plane, where the potential is negative and bound states are possible. The parity of the potential shows up in the wavefunctions being either symmetric or antisymmetric about the x-axis, although states of such “odd” and “even” parity do not always alternate. For example, the 2nd and 4th excited states are “odd”, and the 3rd excited state correspondingly “even”, but the ground state and 1st excited states are both “even”. Similarly the 10th, 50th and 100th excited states are all “odd” while the 23rd and 24th are “odd”. The spatial extent of the wavefunctions is seen to be generally higher for higher excited states, but this is not always the case. The extent does not scale monotonically with quantum number. Some cases are found where a higher excited state has less spatial

extent than a lower one. For example we see in Fig. 2-5, that the 24th excited state is less extended in the x-direction compared to the 23rd. We do not have any satisfactory explanation yet for these irregular features.

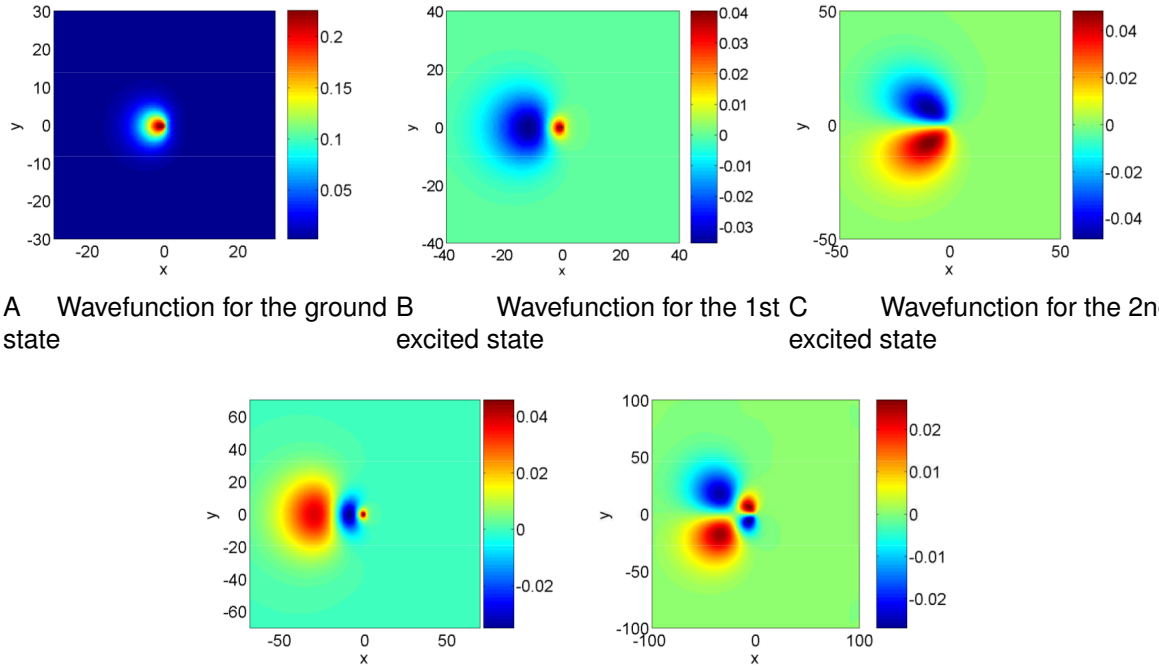

Figure 2-4. Eigenfunctions of the first five states of the 2D quantum dipole problem. For clarity of presentation, the range of the x and y axes have been increased for the higher excited states. Reprinted with permission from Ref. [79] [K. Dasbiswas, D. Goswami, C.-D. Yoo and A. T. Dorsey, Phys. Rev. B **81**, 64516 (2010)], ©APS, 2010

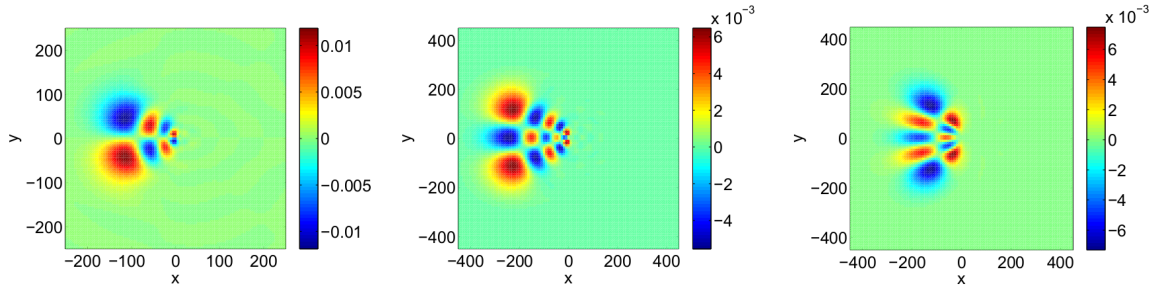

A Wavefunction for the 10th excited state B Wavefunction for the 23rd excited state C Wavefunction for the 24th excited state

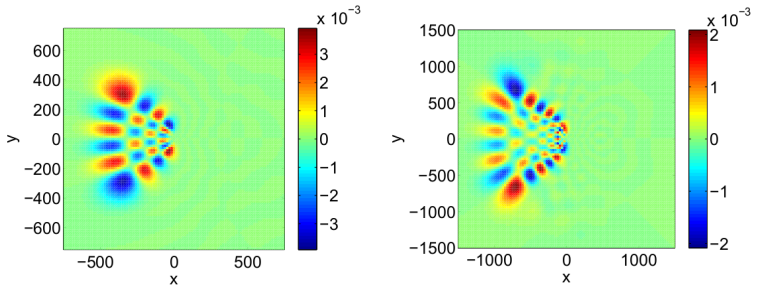

D Wavefunction for the 50th excited state E Wavefunction for the 100th excited state

Figure 2-5. Eigenfunctions of five higher excited states of the 2D quantum dipole problem. For clarity of presentation, the range of the x and y axes have been increased for the higher excited states. Reprinted with permission from Ref. [79] [K. Dasbiswas, D. Goswami, C.-D. Yoo and A. T. Dorsey, Phys. Rev. B **81**, 64516 (2010)], ©APS, 2010.

CHAPTER 3
SUPERFLUIDITY IN THE PRESENCE OF MULTIPLE DISLOCATIONS

In Chapter 2, we considered the superfluidity induced by a single, quenched, dislocation line by coupling the elastic strains induced by it to the superfluid order parameter. However a real crystal prepared in the laboratory is likely to contain grain boundaries (which can be thought of as regular arrays of dislocations), or a tangled network of dislocation lines. In this chapter, we follow a similar approach to derive the Landau theoretic model for superfluidity in dislocation arrays and networks by considering the overlap between superfluid regions induced by each dislocation line and find their effect on superfluid critical temperature T_c. This superfluid ordering in grain boundaries or networks are quasi long range (in 2D) and long range (in 3D) respectively, and thus have the thermodynamic characteristics of a phase transition, unlike the local 1D superfluid ordering induced by a single dislocation. The network model, we argue, could also be responsible for some of the anomalous effects seen in torsion oscillator experiments in solid ^{4}He. Further questions that could be addressed are the effects of the elastic interactions between dislocation lines on the superfluidity, and also of their motion.

3.1 Grain Boundary Superfluidity

A grain boundary is an interface between two regions of different crystal orientation in a polycrystal [50, 70, 71], where the atoms are locally disordered because of the competing effects of neighboring crystalline regions. Theoretical studies, both Quantum Monte Carlo methods [72] and Landau theoretic models [73], indicate that superfluidity can be locally induced in a defect structure such as a grain boundary. Also, there is some experimental evidence for mass superflow through grain boundaries in solid ^{4}He [31]. A low angle grain boundary can be interpreted as a surface containing a sequence of dislocations [50, 74]. In particular, a low angle tilt grain boundary is a periodic array of edge dislocations [see Fig. 3-1], and we have shown in Chapter 2 that each such

dislocation is capable of locally inducing superfluidity around itself. These local regions of superfluidity can overlap forming 2D superfluid order in the grain boundary. This superfluidity would be anisotropic, with differing properties along the dislocation lines and transverse to them. The superfluid coupling between neighboring dislocation lines and consequently, the critical temperature (T_c) would depend sensitively on the spacing between them. The Mermin-Wagner theorem [75] forbids the presence of long-range

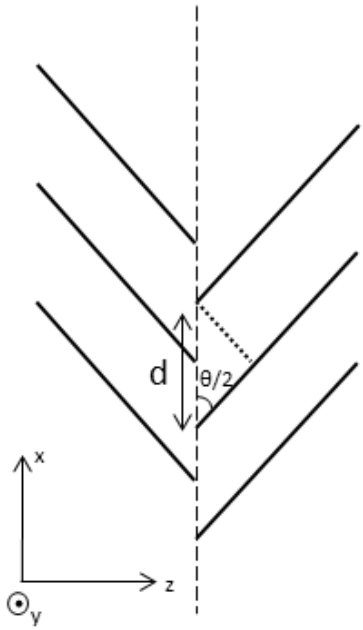

Figure 3-1. A symmetric tilt grain boundary showing the crystal planes. Each half plane on the left can be considered to be an extra half plane inserted between two half planes on the right, thus giving rise to an array of straight dislocation lines each of which point along the y-axis. The spacing between dislocations lines is d and the grain boundary angle is θ.

order in a 2D system because of the large role played by fluctuations, but quasi-ordering can result from the Berezinskii-Kosterlitz-Thouless (BKT) mechanism [17, 18]. In a BKT superfluid, vortices and antivortices are bound into ordered pairs. This order can be lost above a certain critical temperature when these vortex-antivortex pairs dissociate. In the rest of this section we discuss this anisotropic grain boundary superfluidity and address some of its BKT properties.

Consider a tilt grain boundary with angle of tilt θ and spacing d between the neighboring dislocations that make up this grain boundary[see Fig. 3-1]. Let the dislocation lines be oriented along the y direction and a series of them placed distance d apart (in units of lattice spacing) along the x-axis. The grain boundary interface is then just the $x-y$ plane. The Burger's vector of each dislocation is perpendicular to this plane, $\mathbf{b} \parallel x$. It follows from the geometry of the system that these quantities are related as

$$d = \frac{b}{2\sin(\theta/2)}, \tag{3–1}$$

where b is the Burger's vector of each dislocation line. This is called the Frank formula in metallurgy literature [50]. In the limit of small angles, this becomes

$$d \simeq \frac{b}{\theta}. \tag{3–2}$$

The Landau theory for grain boundary superfluidity in an isotropic solid proceeds in the same way as for a single dislocation introduced in Chapter 2,

$$F = \int d^3x \left[\frac{c}{2}|\nabla\psi|^2 + \frac{1}{2}a(\mathbf{x})|\psi|^2 + \frac{1}{4}u|\psi|^4\right], \tag{3–3}$$

where the superfluidity couples to the crystallinity through the trace of the grain boundary strain tensor, $a(\mathbf{x}) = a_0(T - T_0)/T_0 + a_1 u_{ii}(x, z)$. As in the case of the single dislocation, the grain boundary strains can locally enhance the superfluid critical temperature (T_c), the change in T_c being related to the ground state eigenvalue of the corresponding linear problem.

The stress from a grain boundary can be calculated by considering it as a sum of the stresses generated by each individual dislocation in the periodic array [1] :

$$\sigma_{xz}(x,z) = bBx \sum_{n=-\infty}^{\infty} \frac{z^2-(x-nd)^2}{[z^2+(x-nd)^2]^2}. \tag{3–4}$$

This may be written in the convenient form,

$$\sigma_{xz}(x,z) = -bB\frac{\alpha}{d}\left[J(\alpha,\beta)+\alpha\frac{\partial J(\alpha,\beta)}{\partial\alpha}\right], \tag{3–5}$$

where $J(\alpha,\beta) = \sum_{n=-\infty}^{\infty} \frac{1}{\alpha^2+(\beta-n)^2}$, $\alpha = z/d$ and $\beta = x/d$ are the nondimensional distances in the z and x- directions respectively. Using the Poisson summation formula,

$$\sum_{n=-\infty}^{\infty} f(n) = \sum_{k=-\infty}^{\infty} \int_{-\infty}^{\infty} dx\, f(x) e^{2\pi i k x},$$

we find

$$\begin{aligned} J(\alpha,\beta) &= \int_{-\infty}^{\infty} \frac{d\xi}{\alpha^2+\xi^2} + 2Re\sum_{k=1}^{\infty} e^{2\pi i k\beta} \int_{-\infty}^{\infty} d\xi \frac{e^{2\pi i k\xi}}{\alpha^2+\xi^2} \\ &= \frac{\pi}{\alpha} + \sum_{k=1}^{\infty} e^{-2\pi k\alpha}\cos(2\pi k\beta). \end{aligned} \tag{3–6}$$

The stress far away from the plane of the grain boundary is obtained by setting $\alpha >> 1$ in the above expression. In that case, only the first term of the sum would matter, and the resultant "far-field" stress is of the simplified form

$$\sigma_{xz}(x,z) = 4\pi^2 B\frac{bz}{d^2} e^{-2\pi z/d}\cos(2\pi x/d). \tag{3–7}$$

This stress is periodic in the x-direction as expected. The crystal is more stressed for a higher angle grain boundary, where the dislocations are placed closer together. Far away from the plane of the grain boundary, the stress decays exponentially with

[1] The subsequent derivation is provided in Chapter 4 of the text *Theory of Elasticity* by L. D. Landau and E. M. Lifshitz [74].

distance along the z-direction. This implies that although the stress fields from individual dislocations are long range (decay as a power law), there are cancellations from the different dislocations of the periodic array, thus leading to a short range form of the stress (or strain) field. The other stress components can be found similarly by summing over the respective dislocation stress components using the property of Poisson summation. Particularly, the trace of the far-field stress tensor (which couples to the superfluidity in our Landau theoretic framework) is

$$\sigma_{ii} = -2\pi B \frac{b}{d} e^{-2\pi z/d} \sin(2\pi x/d). \tag{3–8}$$

The linearized Landau equation can now be written in a nondimensionalized form as

$$-\nabla^2 \psi + [V_{gb}(x, z) - E]\,\psi = 0, \tag{3–9}$$

where E is proportional to the reduced temperature, and V_{gb} is a nondimensional potential corresponding to the trace of the grain boundary strain field [proportional to the hydrostatic stress found in Eq. (3–8)]. We can now see that the separation *Ansatz* used for the dislocation superfluidity problem cannot be simply carried over to the grain boundary situation. The "fast" degree of freedom of the order parameter is the z-direction, transverse to the grain boundary. If the z direction is separated out from the order parameter amplitude, we are left with an order parameter dependent on x and y. The eigenfunction of the linear problem Eq. (3–9) is however a function of x and z and cannot be used to "integrate out" the fast degree as was done for dislocations. The grain boundary strain field takes a simple form far away from the boundary, but we are interested in the order parameter in the plane of the grain boundary. The linear equation Eq. (3–9) is not analytically tractable in that plane because of the complicated form of the potential. We therefore analyze this problem approximately in two different limits, where the coherence length is much bigger (smaller) than the dislocation separation : $\xi \gg d$ ($\xi \ll d$). In the former case, we expect the superfluid regions from neighboring

dislocations to overlap strongly. The order parameter will then have a large uniform background piece with small amplitude corrugation on top of it. In the latter case the overlap will be exponentially small. We give some heuristic arguments to obtain the dependence of the T_c on the grain boundary angle in each case.

We first analyze the case of long coherence lengths following the work of Gurevich and Pashitskii [73]. The strain field, order parameter and all physical quantities are periodic in the x-direction because of the way the constituent dislocations are placed. In this limit of strong overlap between neighboring dislocations, the order parameter has a large constant piece along the grain boundary and rapid but small fluctuations about this average. We can thus decompose the order parameter into "slow" and "fast" parts as

$$\psi(x,z) = \psi_0(z) + \psi_1(x,z), \tag{3–10}$$

where $\psi_0(x) = \langle \psi(x,z) \rangle_x$. Here $\langle\ \rangle_x$ indicates averaging over a period d in the x-direction (the direction of periodicity), i. e. $\langle A(x,z) \rangle_x = \frac{1}{d}\int_0^d dx A(x,z)$. We separate Eq. (3–9) using a standard technique developed for rapidly oscillating systems [76]. First we consider only the quantities up to leading order on both sides of Eq.(3–9). In the limit we are considering, the gradients of $\psi_1(x,z)$ are much bigger than that of $\psi_0(z)$, although the amplitude of $\psi_1(x,z)$ is much smaller than that of $\psi_0(z)$. Therefore,

$$\nabla^2 \psi_1 = V_{gb}\psi_0. \tag{3–11}$$

Now we average over the rapidly oscillating degree of freedom, i.e. the $x-$ coordinate to get

$$-\nabla^2\psi_0 - E\psi_0 + \langle V_{gb}\psi_1 \rangle_x = 0. \tag{3–12}$$

In order to obtain this result we have used $\langle V_{gb} \rangle_x = \langle \psi_1 \rangle_x = 0$, which is due to the potential and corrugation on the order parameter being both sinusoidally oscillating functions in the $x-$ direction. The corrugation term can be expressed explicitly in terms

of the potential by Fourier transforming Eq.(3–11), which yields

$$\psi_1(k, G) = \frac{V_{gb}(k, G)\psi_0}{k^2 + G^2}, \tag{3–13}$$

where the (inverse) Fourier transform of the potential is defined as

$$V_{gb}(x, y) = \sum_{G\neq 0} \int_{-\infty}^{\infty} \frac{dk}{2\pi} V_{gb}(k, G) e^{ikx+iGy}. \tag{3–14}$$

The function is periodic in the x-direction and so is represented as a Fourier series over the reciprocal lattice vectors, $G = 2\pi n/d$, and $n = .., -2, -1, 1, 2, ...$ For a symmetric grain boundary, the term with $G = 0$ is absent because each dislocation causes a dipole strain field which has zero average along the x-direction. We have shown previously that at distances far away from the grain boundary compared to the dislocation spacing d, the stresses decay exponentially. The order parameter $\psi_1(x, z)$ is also expected to decrease rapidly with distance transverse to the grain boundary. In the limit of small spacing $d \ll \xi$ we are considering, the function $\tilde{V(z)} = \langle V_{gb}\psi_1 \rangle_x$ describes a short range potential well, $\tilde{V(z)} = V_0\delta(z)$. Integrating over z and using the Fourier transformed expression for $V_{gb}(x, z)$, we obtain

$$V_0 = \sum_{G\neq 0} \int_{-\infty}^{\infty} \frac{dk}{2\pi} \frac{|V_{gb}(k, G)|^2}{k^2 + G^2}. \tag{3–15}$$

The linearized Landau equation for the large, “slow” piece of the order parameter, Eq. (3–12), then reduces to a 1D Schrödinger equation for a particle in a “delta” potential well:

$$-[\nabla^2 + V_0\delta(z)]\psi_0 = E\psi_0. \tag{3–16}$$

The groundstate eigenvalue of this problem, $E_0 = V_0^2/4$, is related to the shift in the T_c of the superfluidity in the grain boundary. We can derive the dependence of this shift in T_c on the grain boundary angle (or dislocation spacing) with a simple scaling analysis at this point. This is the essential point of this section. The grain boundary potential is the trace of the strain tensor and varies with dislocation spacing as $b/d \sim \theta$. On calculating

its Fourier transform and using the expression in Eq.(3–15), we find (after scaling out the dependence on d) that $V_0 \sim d$. The shift in T_c goes as the square of V_0 (as known from the ground state eigenvalue) and therefore as an inverse square power law in the grain boundary angle. From dimensional considerations, we have derived the relative increase in T_c as

$$\frac{\Delta T_c}{T_c} = \left(\frac{\theta_e}{\theta}\right)^2, \tag{3–17}$$

where θ_e is some characteristic angle depending on the elastic properties of the crystal under consideration.

For the limit where dislocation spacing is larger than superfluid coherence length, we have a situation of weak overlap, and the T_c for grain boundary superfluidity is proportional to the Josephson superfluid coupling between neighboring dislocations, and is exponentially sensitive on the spacing, $T_c \sim e^{-d/b} \sim e^{-1/\theta}$. Thus we uncover the separate power law and exponential dependence of the critical temperature on the grain boundary angle in different limits. We presume the latter is likelier in the case of solid helium, because the coherence lengths are known to be about as small as the atomic spacing (a few Angstroms) in superfluid helium. The former situation analyzed by Gurevich and Pashitskii [73] could be found for example in superconductors with grain boundaries.

3.2 Berezinskii-Kosterlitz-Thouless Superfluid in a Grain Boundary

As mentioned earlier, the superfluidity in a 2D system like a grain boundary can arise through the vortex-binding BKT mechanism. In this Section, we discuss some of the BKT properties of the grain boundary induced superfluid described above, especially focusing on how these properties are affected by the inherent anisotropy of the grain

boundary. To understand the BKT argument, we first need to understand the basic properties of a vortex and calculate its energy[2] .

Vortices are ubiquitous topological defects found in 2D systems with continuously broken U(1) symmetry, that are best described as singularities in the phase of the order parameter. It is often useful to think of them as analogous to point charges in electrodynamics problems. Consider, for example, an XY spin model in 2D, which belongs to the same U(1) universality class as a superfluid. A simple *Ansatz* for the phase in a 2D system with a single vortex located at the origin of coordinates is

$$\theta_v = e_v \phi, \tag{3–18}$$

where e_v is an integer called the "winding number" or "charge" of the vortex, and r and ϕ are the polar coordinates in 2D. The long wavelength or elastic energy of the vortex is then given by

$$E_{el} = \frac{1}{2}\rho_s \int d^2x \left(\nabla\theta_v\right)^2 = \frac{1}{2}\rho_s (2\pi)(e_v)^2 \int \frac{rdr}{r^2} = \pi (e_v)^2 \rho_s \ln(R/a), \tag{3–19}$$

where a is the core radius of the vortex. and R the system size. In addition there is an energy cost E_c associated with the core of the vortex. The superfluid phase stiffness ρ_s is usually identified with the square of the amplitude of the order parameter, but can be "renormalized" by fluctuations of this amplitude, as introduced for example by vortices.

A simple heuristic argument first given by Kosterlitz and Thouless [18] shows how vortices can lead to a second-order phase transition in the XY model. The energy of a singly charged vortex in sample of linear dimension R, as calculated in Eq. (3–19), is $\pi\rho_s \ln(R/a)$. The vortex core could lie anywhere in the sample, and so carries an entropy proportional to the area, $\ln(R/a)^2$. The free energy of an XY-system with a single vortex

[2] Most of the development in this section closely follows Section 9.4 in the text *Principles of Condensed Matter Physics* by P. M. Chaikin and T. C. Lubensky [70]

is then

$$F = E - TS = (\pi\rho_s - 2T)\ln(R/a). \tag{3–20}$$

Thus it is reasonable to identify

$$T_c = \frac{\pi}{2}\rho_s, \tag{3–21}$$

with the critical temperature above which it becomes energetically favorable to have a free vortex. A more detailed analysis shows that there exists an algebraically (quasi long-ranged) ordered phase below such a T_c in which the vortices are bound into pairs with their antivortices. The spin wave stiffness of the XY model, ρ_s, is modified by the presence of the vortices, and this changes the T_c from the "bare" form derived here.

Vortices are mobile degrees of freedom that arrange themselves so as to minimize the free energy of any imposed gradient of the phase of the order parameter. The macroscopic spin wave stiffness, ρ_s^R, is renormalized by vortex fluctuations. It is expressed as the difference in free energy between the system with and without an externally imposed "flow velocity":

$$F(\mathbf{v}) - F(0) = \frac{1}{2}V\rho_s^R\mathbf{v}^2. \tag{3–22}$$

Here $v_s = \nabla\theta(\mathbf{x})$ is the uniform gradient of the phase of the XY model, to be identified with the superfluid velocity after incorporating a suitably dimensionful factor of h/m. V is the total volume of the system. The free energy is found by statistically averaging the Hamiltonian over phase fluctuations (in the following treatment we take the Boltzmann factor $k_B = 1$),

$$F(\mathbf{v}) = -T\ln \mathrm{Tr}\exp\big[-H(\mathbf{v})/T\big], \tag{3–23}$$

where the Hamiltonian for low energy phase fluctuations is given by

$$H(\mathbf{v}) = \frac{1}{2}\rho_s\int d^2x\big(\nabla\theta\big)^2. \tag{3–24}$$

The phase $\theta(\mathbf{v})$ in the above relations can be decomposed into a singular, transverse part from the vortex, an analytic, longitudinal and spin-wave part, and a constant piece corresponding to the uniform gradient or velocity:

$$\nabla\theta = \mathbf{v}_s^{\perp} + \mathbf{v}_s^{||} + \mathbf{v}. \tag{3–25}$$

After expanding in the uniform gradient to quadratic order and averaging over the fluctuations, we obtain an expression for the renormalized stiffness in terms of the bare stiffness and a correlation function of transverse velocities (associated with the vortices),

$$\rho_s^R = \rho_s - \frac{\rho_s^2}{T}\int d^2x \langle \mathbf{v}_s^{\perp}(\mathbf{x}).\mathbf{v}_s^{\perp}(0)\rangle. \tag{3–26}$$

Using standard relations for vortex velocities and source functions, and the energy of a system of dilute vortices at low temperature, it can be shown that the renormalized stiffness (see appendix for derivation) is related to the bare stiffness and vortex fugacity $f = e^{-E_c/T}$ as

$$K_R^{-1} = K^{-1} + 4\pi^3 f^2 \int_a^{\infty} \frac{dr}{a}\left(\frac{r}{a}\right)^{(3-2\pi K)}. \tag{3–27}$$

The notation in this equation has been made simpler by defining a reduced spin stiffness, $K = \rho/T$. By simple power counting, the above integral converges when $(3 - 2\pi K) < -1$, i.e. at temperatures lower than $T_c = \frac{\pi}{2}\rho_s(T_c)$. When the temperature is higher than this self-consistently determined T_c, the integral diverges for large r, and the perturbation theory in fugacity breaks down. The difficulty associated with the divergence can be handled through a renormalization procedure [77]. Instead of going into the details of this real space renormalization procedure, we mention some of the key results of this renormalized XY model in 2D. Below the T_c which is the fixed point of the RG flow, the fugacity is found to be irrelevant, which qualitatively implies that there are no free vortices. Any vortices present are bound into pairs, and so their presence is not felt as one "coarsens" the scale. Above T_C, the fugacity "flows" towards higher values implying the existence of free vortices. These conclusions are consistent with

the expression for the energy of a system of dilute, interacting vortices: the energy of a free vortex actually diverges with system size. So at low temperatures, it is energetically favorable to have only bound vortex pairs with total charge, $\sum e_v = 0$.

Modifications for an anisotropic theory. We have remarked before that the 2D grain boundary superfluid is expected to be anisotropic, as the phase stiffness along the dislocation lines, the y-direction, is expected to be stronger than the coupling transverse to them (the x-direction). The situation can be described by an anisotropic XY model with different phase stiffness values along x and y. The Hamiltonian for the low energy phase fluctuations of such a model is

$$\mathcal{H} = \frac{1}{2}\rho_x(\partial_x\theta)^2 + \frac{1}{2}\rho_y(\partial_y\theta)^2. \tag{3–28}$$

The ratio of the phase stiffnesses should vary with the grain boundary angle as, $\rho_x \sim \rho_y e^{-\frac{1}{\theta}}$. Following the same analysis as in the isotropic case, the renormalized stiffnesses are found to have forms similar to Eq. (3–26).

$$\begin{aligned} \rho_x^R &= \rho_x - \frac{\rho_x^2}{T}\int d^2x \langle v_x^\perp(\mathbf{x}).v_x^\perp(0)\rangle, \\ \rho_y^R &= \rho_y - \frac{\rho_y^2}{T}\int d^2x \langle v_y^\perp(\mathbf{x}).v_y^\perp(0)\rangle. \end{aligned} \tag{3–29}$$

Using an expression for the transverse velocity in terms of the vortex source function $\mathbf{m}(\mathbf{x})$,

$$\mathbf{v}^\perp(\mathbf{x}) = \nabla \times \int d^2x\, G(\mathbf{x}-\mathbf{x}')\mathbf{m}(\mathbf{x}), \tag{3–30}$$

the expression for renormalized stiffness as given in Eq. (3–29) yield,

$$\begin{aligned} \rho_x^R &= \rho_x - (2\pi)^2\frac{\rho_x^2}{2T}\int d^2x\, y^2\langle n(\mathbf{x})n(0)\rangle, \\ \rho_y^R &= \rho_y - (2\pi)^2\frac{\rho_y^2}{2T}\int d^2x\, x^2\langle n(\mathbf{x})n(0)\rangle. \end{aligned} \tag{3–31}$$

The anisotropy is dealt with by rescaling the length scales to render the problem isotropic. It is useful to define the following quantities: an effective stiffness $\rho_e \equiv \sqrt{\rho_x\rho_y}$

and an anisotropy factor $\zeta = \sqrt{\rho_x/\rho_y}$. The rescaled radial polar coordinate is then $R = \sqrt{x^2 + \zeta^2 y^2}$. The correlation function for vortex densities for a small fugacity (low temperature) can be derived by statistically averaging over the Hamiltonian for a dilute gas of interacting vortices, in the same way as Eq.(3–27), giving

$$\begin{aligned} K_x^R &= K_x - 4\pi^3 f^2 \frac{K_e^2}{2T} \int \frac{dR}{a} \left(\frac{R}{a}\right)^{3-2\pi K_e}, \\ K_y^R &= K_y - 4\pi^3 f^2 \frac{K_e^2}{2T} \int \frac{dR}{a} \left(\frac{R}{a}\right)^{3-2\pi K_e}. \end{aligned} \tag{3–32}$$

K is as usual a quantity defined to denote the stiffness divided by temperature, to make the notation in the RG procedure simpler. The $x-$ and $y-$ equations in Eq.(3–32) can be combined as a single equation for the effective stiffness K_e by multiplying and expanding upto quadratic order in the fugacity.

$$(K_e^R)^{-1} = (K_e)^{-1} + 4\pi^3 f^2 \frac{K_e^2}{2T} \int_a^\infty \frac{dR}{a} \left(\frac{R}{a}\right)^{3-2\pi K_e} + \mathcal{O}(f^4). \tag{3–33}$$

This is essentially the same renormalized stiffness as was obtained in Eq. (3–27) for the isotropic case. Similarly an equation for the renormalized anisotropy can be obtained from Eq. (3–32) as

$$\zeta^R = \sqrt{K_x^R (K_y^R)^{-1}} = \zeta + \mathcal{O}(f^4). \tag{3–34}$$

This shows that the anisotropy is irrelevant and the effective stiffness defined as the geometric mean of the two stiffnesses in the x- and y- directions is renormalized in exactly the same way as in the isotropic superfluid. So we do not expect any qualitative differences in the coarse-grained behavior of the anisotropic BKT superfluid in a grain boundary from an isotropic 2D superfluid.

3.3 Network of Dislocation Lines and a Model Supersolid

In Chapter 2, we considered a single edge dislocation, reducing the full three-dimensional Landau theory to an effective one-dimensional theory for a superfluid tube localized near the dislocation core. Then, in the preceding section, we considered a grain boundary which can be thought of as a regular array of dislocations. However, real crystals including solid ^{4}He, will consist of a tangle of dislocations many of which will "cross" when they come within a transverse correlation length of each other. Conceptually, we can model this as a random lattice (or network) of dislocations with the crossing points serving as lattice sites as illustrated in Fig. 3-2. While thermal fluctuations destroy any long range order in a single, one-dimensional tube, the lattice of tubes will generally order at a temperature characteristic of the phase stiffness between adjacent lattice sites of this random network of intersecting dislocation lines. This is the motivation behind the models developed by Shevchenko [80] and Toner [78]. In this Section we revisit the Shevchenko and Toner models with a systematic approach for calculating the coupling between adjacent lattice sites in the network model, and obtain new results on the length scaling of the coupling constant. We conclude with some observations regarding implications of our results for experiments on the putative supersolid phase of ^{4}He.

We start by considering the correlations between two points along a single superfluid tube, separated by a distance L. Using the notation of the previous section, $\varphi(0) = \varphi_1$ and $\varphi(L) = \varphi_2$ are the values of the superfluid order parameter at two sites along the tube. The correlations are captured by the propagator $K(\varphi_2, \varphi_1; L)$, which can

---

Parts of this section are reproduced from the published article: "D. Goswami, K. Dasbiswas, C.-D. Yoo and A. T. Dorsey, Phys. Rev. B **84**, 054523 (2011)."

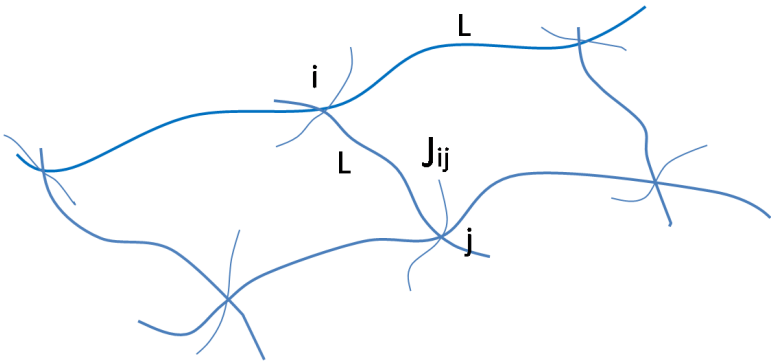

Figure 3-2. A tangled network of dislocation lines one is likely to find in a real crystal. In our picture, bulk superfluid order develops along this defect structure embedded in 3D. The average spacing between the nodes or lattice points in this network is L, and the XY model like exchange coupling between the superfluid order between the ith and jth nodes is J_{ij}.

be obtained from the functional integral

$$K(\varphi_2,\varphi_1;L)=\exp(-\beta H_{\text{eff}})=\int_{\varphi(0)=\varphi_1}^{\varphi(L)=\varphi_2}\mathcal{D}(\varphi,\varphi^*)\exp\left\{-\beta\int_0^L dz\left[\frac{c}{2}|\partial_z\varphi|^2+\frac{a}{2}|\varphi|^2+\frac{b}{4}|\varphi|^4\right]\right\}, \tag{3–35}$$

where a, b and c are the parameters of the one-dimensional Landau theory derived in the previous section, and H_{eff} is the effective Hamiltonian that characterizes the coupling between the lattice sites. Cast in this form, we see that the functional integral for the classical one-dimensional system is equivalent to the Feynman path integral for a quantum particle in a two-dimensional quartic potential (two-dimensional because the order parameter φ is complex), with z in the classical problem replaced by the imaginary time τ for the quantum system [86]. Indeed, previous authors have used this analogy to study the effect of thermal fluctuations on the resistive transition in one-dimensional superconductors [87, 88], obtaining essentially exact results for the correlation length and thermodynamic properties. Consistent with the Mermin-Wagner theorem [75], these authors find no singularities in the thermodynamic properties, and a one-dimensional correlation length that grows as the temperature is reduced, but never diverges [88]. Most of these results are conveniently captured using a simple Hartree approximation [89], in which the quartic term is absorbed into the quadratic term with the quadratic

coefficient redefined as

$$\bar{a} = a + \frac{1}{2} b \langle |\varphi|^2 \rangle, \tag{3–36}$$

where $a = a_0(T - T_{\text{cond}})/T_{\text{cond}}$ and $\langle |\varphi|^2 \rangle$ a statistical average with respect to the effective quadratic theory. Carrying out the averaging, we obtain [89]

$$\langle |\varphi|^2 \rangle = \frac{k_B T}{c \xi_\perp^2} \xi, \tag{3–37}$$

where $\xi = (c/\bar{a})^{1/2}$ is the correlation length for the one-dimensional system along the superfluid tube, and $\xi_\perp$ is the cross-sectional dimension of the 1D superfluid region (the transverse correlation length, as shown in Fig. 2-1 in Chapter 2). Inserting this result into the Hartree expression of Eq. (3–36), we obtain a cubic equation for the correlation length as

$$\frac{1}{\xi^2} = \frac{1}{\xi_0^2} + \left(\frac{k_B T b}{2 c^2 \xi_\perp^2} \right) \xi, \tag{3–38}$$

where $\xi_0 = (c/a)^{1/2}$ is the Gaussian correlation length. While the mean-field correlation length ξ_0 diverges at T_{cond}, the "Hartree" correlation length ξ remains finite at all temperatures [88] [see Fig. 3-3], reflecting the lack of long-range order in the one-dimensional superfluid tube.

Continuing with the Hartree approximation, we can find the explicit form of the propagator by exploiting an analogy with the partition function for a two-dimensional quantum harmonic oscillator; the result is [86]

$$\begin{aligned} K(\varphi_2, \varphi_1; L) &= k(L) \exp \left\{ - \frac{\beta c}{2 \xi \sinh(L/\xi)} \right. \\ &\left. \left[(|\varphi_2|^2 + |\varphi_1|^2) \cosh(L/\xi) - 2 |\varphi_2| |\varphi_1| \cos(\theta_1 - \theta_2) \right] \right\}, \end{aligned} \tag{3–39}$$

where the prefactor $k(L) = \beta c / 2\pi \xi \sinh(L/\xi)$, and $\varphi_1 = |\varphi_1| e^{i\theta_1}$ and $\varphi_2 = |\varphi_2| e^{i\theta_2}$. The effective Hamiltonian (up to an additive constant) is given by

$$H_{\text{eff}} = \frac{c}{2\xi} \coth(L/\xi)(|\varphi_2|^2 + |\varphi_1|^2) - J_{12}(L) \cos(\theta_1 - \theta_2), \tag{3–40}$$

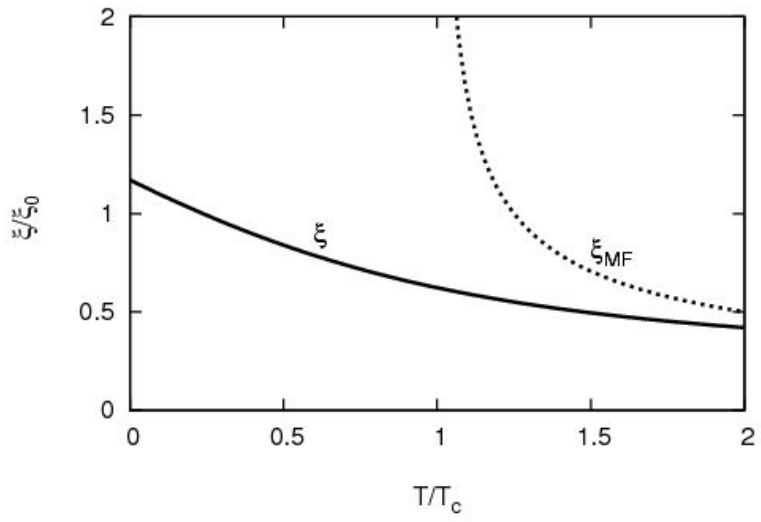

Figure 3-3. Dependence of Hartree and mean field correlation lengths on temperature: the ξ does not diverge at T_c unlike ξ_{MF}. The latter is obtained directly from the Landau theory while the former takes Gaussian fluctuations into account.

where

$$\begin{aligned} J_{12}(L) &= \frac{c|\varphi_2||\varphi_1|}{\xi \sinh(L/\xi)} \\ &= \begin{cases} c|\varphi_2||\varphi_1|/L, & L/\xi \ll 1; \\ (2c|\varphi_2||\varphi_1|/\xi)e^{-L/\xi}, & L/\xi \gg 1. \end{cases} \end{aligned} \tag{3–41}$$

The last term in Eq. (4–3) is the one of interest, as it couples the phases at the neighboring sites through an effective "ferromagnetic" coupling constant J_{12}. The behavior of J_{12} as a function of the inter-site separation L is one of our important results–for small L/ξ, $J_{12} \sim 1/L$, reproducing the result of Toner [78], whereas for large L/ξ, $J_{12} \sim e^{-L/\xi}$. Since ξ is finite for all T, for a sufficiently dilute network of dislocations we will always satisfy the latter condition–i.e., dilute networks of dislocations possess coupling constants exponentially small in the dislocation density. It might be reemphasized here that since true long range order is not possible in one-dimension,

the phase of the order parameter is also not well defined in one-dimension. Hence, a "phase only" approximation of the problem as shown by Toner [78] would be inadequate in capturing the complete behavior of the coupling constant and a complete order parameter description as shown here, in the spirit of the work by Scalapino *et al.* [88] is necessary. Toner's phase-only description would be valid when the correlation length ξ is larger than the dislocation network length scale L as then there would be phase ordering between neighboring lattice sites of the dislocation network, and it is in such a limit ($L \ll \xi$) that we recover a dependence similar to Toner's [see Eq. (3–41)].

So far we have systematically derived an effective Hamiltonian that describes the phase coupling between two points (lattice sites) on a single dislocation. To make the conceptual leap to the dislocation network, we propose that the appropriate model for the network is a random bond XY model of the form

$$H = -\sum_{\langle ij \rangle} J_{ij} \cos(\theta_i - \theta_j), \tag{3–42}$$

where $\langle ij \rangle$ represents nearest-neighbor lattice sites and J_{ij} is a (positive) coupling between the sites that scales as $e^{-L_{ij}/\xi}$ for a sufficiently dilute network of dislocations. As noted by Toner [78], the randomness is irrelevant in the renormalization-group sense [90], and in three dimensions we expect the superfluidity in the network to order when the temperature is of order the typical coupling strength $[J_{ij}]$; i.e., $k_B T_c = \mathcal{O}([J_{ij}])$. Again, for a dilute network of dislocations (with areal dislocation density $n \sim 1/L^2$), we would find $T_c \sim e^{-1/(n^{1/2}\xi)}$, a remarkably sensitive dependence on the dislocation density.

It is natural to ask here how well these theoretical findings relate with the recent torsional oscillator experiments on solid helium. The recent consensus from experimental studies, such as by Rittner and Reppy [25], is that the putative supersolid response depends on sample quality and preparation. According to these experiments, the NCRI fraction shows much more sensitive dependence on the sample quality (varying from as much as 20% for samples prepared by the blocked capillary method and thus

having more disorder to 0.5% for those prepared under constant pressure [26]) than the onset temperature itself, which shows no clear dependence on disorder. This seems to contradict the exponential dependence of T_c on dislocation density that we predict but we would like to point out that so far there have been no systematic studies characterizing samples of solid ^{4}He for their dislocation density, and relating this to the onset temperature of supersolid signal found in these samples. Ultrasound attenuation experiments on solid ^{4}He in the past [91, 92] have revealed dislocation densities ranging from 10^4-10^6 cm^{-2}. This means the density cannot be determined to even within an order of magnitude.

What makes relating our theory to experiment even more difficult is the fact that we cannot make quantitative predictions for the T_c from our theory. That would require knowledge of the Landau theory parameters for solid ^{4}He in order to be able to calculate the correlation length (ξ in Eq. (3–41)). These are not known for solid ^{4}He, unlike for example, in conventional superconductors, where the Landau parameters can be obtained through experiment by relating to the microscopic theory. This lack of certain knowledge of at least two variables in our theory (L and ξ) make any comparison with experiment inconclusive. It is also entirely possible, that while dislocation superfluidity is a real effect, there might be other factors at work behind the high NCRI fraction observed in disordered samples which tend to swamp out the sensitive dependence of T_c that our model for dislocation superfluidity predicts. Also our theory at present doesn't include dynamics (see Appendix C for a rudimentary discussion of dynamics) and cannot comment on experiments that study the rate of superflow, such as by Ray and Hallock [93]. However we believe that the model proposed above serves as a useful starting point to numerically simulate and understand some of these effects.

CHAPTER 4
VORTICES IN TRAPPED, DILUTE BOSE-EINSTEIN CONDENSATE

The generation of quantized vortices in gaseous samples has been the subject of much study [39] since the first observation of Bose-Einstein condensation in atomic gases. The degree of control and the ease with which vortices can be observed in a BEC in a trap make it an exciting alternative neutral superfluid system to liquid helium, where vortex creation and dynamics can be studied. In this chapter, we review some of the known results related to the stability and motion of a single vortex in a BEC in a trap, and sketch a derivation of the dynamics of a vortex in a rotating frame of reference from a hydrodynamics perspective. These results are ostensibly different from that of a vortex in liquid helium, because of the effect of a time-dependent potential (that rotates the trap), and the inhomogeneities of the confining potential.

4.1 Gross-Pitaevskii Formulation

The zero temperature properties of a dilute, interacting, Bose gas of ultracold atoms in a trap is described by the Gross-Pitaevskii (GP) equation [102]. Here we sketch a brief derivation of this GP formalism, followed by a discussion of some of its basic mathematical features. A collection of interacting (bosonic) atoms in a trap is characterized by its many body wave function. We employ a Hartree or mean field approach where this many body wave function is replaced by its statistically averaged mean field wavefunction, which can be written as a suitably symmetrized product of single-particle wavefunctions. A further simplification is achieved in the fully condensed state when all atoms occupy the same single-particle state, $\phi(\mathbf{r})$. Therefore the wavefunction of the N-particle system can be written as

$$\Psi(\mathbf{r}_1, \mathbf{r}_2, \ldots . \mathbf{r}_N) = \prod_{i=1}^{N} \phi(\mathbf{r}_i), \tag{4–1}$$

where the single-particle wavefunction is normalized as $\int d\mathbf{r}|\phi(\mathbf{r})|^2 = 1$. This wavefunction does not take into account correlations between single-particle particle

wavefunctions that are produced by their interactions. For the dilute gases of neutral alkali atoms we typically consider, the interacting forces are short range and can be taken into account by an effective interaction $g\delta(\mathbf{r}-\mathbf{r}')$ which includes the influence of short-wavelength degrees of freedom that have been integrated out. In fact for short range scattering, g is related to the scattering length a_s as [103]

$$g = \frac{4\pi\hbar^2 a_s}{m}. \tag{4–2}$$

The effective Hamiltonian may be written as

$$H = \sum_{i=1} N\big[\frac{p_i^2}{2m} + V_{tr}(\mathbf{r}_i)\big] + g\sum_{i<j}\delta(\mathbf{r}_i - \mathbf{r}_j), \tag{4–3}$$

$V_{tr}(\mathbf{r})$ being the external potential applied by a magneto-optic trap in actual experiments. The energy of the state in Eq. (4–1) is the expectation value of the Hamiltonian in Eq. (4–3), and is given by

$$E = N\int d\mathbf{r}\left[\frac{\hbar^2}{2m}|\nabla\phi(\mathbf{r})|^2 + V_{tr}(\mathbf{r})|\phi(\mathbf{r})|^2 + \frac{(N-1)}{2}g|\nabla\phi(\mathbf{r})|^4\right]. \tag{4–4}$$

The factor of $N(N-1)/2$ corresponds to the number of interacting pairs of particles. In the Hartree approximation above we suppose that all particles are in the ground state ϕ, but the correlations resulting from interactions of particles at small separations will result in some atoms being in excited states. The fraction of such atoms in the condensate can however be shown to be very small of the order of a_s/r_s, where a_s is the scattering length of the interaction, and r_s the average inter-particle separation (these are typically in nanometers and micrometers respectively in a dilute BEC). The condensate wave function, $\psi(\mathbf{r}) \equiv N^{1/2}\phi(\mathbf{r})$ is a convenient rescaling of the single-particle ground state wavefunction, related to the density of particles as

$$n(\mathbf{r}) = |\psi(\mathbf{r})|^2. \tag{4–5}$$

The GP energy functional of the dilute BEC can then be written in terms of the condensate wave function as

$$E[\psi] = \int d\mathbf{r}\left[\frac{\hbar^2}{2m}|\nabla\psi|^2 + V_{tr}(\mathbf{r})|\psi|^2 + \frac{1}{2}g|\psi|^4\right]. \tag{4–6}$$

The external trapping potential will typically be assumed to be that of a 3D spherical harmonic oscillator,

$$V(\mathbf{r}) = \frac{1}{2}m\omega^2 r^2. \tag{4–7}$$

To nondimensionalize Eq. (4–6), we choose the harmonic oscillator length scale obtained from the linear Schrödinger equation part of the problem as the appropriate length scale in the problem $l \equiv a_{ho} \equiv \sqrt{\frac{\hbar}{m\omega}}$, and wavefunction amplitude scale, $\chi \equiv \sqrt{\frac{\hbar\omega}{g}}$. Using the above to rescale only the length, the free energy functional is nondimensionalized as

$$E/E_0 = l^3\int d^3x\left[|\nabla\psi|^2 + r^2|\psi|^2 + \lambda|\psi|^4\right], \tag{4–8}$$

where the scale of free energy is $E_0 \equiv \frac{1}{2}\hbar\omega$. This is the fundamental energy scale in this problem, and is related to the ground state energy E_0 of the harmonic oscillator. In the units of E_0, the ground state energy is 3. The dimensionless parameter λ is a measure of the strength of the nonlinearity in the GP functional and its form can be derived from Eq. (4–2) as

$$\lambda \equiv \frac{g}{\hbar\omega} = \frac{Na_s}{a_{ho}}. \tag{4–9}$$

This form is particularly useful as it tells us whether we are in a regime of strong nonlinearity (large condensate wavefunction and density) or weak nonlinearity (small condensate wavefunction and density) in terms of experimentally known parameters: the particle number, the scattering length of the inter-atomic interaction and the harmonic trap length scale (related to its frequency). We apply accordingly a Thomas-Fermi or a perturbative approximation. Both these methods are discussed in subsequent sections. For completeness of the discussion, we now present the fully nondimensionalized GP

functional after scaling out the wavefunction amplitude as well as the length,

$$E/E_0 = l^3\chi^2 \int d^3x \left[|\nabla\psi|^2 + r^2|\psi|^2 + |\psi|^4 \right], \tag{4–10}$$

To get the equation of motion for the condensate we vary the above free energy with respect to ψ under the constraint that total number of atoms in the trap is fixed. This gives

$$\frac{\delta\mathcal{E}}{\delta\psi^*} = 0 = -\nabla^2\psi + [r^2 - \mu]\psi + |\psi|^2\psi, \tag{4–11}$$

where μ is the nondimensionalized chemical potential (in units of E_0) which serves as the Lagrange multiplier for this constraint.

4.1.1 "Weakly nonlinear" Analysis for Small Condensates

The GP Eq. (4–11) is mathematically similar to the Landau theory for second order phase transitions with chemical potential playing the role of temperature. When the chemical potential is close to the ground state energy, there are very few atoms in the trap, and we are in a low density limit. The cubic term in the GP equation is then small compared to the linear terms and can be treated perturbatively following the prescription of the weakly nonlinear analysis introduced in Chapter 2. To see this clearly, we introduce a control parameter

$$\epsilon \equiv \mu - \epsilon_0, \tag{4–12}$$

where μ is the chemical potential and ϵ_0 the ground state eigenvalue of the linear part of the problem, which is basically the Schrödinger equation for the trap potential, in this case a 3D isotropic harmonic oscillator. Now rescale the condensate wavefunction as,

$$\psi = \epsilon^{1/2}\phi. \tag{4–13}$$

The GP equation can then be recast in a form convenient for a perturbative analysis,

$$\hat{L}\phi = \epsilon\left[\phi - |\phi|^2\phi\right], \tag{4–14}$$

where the Hermitian linear operator $\hat{L}$ is given by

$$\hat{L} = -\nabla^2 + r^2 - E_0. \tag{4–15}$$

Next, we expand ϕ in powers of ϵ,

$$\phi = \phi_0 + \epsilon\phi_1 + \epsilon^2\phi_2 + \dots . \tag{4–16}$$

Collecting terms, we obtain the following hierarchy of equations:

$$\begin{aligned} \mathcal{O}(1): &\qquad \hat{L}\phi_0 = 0, \\ \mathcal{O}(\epsilon): &\qquad \hat{L}\phi_1 = \phi_0 - |\phi_0|^2\phi_0, \\ \mathcal{O}(\epsilon^2): &\qquad \hat{L}\phi_2 = (1 - 3\phi_0^2)\phi_1. \end{aligned} \tag{4–17}$$

The solution of the $\mathcal{O}(1)$ equation is the normalized ground state eigenfunction, $\Psi_0(\mathbf{r}) = 1/\pi^{\frac{3}{4}} e^{-r^2/2}$; there is an overall integration constant A_0, so that

$$\phi_0 = A_0\Psi_0(\mathbf{r}). \tag{4–18}$$

Substitute this into the right hand side of the $\mathcal{O}(\epsilon)$ equation,

$$\hat{L}\phi_1 = \Psi_0 A_0 - \Psi_0^3|A_0|^2 A_0. \tag{4–19}$$

We can determine A_0 by left multiplying this equation by Ψ_0, integrating on d^3r, and using the fact that $\hat{L}$ is Hermitian, to find

$$A_0 - \gamma|A_0|^2 A_0 = 0, \tag{4–20}$$

where the constant γ is given by

$$\gamma = \int d^3r\, \Psi_0^4(\mathrm{r}), \tag{4–21}$$

the integral of the normalized ground state wavefunction raised to the fourth power. Calculating for the harmonic oscillator wavefunction, we get $\gamma = 1/(2\pi)^{\frac{3}{2}}$. From

Eq. (4–19), $A_0 = 1/\sqrt{\gamma}$, and therefore $\phi_0 = 2^{3/4}e^{-r^2/2}$. The overall wave function is therefore

$$\psi(\mathbf{r}) = \epsilon^{1/2}2^{3/4}e^{-r^2/2} + \mathcal{O}(\epsilon^{3/2}). \tag{4–22}$$

The next higher order term requires the solution of an inhomogeneous differential equation. This result is expected to hold in the low density limit when μ is close to the ground state value of 3 (in our units). In this limit, the total number of particles up to the zeroeth order, is obtained by finding the normalization of the condensate wave function in Eq. (4–22) and putting the dimensionful length and amplitude scales back in,

$$N = (2\pi)^{3/2}(\mu - 3)\chi^2 l^3 = \sqrt{\frac{\pi}{2}}\epsilon\frac{a_{ho}}{a_s}. \tag{4–23}$$

Thus we identify an important experimental parameter $\lambda = \frac{Na_s}{a_{ho}}$ identical up to a multiplicative constant with the ϵ defined earlier as the shift in chemical potential, that has to be small ($\lambda \ll 1$) for the problem to be weak nonlinear, and the above perturbative analysis to hold.

4.1.2 Thomas Fermi Analysis

In the opposite limit of high density (quantitatively expressed as $\lambda \equiv Na_s/a_{ho} \gg 1$), the nonlinear term in the GP equation becomes significant and away from the edges of the trap it is the gradient term that can be neglected. The condensate wavefunction in this limit is

$$\psi(r) = \psi(0)\sqrt{\mu - r^2}, \tag{4–24}$$

where r is the radial distance from the center of the trap. The condensate density thus goes to zero at a radial distance of R in the TF description, and it is the vicinity of $r \sim R$ that this approximation breaks down. We now list several quantities associated with the high density condensate and their expressions in terms of other quantities, in the TF limit.

- chemical potential,
$$\mu = \frac{15^{2/5}}{2}\lambda^{\frac{2}{5}}\hbar\omega;$$

- condensate size or trap radius,
$$R^2 = \frac{2\mu}{m\omega^2};$$

- density at the center of the trap,
$$n_0 = \mu/g = \frac{15^{2/5}}{2}\left(\frac{\lambda^{\frac{2}{5}}}{a_s a_{ho}^2}\right);$$

- total number of particles:
$$N = 8\pi/15\mu^{5/2};$$

- healing length or size of the vortex core.
$$\xi = \frac{a_{ho}^2}{R}.$$

4.2 Vortex Energetics and Stability

We consider an axially symmetric trap, and calculate the energy cost of creating a vortex in its center from a time-independent mean field theory. The results obtained in this section hold only for a stationary vortex. The dynamics have to be incorporated through a time-dependent theory, which we discuss later Let the axis of the trap be directed along the z-axis, and we work in a cylindrical system of coordinates with ρ the radial distance in the plane, and ϕ the azimuthal angle. In the subsequent presentation, we will first address the simplest case of a uniform condensate, and then address the issue of inhomogeneities introduced by a trap. We discuss first the case of the 2D condensate, and then generalize our conclusions to the 3D case. A 2D situation can be realized in a flat or “pancake” condensate where the trapping is much stronger in the z-direction, than in the plane transverse to it ($\omega_z \gg \omega_x = \omega_y = \omega$). The axial extent of such a trap is going to be much smaller than the transverse extent. We then

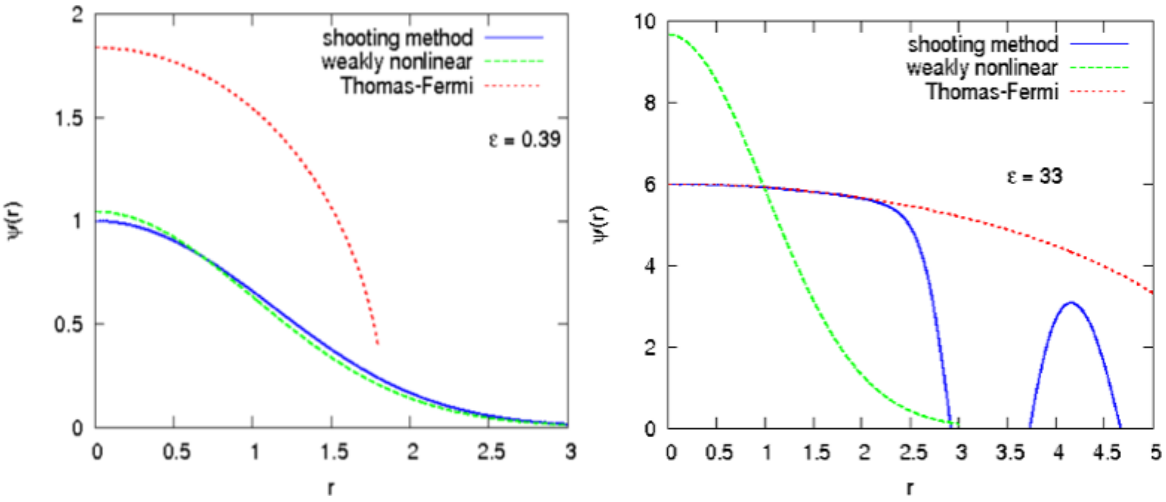

Figure 4-1. Condensate wavefunction $\psi(r)$ versus r. ϵ corresponds to proximity of the chemical potential to the ground state eigenvalue of the trap. The solid blue line is the numerical solution, the dotted red line is the naive one-term perturbative result, and the dashed green line is the Thomas Fermi approximated result. The panel on the left is in the low density limit (lower value of ϵ) where the numeric result is close to the perturbative one. The panel on the right is for a high density limit (high value of ϵ) and the numeric result matches the TF result closely, as expected. The oscillation in the numeric result is an artifact and can be removed by progressively refining the value of the shooting parameter to greater number of significant figures.

make necessary modifications in our calculation to describe a 3D or spherical trap, where the trapping frequencies and condensate size are the same in all directions ($\omega_x = \omega_y = \omega_z = \omega$). Wherever otherwise mentioned, we assume that the condensate has a large density of atoms, and the Thomas Fermi (TF) limit applies. The appearance of a vortex changes the density only locally around itself without affecting the bulk condensate profile, and the healing length is much smaller than the condensate size, $\xi \ll R$.

A vortex with winding number l located in the center of the trap can be described by the condensate wavefunction

$$\psi(\mathbf{r}) = f(\rho, z)e^{il\phi}, \tag{4–25}$$

where the phase of the wavefunction is simply an integral multiple of the azimuthal angle, $\theta = l\phi$. It is easy to check that this phase satisfies the vortex quantization

condition, $\oint \nabla\theta.d\mathbf{l} = 2\pi l$, and minimizes the elastic energy, $\nabla^2\theta = 0$. The superfluid velocity induced by the vortex $\mathbf{v}_s = (\hbar/m)\nabla\theta = \frac{l\hbar}{m}(1/\rho)$ has the requisite quantized circulation, and falls off slowly with distance. Recall from Eq. (4–6) that the Gross Pitaevskii (GP) energy of a condensate (strictly valid at zero temperature when there are no thermal excitations that deplete the condensate) is given as a functional of the condensate wave function. Using our *Ansatz* of Eq. (4–25) for a wavefunction with a vortex, in the GP energy functional of Eq. (4–6), we find

$$E = \int d\mathbf{r}\left\{\frac{\hbar^2}{2m}\left[\left(\frac{\partial f}{\partial \rho}\right)^2 + \left(\frac{\partial f}{\partial z}\right)^2 + l^2\frac{f^2}{\rho^2}\right] + V_{tr}(\rho, z)f^2 + \frac{1}{2}gf^4\right\}. \tag{4–26}$$

The only difference between this result and the one for a condensate without a vortex, and no spatial dependence of the condensate phase, is the $1/\rho^2$ term which comes from the kinetic energy density of the azimuthal superflow induced by the vortex. The energy required to create a vortex at the center of the trap is the difference in GP energy calculated for a condensate of the same density, with and without the vortex, and so corresponds to this azimuthal kinetic energy term. Simple power counting shows that the energy is logarithmically divergent in the radial coordinate. In a condensate of finite size, as one would expect in a confined trap, the large distance cutoff is naturally given by the condensate size or radius R, whereas a natural lower length scale is the healing length ξ. The leading order term of the vortex energy is thus expected to be $\epsilon_v \simeq (\hbar^2 l^2 n_0/2m)\ln(R/\xi_0)$ where n_0 is some characteristic condensate density[1] .

4.2.1 Energy of a Vortex at the Center of the Trap

We now present a derivation of this vortex energy and calculate higher order corrections to it using the GP energy functional presented in Eq. (4–26). For a large

[1] The size of a l-fold vortex is actually $|l|\xi$ (can be verified by comparing terms in GP functional) but this factor of l will only be a logarithmic correction and hence is dropped in the rest of this analysis.

uniform condensate with a vortex (in a TF limit), the condensate density heals to its bulk value of $n_0 = N/V$ within the coherence length ξ, and the radial integral is easily performed (the condensate density can be assumed to be zero within the vortex core radius) to get the energy per unit length of a vortex

$$\epsilon_v = \int_{\xi_0}^{R} \frac{2\pi d\rho}{\rho} \frac{l^2\hbar^2 n}{m} \simeq \pi n_0 \frac{\hbar^2 l^2}{2m} \ln\left(\frac{R}{\xi_0}\right). \tag{4–27}$$

The more accurate result is found by using the numerical solution of the GP equation in the vortex energy as [42]

$$\epsilon_v = \pi n_0 \frac{\hbar^2 l^2}{m} \ln\left(1.464\frac{R}{\xi_0}\right). \tag{4–28}$$

Now consider the added complication of a harmonic trap. The condensate density instead of being uniform outside the vortex core, now follows a parabolic profile, $n(\rho) = n_0\left(1 - \frac{r^2}{R^2}\right)^{\frac{1}{2}}$. The density varies slowly on the length scale of the condensate size. So for length scales much smaller than that but larger than the vortex size, $\xi_0 \ll \rho_1 \ll R$, the system is essentially like a uniform condensate with a vortex and its energy can be found in the same way as shown above in Eq. (4–27) or Eq. (4–28). At distances larger than this, the density profile has the parabolic TF dependence. Putting the two contributions together, we calculate the energy of a vortex per unit length in a 2D trap as,

$$\begin{aligned} \epsilon_v &= \pi n_0 \frac{\hbar^2 l^2}{m}\left[\ln\left(\frac{\rho_1}{\xi_0}\right) + \int_{\rho_2}^{R} \frac{\rho d\rho}{\rho^2}\left(1 - \frac{\rho^2}{R^2}\right)\right] \\ &= \pi n_0 \frac{\hbar^2 l^2}{m}\left[\ln\left(\frac{R}{\xi_0}\right) - \frac{1}{2}\right] + \mathcal{O}\left(\frac{\rho_1^2}{R^2}\right). \end{aligned} \tag{4–29}$$

The logarithmic term is a contribution of the near-uniform slowly varying condensate profile, but there is a slight reduction from that because of the sharply reduced density near the edge of the condensate.

If the condensate size is also large in the z-direction ($\xi_0 \ll R_z$), as would be the case for a spherical 3D trap in the TF limit, the total energy of a vortex is calculated by

summing over each horizontal slice of the condensate and ignoring gradients in the z-direction. The radius of the cloud at each such slice depends on the vertical position as $R(z) = R\left(1 - \frac{z^2}{R^2}\right)^{\frac{1}{2}}$, and the density is a function of both the radial and axial distance. The coherence length depends on the inverse square of the condensate density and on the axis, goes as $\xi(z) = \left(n(0,0)/n(0,z)\right)^{\frac{1}{2}}$. Using the expression for kinetic energy contribution in 2D found in Eq. (4–29), we calculate the total kinetic energy of a 3D condensate with a vortex as

$$\begin{aligned} E &= \frac{\pi\hbar^2 l^2}{m}\int_{-R_z}^{R_z} dz\, n(0,z)\left[\ln\left(\frac{R(z)}{\xi(z)}\right) - \frac{1}{2}\right] \\ &= \frac{\pi\hbar^2 l^2 n(0,0)}{m}\int_{-R_z}^{R_z} dz\left(1 - \frac{z^2}{R^2}\right)\left[\ln\left(\frac{R}{\xi_0}\left(1 - \frac{z^2}{R^2}\right)\right) - \frac{1}{2}\right] \\ &= \frac{4\pi\hbar^2 l^2 n(0,0)}{3m} R_z \ln\left(0.458\frac{R}{\xi_0}\right). \end{aligned} \tag{4–30}$$

4.2.2 Energy of an Off-center Vortex

We now determine the dependence of the energy of a vortex on its position within the condensate. Since the condensate density is suppressed in a region of the order of the healing length around the vortex, it is expected that the energy cost of creating a vortex would be more near the center of the trap where the condensate density is higher. For an axially symmetric trap, the energy will depend only on the radial distance of the vortex from the center, $\rho_v = \sqrt{x_v^2 + y_v^2}$ where the vortex coordinates are labeled (x_v, y_v). We will generally refer to the vortex position, $\mathbf{x}_v \equiv (\rho_v, \phi_v, 0)$, reserving use of ρ_v only when we want to explicitly refer to the radial distance of the vortex from the center of the trap/axis of rotation. The dominant logarithmic contribution to the energy of an off-center vortex is calculated using the same ideas as for a vortex at the center: Eq. (4–27) to Eq. (4–29). The uniform condensate density at the vortex position in the absence of a vortex determines this energy contribution. Thus for a 2D condensate, the

energy per unit length of the vortex is given by

$$\epsilon_v \simeq \pi n(\mathbf{r}_v)\frac{\hbar^2 l^2}{2m}\ln\left(\frac{R}{\xi_0}\right) = \pi n_0 \frac{\hbar^2 l^2}{2m}\ln\left(\frac{R}{\xi_0}\right)\left(1-\frac{\mathbf{r}_v^2}{R^2}\right), \tag{4–31}$$

where we have used the TF density profile. Following the same steps for a vortex in the center of a trap that lead from Eq. (4–29) to Eq. (4–30), which is basically integrating along the axial direction, we find the energy of a vortex in a 3D trap:

$$E = \frac{\pi\hbar^2 l^2}{m}\int_{-R_z}^{R_z} dz\, n(\rho_v, z)\ln\left(\frac{R(z)}{\xi(\rho_v, z)}\right) \simeq E_0\left(1-\frac{\mathbf{r}_v^2}{R^2}\right)^{3/2}, \tag{4–32}$$

where $E_0 = \frac{4\pi\hbar^2 l^2 n(0,0)}{3m} R_z \ln\left(R/\xi_0\right)$ is the energy to leading order of a vortex at the center of the trap, as found in Eq. (4–30). In the above relations, the off-center vortex energy is smaller than the central vortex by a factor of $\left(1-\frac{r_v^2}{R^2}\right)^{1/2}$, which is from the lower density of the condensate at the vortex position. An extra factor of $\left(1-\frac{r_v^2}{R^2}\right)^{1/2}$ arises in Eq. (4–32) for the 3D trap because the z-height of the condensate is smaller at the vortex position than at the center of the trap.

4.2.3 Vortex Stabilization in a Rotating Trap

The stationary GP development so far suggests that the vortex energy is always highest at the center of the trap and decreases monotonically with outward radial distance. So if there is any dissipative mechanism for example, a vortex created at the center would tend to lose energy and move towards the periphery of the trap. We will now show that this tendency can be compensated to some extent by the effect of rotation of the trap, and that for some range of angular frequencies, the vortex at the center can actually be in an energetically stabilized or metastable state.

The additional complication when the trap is being rotated is that the external potential felt by the condensate atoms becomes time-dependent in the laboratory frame of reference. This difficulty can be circumvented by transforming to a comoving frame that rotates with the trap. In this case the trap potential remains time-independent, and the static description we have used so far still holds. Quantities in the rotating (primed)

and laboratory (unprimed) frame of reference are related through a well-known transport theorem from mechanics [76],

$$\frac{d\mathbf{A}'}{dt} = \frac{d\mathbf{A}}{dt} - \mathbf{\Omega} \times \mathbf{A}, \tag{4–33}$$

where $\mathbf{\Omega}$ is the angular velocity with which the trap is rotating and $\mathbf{A}$ is any vector. The result of interest to us (which can be derived from this basic relation) is that energies in the rotating and laboratory frames of reference are related by

$$E' = E - \mathbf{\Omega} \cdot \mathbf{L}, \tag{4–34}$$

where $\mathbf{L}$ is the angular momentum of the condensate calculated in the laboratory frame.

Calculation of condensate angular momentum. For the sake of simplicity we consider a situation in which the trap is being rotated about its axis of symmetry, i.e. the $z-$ direction. Eq. (4–34) suggests that we need to calculate the expectation value of the $z-$component of the angular momentum about the axis of the trap, produced by the superflow induced by a vortex located at a radial distance ρ_v from the axis of the trap. This is given by the expression

$$\left\langle \hat{L_z} \right\rangle = \int d\mathbf{r}\, i\hbar\psi\hat{z} \cdot \left(\mathbf{r} \times \nabla\psi\right), \tag{4–35}$$

where the condensate wave function for an off-center vortex configuration is given by a modification of the *Ansatz* in Eq. (4–25),

$$\psi(\mathbf{r}) = f(\rho, z)e^{il\phi'}, \tag{4–36}$$

$$\phi' = \arctan\left(\frac{y - y_v}{x - x_v}\right). \tag{4–37}$$

The phase is now measured in a coordinate frame centered at the vortex position. The dominant contribution to the angular momentum (like for the kinetic energy) is going to come from the azimuthal superfluid velocity induced by the presence of the vortex according to the definition of superfluid velocity, $\mathbf{v} = i\hbar\nabla\theta$. Another way to see this is

that the gradient of the density is ignored in the TF limit. A finite gradient of the phase is imperative because a vortex is an excitation in the phase field of the order parameter. This is plausible because the energy cost associated with an amplitude fluctuation is more than in phase as seen from the Gross-Pitaevskii functional. This discussion suggests that the expression of the angular momentum in Eq. (4–35) can be written in the form,

$$L_z \simeq \int d\rho d\phi \; mn\rho v_\phi, \tag{4–38}$$

for a 2D condensate, which is also classically intuitive. Here, v_ϕ is the azimuthal component of the superfluid velocity, and m is the mass of each particle in the condensate. The density n in the above expression is actually $n(\mathbf{r}_v)$, i.e. the density evaluated at the position of the vortex and the correction coming from the inhomogeneities in density due to the trap potential at larger length scales is found to be small, as was the case in the derivation of vortex energy in the TF limit Eq. [4–27 to Eq. (4–29)]. The integral in Eq. (4–38) can be evaluated simply by realizing that

$$\begin{aligned} \int d\phi \rho v_\phi = \oint \mathbf{v}.d\mathbf{l} &= \oint (\nabla \times \mathbf{v}).d\mathbf{a} \\ &= \frac{2\pi l\hbar}{m} \int da \delta^{(2)}(\rho - \rho_v) = \begin{cases} 2\pi l\hbar m \text{ if } \rho > \rho_v, \\ 0 \qquad \text{if } \rho < \rho_v. \end{cases} \end{aligned} \tag{4–39}$$

Here we have used Stoke's theorem and the idea of a vortex as a source of the rotational part of the superfluid velocity, to realize that the circulation of velocity is non-zero only when the contour of integration encloses the position of the vortex. This result can then be used to calculate the angular momentum for a 2D condensate with a vortex from Eq. (4–38) and using the TF expression for density,

$$L_z \simeq 2\pi\hbar n(\rho_v) \int_{\rho_v}^{R} d\rho\rho = Nl\hbar \left(1 - \frac{\mathbf{r}_v^2}{R^2}\right)^2. \tag{4–40}$$

This implies that for a vortex on the axis each atom carries a quantized angular momentum of $l\hbar$. This is expected because the atoms are condensed to the same ground state wavefunction, and the total energy or angular momentum is an extensive quantity that is a multiple of the quantity carried by each atom. In this picture each atoms rotates about the central axis, wheras an off-axis vortex implies that rotation is about an axis different from the central axis about which angular momentum was computed. We can now work out the angular momentum of a 3D condensate by integrating along the axial (z) direction,

$$L_z \simeq 2\pi\hbar \int_{-R_z}^{R_z} dz n(\rho_v, z) \int_{\rho_v}^{R} d\rho\rho = Nl\hbar\left(1 - \frac{\mathbf{r}_v^2}{R^2}\right)^{\frac{5}{2}}. \tag{4–41}$$

The angular momentum in the 3D trap has an extra factor of $(1 - \mathbf{r}_v^2/R^2)^{1/2}$ over the 2D case as was seen in the expressions for energy.

Vortex energy in the rotating frame. Now that we have calculated both energy and angular momentum for a general vortex state of the condensate in the laboratory frame of reference, we are in a position to calculate the energy cost of creating a vortex in the rotating frame that is comoving with the trap. Using Eq. (4–34), we find the energy per unit length of a vortex in the rotating frame for a 2D condensate

$$\epsilon_v' = \epsilon_0 \left[\left(1 - \frac{\mathbf{r}_v^2}{R^2}\right) - \frac{\Omega}{\Omega_c^{2D}}\left(1 - \frac{\mathbf{r}_v^2}{R^2}\right)^2\right], \tag{4–42}$$

where the prefactor $\epsilon_0 = \pi n_0 \frac{\hbar^2 l^2}{2m} \ln\left(\frac{R}{\xi_0}\right)$ is the energy per unit length of a vortex on the axis of a 2D condensate calculated in Eq. (4–31). Ω_c^{2D} is the critical angular velocity at which the trap needs to be rotated above which the vortex at the center of the trap is stabilized. This is determined by the ratio of energy and angular momentum of the condensate for a vortex at the center in the laboratory frame :

$$\Omega_c^{2D} = \frac{\hbar l^2}{2mR^2} \ln\left(\frac{R}{|l|\xi_0}\right). \tag{4–43}$$

The corresponding energy of a vortex in the rotating frame for a 3D condensate is

$$E_v = E_0\left[\left(1-\frac{\mathbf{r}_v^2}{R^2}\right)^{3/2} - \frac{\Omega}{\Omega_c}\left(1-\frac{\mathbf{r}_v^2}{R^2}\right)^{5/2}\right], \tag{4–44}$$

where the prefactor E_0 is the energy of a vortex on the axis of a 3D condensate calculated in Eq. (4–32), and Ω_c is the critical velocity (same up to some numerical factor in 2D and 3D cases), which is defined similarly as in Eq. (4–43) to be

$$\Omega_c = \frac{5}{2}\frac{\hbar l^2}{mR^2}\ln\left(\frac{R}{|l|\xi_0}\right). \tag{4–45}$$

The energy profiles for a vortex in the rotating frame, when plotted against its radial distance from the trap center for various regimes of rotation, has the same behavior as shown in Fig. 5-1 in the Chapter 5. This shows that the vortex at the center of the trap can be in stable, metastable or unstable configurations depending on how fast the trap is being rotated. The metastable state is of particular importance to us as this suggests that there is some finite, possibly measurable, time at which a vortex at the center can tunnel through this potential barrier towards the periphery of the trap.

4.2.4 Vortex in a Small Condensate

So far we have considered the energetics of a vortex in a condensate of large density or particle number where the TF analysis is applicable. There the presence of a vortex does not alter the density of the condensate except around a small distance, which corresponds to the healing length ξ, that is much smaller than the condensate size R in this limit. Now we consider the opposite limit, where the nonlinear term can be treated perturbatively by the “weakly nonlinear” method introduced in Section 4.1. Here the density is small to begin with and the presence of the vortex radically alters the condensate density, all over the trap. The healing length is now of the same order as the condensate size, which means that the vortex occupies almost the whole of the trap. The long length scale hydrodynamics valid far away from the vortex core thus fail in this limit, making this a harder case to deal with.

The nondimensionalized GP energy functional for a vortex at the center of a trap is,

$$E = \int d^3x \left\{ \frac{\hbar^2}{2m} \left[\left(\frac{\partial f}{\partial \rho} \right)^2 + \left(\frac{\partial f}{\partial z} \right)^2 + l^2 \frac{f^2}{\rho^2} \right] + V(\rho, z) f^2 + \frac{1}{2} g f^4 \right\}, \tag{4–46}$$

where the $1/\rho^2$ term is the contribution of the rotation to the kinetic energy (i.e. the "centrifugal barrier"). The length and amplitude scales $l = a_{ho}$ and χ are the same as defined earlier in Eq. (4–8).

For illustrative purposes, we consider the commonest (lowest energy) situation of a vortex with a single quantum of circulation, i.e. $l = 1$. In the ground state the wavefunction should not have any z-dependence. The trapping potential is isotropic and harmonic. The nondimensionalized GP equation is,

$$-\frac{1}{x}\frac{d}{dx}\left(x \frac{df}{dx} \right) + \frac{f}{x^2} + (x^2 - \mu) f + f^3 = 0, \tag{4–47}$$

where $x = \rho/l$ is the nondimensionalized radial coordinate in a cylindrical coordinate system. The linearized version of this problem is therefore a Schrödinger equation separable into an axial part along the $z-$axis which corresponds to the ground state of a 1D harmonic oscillator, and a radial part which corresponds to the first excited state of a 2D harmonic oscillator problem (l=0 in ground state, $l = 1$ is the first excited state). The eigenvalue of the linear problem in our units (1 unit of energy $\equiv \frac{1}{2}\hbar\omega$) is $1 + 4 = 5$.

Following the weakly nonlinear analysis of the previous section, the $\mathcal{O}(1)$ equation is the normalized product of a 1D harmonic oscillator's ground state eigenfunction and a 2D harmonic oscillator's 1st excited state eigenfunction. There is an overall integration constant A_0, which is recovered from the solvability condition of the $\mathcal{O}(\epsilon)$ equation, as $A_0 = 2\sqrt{\pi}$. The overall amplitude of the wavefunction is therefore,

$$f(x) = 2^{5/4}\sqrt{\epsilon}\rho e^{-\rho^2/2 - z^2/2} + \mathcal{O}(\epsilon^{3/2}), \tag{4–48}$$

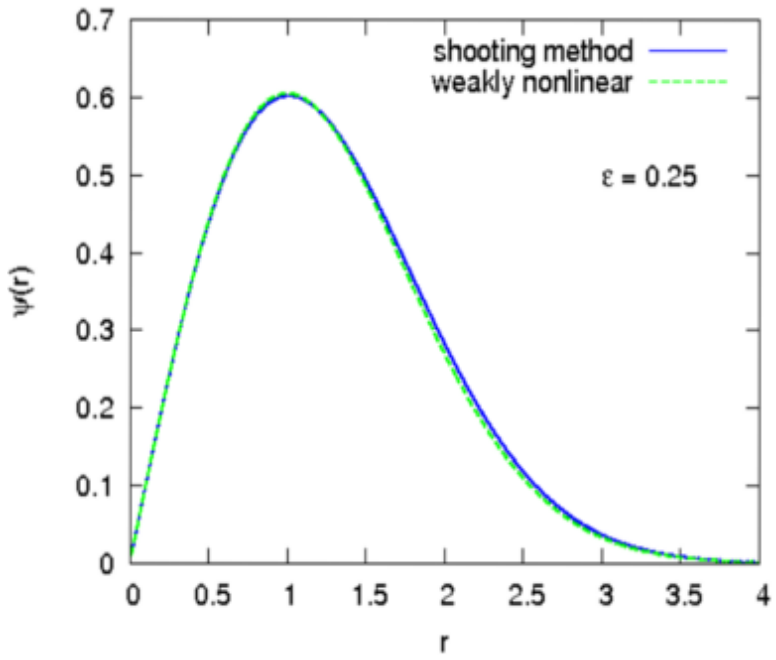

Figure 4-2. Condensate wavefunction $\psi(r)$ versus r for the $l = 1$ vortex state in a small condensate. The solid blue line is the numerical solution, and the dashed green line is the one-term perturbative result.

where the coordinates ρ and are polar coordinates nondimensionalized by the length scale a_{ho}. The result is expected to hold when μ is close to 5 and ϵ is the small parameter in the problem defined as $\epsilon \equiv \mu - 5$.

The energy needed to create a vortex is the difference of the GP energy of a condensate with and without a vortex. This was readily done in the TF limit, because the kinetic energy from the azimuthal superflow was the only extra term in the GP energy functional of a vortex state. We assumed that the density of the condensate remained the same while integrating over this kinetic energy density. This assumption would not be right in the case of the small condensate being considered here, because the density of the condensate is altered over a length scale comparable to the condensate size by the presence of a vortex. So we have to be more careful with our analysis.

We first calculate the total energy of a condensate (in our appropriately nondimensionalized units) with a singly quantized vortex at its center, and with a chemical potential determined by ϵ. In nondimensional units, this is obtained by inserting the wavefunction

of Eq. (4–48) into a suitably nondimensionalized GP energy functional as

$$\begin{aligned}\mathcal{E} &= \int_{-\infty}^{\infty} dz \int_0^{\infty} 2\pi\rho d\rho \left[\left(\frac{\partial f}{\partial \rho}\right)^2 + \left(\frac{\partial f}{\partial z}\right)^2 + \left(\frac{1}{\rho^2} + \rho^2 + z^2\right) f^2 + f^4 \right] \\ &= 20\sqrt{2}\pi^{3/2}\epsilon + \mathcal{O}(\epsilon^2). \end{aligned} \tag{4–49}$$

The total number of particles in this state is

$$N = \int_{-\infty}^{\infty} dz \int_0^{\infty} 2\pi\rho d\rho |f(\rho, z)|^2 = 4\sqrt{2}\pi^{3/2}\epsilon + \mathcal{O}(\epsilon^2). \tag{4–50}$$

Now to find the actual extra energy cost of creating a vortex, we have to calculate the energy of the condensate in Eq. (4–49) to a vortex-free reference system which has the same number of particles. The wavefunction of such a system will be described by the ground state of a 3D harmonic oscillator

$$f^R(\rho, z) = 2^{3/2}\sqrt{\epsilon^R} e^{-\rho^2/2 - z^2/2} + \mathcal{O}((\epsilon^R)^{3/2}), \tag{4–51}$$

where the quantities associated with this reference system have been labeled with a superscript R. In particular we expect the chemical potential of the original and reference states to be different. Equating the total number of particles for the vortex-free reference state to that of the original state we discover a simple relationship between their respective chemical potentials

$$\epsilon^R = 2\epsilon. \tag{4–52}$$

The energy of the reference system is found by inserting the wavefunction of Eq. (4–51) into the GP energy functional

$$\begin{aligned}\mathcal{E}^R &= \int_{-\infty}^{\infty} dz \int_0^{\infty} 2\pi\rho d\rho \left[\left(\frac{\partial f^R}{\partial \rho}\right)^2 + \left(\frac{\partial f^R}{\partial z}\right)^2 + \left(\frac{1}{\rho^2} + \rho^2 + z^2\right) (f^R)^2 + (f^R)^4 \right] \\ &= 6\sqrt{2}\pi^{3/2}\epsilon^R + \mathcal{O}((\epsilon^R)^2). \end{aligned} \tag{4–53}$$

The energy cost of creating a vortex is then the difference of Eq. (4–49) and Eq. (4–53):

$$\mathcal{E}_v = \mathcal{E} - \mathcal{E}^R = 8\sqrt{2}\pi^{3/2}\epsilon. \tag{4–54}$$

Similarly since this is a centered vortex, the angular momentum carried by each particle is $\hbar$ and the total angular momentum of the condensate with a singly quantized vortex at its center is

$$L = 4\sqrt{(2)}\epsilon\pi^{3/2} + \mathcal{O}(\epsilon^2), \tag{4–55}$$

where the unit of angular momentum is $\hbar$. The critical velocity of trap rotation at which vortex is stabilized is then (up to zeroeth order in $\mathcal{E}$, and after putting back the units)

$$\Omega_c \equiv \mathcal{E}_v/L \sim \omega \tag{4–56}$$

There will be ϵ corrections to this expression for critical velocity. However we can already see from the zeroeth order result, that for a small condensate, the trap has to be rotated at an angular velocity of the same order of magnitude as the trap frequency to stabilize a vortex at the center of the trap. However the centrifugal forces at this rotation frequency are likely to destroy the trapping. Thus, finding stable or metastable regimes for the vortex, while not destroying the stability of the trap, is ruled out for a small condensate. We concentrate on the dynamics and tunneling of a large TF condensate in the analyses to follow.

4.3 Vortex Dynamics in the Co-rotating Frame

The Gross-Pitaevskii Lagrangian density written in the rotating frame of reference is

$$\mathcal{L}[\psi, \psi^*] = \frac{i\hbar}{2}\left(\psi^*\partial_t\psi - \psi\partial_t\psi^*\right) - \psi^*\left(\hat{H}_0 - \Omega\hat{L_z}\right)\psi - \frac{g}{2}|\psi|^4, \tag{4–57}$$

where

$$\hat{H}_0 = -\frac{\hbar^2}{2m}\nabla^2 + V_{tr}(r) \tag{4–58}$$

is the Hamiltonian for the noninteracting condensate, and

$$\hat{L_z} = i\hbar\hat{z} \cdot \left(\mathbf{r} \times \nabla\right) \tag{4–59}$$

is the component of the angular momentum operator in the z-direction.

We write the above Lagrangian density in terms of superfluid phase and density using the so-called Madelung transform, $\psi(\mathbf{r}, t) = \sqrt{n(\mathbf{r}, t)}e^{i\theta(\mathrm{r},t)}$ [107]:

$$\mathcal{L}\left[n, \theta\right] = -n\left\{\hbar\frac{\partial\theta}{\partial t} + \frac{\hbar^2}{2m}\left[(\nabla\theta)^2 + \frac{(\nabla\sqrt{n})^2}{n}\right] + V_{tr} + \frac{g}{2}n - \hbar\Omega(\hat{z} \times \mathbf{r}).\nabla\theta\right\}. \tag{4–60}$$

The term involving a time derivative of density does not contribute to the dynamics and is neglected. The time derivative of the phase is however important because the phase is not an analytic field in the presence of a vortex.

By varying the above Lagrangian we get the hydrodynamic equations of motion in a rotating frame:

$$\frac{\partial n}{\partial t} - \Omega\frac{\partial n}{\partial \phi} + \frac{\hbar}{m}\nabla \cdot (n\nabla\theta) = 0; \tag{4–61}$$

$$-\hbar\frac{\partial\theta}{\partial t} = \frac{\hbar^2}{2m}\left[(\nabla\theta)^2 - \frac{(\nabla^2\sqrt{n})}{\sqrt{n}}\right] + (V_{tr} - \mu) + gn - \hbar\Omega\frac{\partial\theta}{\partial\phi}. \tag{4–62}$$

The superfluid velocity in the inertial laboratory frame is related to the phase via the Josephson relation, $\mathbf{v} = (\hbar/m)\nabla\theta$. The phase is described in terms of the coordinates of the rotating frame. Re-expressing Eq. (4–61) and Eq. (4–62) in terms of the superfluid velocity, $\mathbf{v}$, we recover the hydrodynamic equations of superfluids in a rotating frame of reference as [2]

$$\frac{\partial n}{\partial t} + \nabla \cdot (n(\mathbf{v} - \mathbf{\Omega} \times \mathbf{r})) = 0, \tag{4–63}$$

and,

$$\frac{\partial \mathbf{v}}{\partial t} + \nabla\left[\frac{v^2}{2} + \frac{V_{tr}}{m} + \frac{g}{m}n - \frac{\hbar^2}{2m^2}\frac{(\nabla^2\sqrt{n})}{\sqrt{n}} - \mathbf{v} \cdot (\mathbf{\Omega} \times \mathbf{r})\right] = 0. \tag{4–64}$$

[2] Note that the equations while in the rotating frame of reference are expressed in terms of the superfluid velocity in the inertial or laboratory frame.

These are the continuity and momentum equations respectively for a superfluid in a rotating frame. The momentum transport equation contains the forces experienced by an infinitesimal element of fluid as a gradient of the external trap potential, the interaction forces from the condensate, terms from the rotating frame of reference (which can be shown to be related to the Coriolis and centrifugal effects) and a "quantum pressure" term (so called because of its dependence on Planck's constant) that goes as the gradient of the density. This term is purely quantum in origin and distinguishes a superfluid from a classical, inviscid and irrotational fluid. In the Thomas-Fermi (TF) approximation, valid for a large, dense condensate where the condensate density varies slowly in space except near the edge of the trap, the "quantum pressure" term is dropped in the above equation. This gives the well-known Euler equation for an inviscid and irrotational, classical fluid in a rotating frame of reference.

Next we integrate out the density fluctuations to obtain the hydrodynamic action solely in terms of the phase. This can be easily done by expressing the density in terms of the phase using Eq. (4–62) and the TF approximation. The TF condensate density is then given by

$$n_{TF}(\mathbf{x}, t) = -\frac{1}{g}\Big[\hbar\frac{\partial\theta}{\partial t} + V_{tr} - \mu + \frac{\hbar^2}{2m}(\nabla\theta)^2 - \hbar\Omega\frac{\partial\theta}{\partial\phi}\Big] \tag{4–65}$$

and the action can then be expressed as,

$$S = \int dt\, \frac{g}{2}\int d^3x \big(n_{TF}\big)^2. \tag{4–66}$$

Now to make contact with the stationary (time-independent) GP equation, we gauge away the time dependence of θ in the stationary case, i.e. define $\hbar\frac{\partial\theta}{\partial t} + \mu$ as the new $\hbar\frac{\partial\theta}{\partial t}$, where μ is the constant chemical potential in the corresponding stationary GP equation, $\mu \equiv gn(0)$. Also define $\rho_s(r) = [\mu - V(r)]/g$ to be the stationary TF condensate density. Using the above notation, the hydrodynamic density can be decomposed into stationary

and non-stationary parts

$$n_{TF}(\mathbf{x},\, t) = \rho_s(r) - \frac{1}{g}\Big[\hbar\frac{\partial\theta}{\partial t} + \frac{\hbar^2}{2m}(\nabla\theta)^2 - \hbar\Omega\frac{\partial\theta}{\partial\phi}\Big]. \tag{4–67}$$

After integrating out the fluctuations in density, we have an action expressed entirely in terms of the phase. The detailed form of the action is written as follows :

$$\begin{aligned}
S &= S_1 + S_2 + S_3 + S_4, \\
S_1 &= -\hbar^2 \int dt \int d\mathbf{x}\rho_s(r)\left(\frac{\partial\theta}{\partial t}\right), \\
S_2 &= \frac{\hbar^2}{2g}\int dt \int d\mathbf{x}\left(\frac{\partial\theta}{\partial t}\right)^2, \\
S_3 &= -\int dt \int d\mathbf{x}\rho_s(r)\left[\frac{\hbar^2}{2m}(\nabla\theta)^2 - \hbar\Omega\frac{\partial\theta}{\partial\phi}\right], \\
S_4 &= -\frac{\hbar^2}{2g}\int dt \int d\mathbf{x}\left[2\Omega\frac{\partial\theta}{\partial\phi}\frac{\partial\theta}{\partial t} + \Omega^2\left(\frac{\partial\theta}{\partial\phi}\right)^2\right].
\end{aligned} \tag{4–68}$$

The reason we make a (purely conceptual) distinction between the four pieces in the action above, will become clearer in the discussion in the subsequent paragraphs.

Let us first consider only the vortex part of the phase, and ignore the phonon modes excited by the motion of the vortex. Our chosen *Ansatz* for the vortex part of the phase is

$$\theta_v(\mathbf{x},\, t) = \frac{\hbar q_v}{m}\arctan\left[\frac{y - y_v(t)}{x - x_v(t)}\right], \tag{4–69}$$

$\mathbf{x}_v(t)$ being the vortex position as a function of time, and for simplicity we consider a single vortex of charge q_v. The same idea could be used to represent a system of multiple vortices. The following relations hold:

$$\nabla\times\nabla\theta_v = 2\pi q_v\delta^{(2)}\big(\mathbf{x} - \mathbf{x}_v\big)\hat{z}, \quad \nabla^2\theta_v = 0.$$

By using the above vortex *Ansatz* in the detailed action stated in Eq. (4–68) and then integrating out the spatial coordinates, we would be left with an action entirely in terms

of the vortex coordinates. Starting from purely hydrodynamic considerations, we would have derived the single-particle dynamics of a vortex. The terms S_1 to S_4 for will be shown to correspond to the superfluid Magnus force, the vortex mass, the static vortex potential, and the noninertial effects of the rotating frame, respectively. We now discuss in some detail, various aspects of the well-established Magnus force felt by a moving vortex in a superfluid, and the not-so-well-established idea of the mass of a vortex, with the above hydrodynamic action sto illustrate the point.

4.3.1 The Magnus Force

The vortex part of S_1 in Eq. (4–68) can be shown to correspond to a transverse force akin to the Lorentz force felt by a charged particle in a magnetic field [109], whereas the analytic part of S_1 is a total derivative and can be dropped from the action. Let us now take a closer look at the vortex contribution to S_1. The time derivative of the vortex phase can be related to the vortex velocity through $\partial_t \theta_v(\mathbf{x} - \mathbf{x}_v) = \mathbf{v}_v.\nabla_v \theta(\mathbf{x} - \mathbf{x}_v(t))$, where $\mathbf{v}_v$ is the velocity of the vortex, and ∇_v denotes the spatial derivative with respect to the vortex coordinates. This identity, which we will make frequent use of, implies that the phase of a moving vortex changes in time because of the change in its coordinates.

This lets us write the S_1 part of the action as

$$-\hbar \int dt \int d\mathbf{x}\, \rho_s(r) \left(\frac{\partial \theta_v}{\partial t} \right) = \int dt q_v \mathbf{v}_v \cdot \mathbf{A}, \tag{4–70}$$

where

$$q_v \mathbf{A}(\mathbf{x}_v) = -\hbar \int d\mathbf{x}\, \rho_s(r) \nabla_v \theta(\mathbf{x} - \mathbf{x}_v). \tag{4–71}$$

The term S_1 as written in Eq. (4–70) resembles the action of a charged particle in a magnetic field, which is known to be $\int dt[(m/2)v^2 + q\mathbf{v} \cdot \mathbf{A}]$, the A defined by Eq. (4–71) being the magnetic vector potential. The effective magnetic field in which the vortex

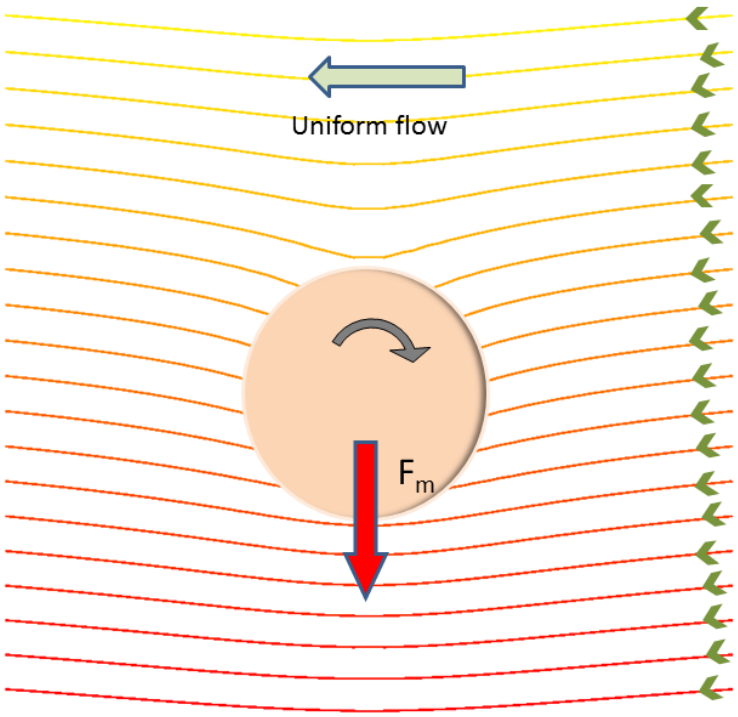

Figure 4-3. Magnus force on a rotating object in a flowing fluid: the object spins clockwise as the fluid flows past it from right to left. The velocity streamlines are shown. The total fluid velocity is a sum of the uniform flow and the rotational flow (which is analogous to a vortex velocity field). The velocities are higher in the bottom half plane in this figure, leading to pressure differences from Bernoulli's principle. The object thus feels a downward Magnus force.

moves is then identified as

$$\mathbf{B}_v = \nabla_v \times \mathbf{A} = -\hbar \int d\mathbf{x} \rho_s(r) \nabla_v \times \nabla_v \theta(\mathbf{x} - \mathbf{x}_v) = -h\rho_s^{2D}(\mathbf{x}_v)\hat{z}. \tag{4–72}$$

The Lorentz-like transverse force $\mathbf{F}_m = q_v(\mathbf{v}_v \times \mathbf{B}_v)$ that originates from this action is exactly like the Magnus force (also called the Kutta-Joukowski force in aerodynamics literature) familiar from classical fluid dynamics [106], with the density of the classical fluid, replaced by the superfluid density. This is a purely classical fluid, and can be understood intuitively by considering a spinning object placed in a classical fluid, as shown in Fig. 4-3. As the objec rotates it entrains some of the surrounding fluid and swirls it around. The net fluid velocity is therefore different on one side of the object from

that on the diametrically opposite side. Bernoulli's principle of energy conservation in a fluid suggests that this leads to the buildup of a pressure difference, and a resulting transverse "lift" or Magnus force. Using the Galilean invariance of the Gross-Pitaevskii formalism and the resultant classical hydrodynamics described above, we can impose an overall constant velocity field $\mathbf{v}_s$ corresponding to the overall superfluid flow in some inertial frame of reference, and the more complete expression of the Magnus force then becomes

$$\mathbf{F}_m = q_v \hbar \rho_s^{2D}(\mathbf{x}_v)\hat{z} \times (\mathbf{v}_v - \mathbf{v}_s). \tag{4–73}$$

We note here that the inhomogeneous potential from the trap is responsible for inhomogeneities in the density, and so ultimately in the "magnetic field", and the magnitude of the Magnus force. For example the force is expected to be stronger when the vortex is near the center of the trap, because that is where the condensate density is the highest. Also note that the $\rho_s(\mathbf{x}_v)$ used in the above treatment is actually the 2D superfluid density at the vortex position, which is obtained by integrating the 3D density along the z-direction.

4.3.2 Vortex Mass

The idea of a vortex mass has been a matter of some debate. Yet the notion of mass is very important in calculating the rate of vortex tunneling, and other such experimentally observable physical phenomena involving vortices. A vortex in a classical, inviscid fluid is usually assumed massless as the fluid density goes to zero in the core of the vortex. This point of view has also been adopted in some approaches to study quantized vortices [110]. Others assume it to be the mass of atoms in the normal vortex core [111], which is the only source of inertia in a strictly incompressible superfluid. Several authors, such as Popov in an older work [112], and Duan and Leggett [113] who take the compressible nature of the superfluid and consequent density fluctuations into account, find a vortex mass that is logarithmically divergent with system size. We note at this point a major difference between vortex

energy in superfluid helium, and a BEC in a trap. The latter always has a finite size, and this condensate radius R provides a natural upper cutoff length scale. The problem of logarithmic divergences is therefore absent in the trapped BEC systems we are considering. In other words $\ln(R/\xi)$ is finite, and of order 1 for most experimental situations, and the above two estimates of mass are not radically different. We will now present an estimate of the vortex mass based on the hydrodynamic action we have written down in Eq. (4–68)[3] .

The vortex part of S_2 in Eq. (4–68) after performing the spatial integral, can be shown to be related to the inertia of the vortex. We begin by noticing that the term S_2 can be cast in a form suggestive of vortex kinetic energy as

$$\frac{\hbar^2}{2g}\int dt \int d\mathbf{x}\left(\frac{\partial\theta}{\partial t}\right)^2 = \int dt \frac{1}{2}\mathbf{v}_v^2 \int d\mathbf{x}\frac{\hbar^2}{g}\left[\nabla_v\theta_v(\mathbf{x}-\mathbf{x}_v)\right]^2. \tag{4–74}$$

This is of the form $\int dt(1/2)M_v v_v^2$ where the vortex "mass" M_v is obtained by performing the spatial integration over the phase term above. We perform this integral by first translating the origin of the spatial coordinates to the position of the vortex, which means that the vortex phase is now simply the azimuthal angle. The gradient of the phase now has the simple form

$$\nabla_v\theta = -\frac{\hat{\phi}'}{\rho'}, \tag{4–75}$$

where ϕ' and ρ' are the azimuthal and radial coordinates respectively in the new coordinate system centered at the vortex position. The vortex "mass" is now obtained by integrating over the new spatial coordinates as

$$M_v \equiv \frac{\hbar^2}{g}\int d\mathbf{x}\left(\nabla_v\theta_v\right)^2 = \frac{\hbar^2}{g}\int dz \int 2\pi\frac{d\rho'}{\rho'} \simeq \frac{2\pi\hbar^2 R_z}{g}\ln\left(\frac{R}{\xi}\right). \tag{4–76}$$

[3] The derivation is similar in spirit to that presented in the book *Inhomogeneous Superconductors* (pp 257) by Simanek in the context of charged superfluids [114].

The idea of a vortex mass is problematic, and estimates in the literature for its value range from 0 to infinite! We have obtained here a working definition of mass, but with the obvious caveat that the vortex *Ansatz* used in this picture is not the whole story to the superfluid phase. A moving vortex is likely to introduce density fluctuations in the form of acoustic waves, and these phonons would couple to the vortex, producing temporally nonlocal "memory" effects in the vortex inertia. This results in a frequency-dependent vortex mass as we find later in this chapter, and as was found by previous authors such as Thouless and Anglin [115]. The expression for vortex "mass" we obtain in Eq. (4–76) is presumably just a local approximation of this more complicated inertial term which we discuss later. For now, we can put the result of Eq. (4–76) on a firmer physical footing by noticing that barring the logarithmic factor, it is simply related to the mass of the atoms in the normal vortex core. This can be easily seen by using the relations between the condensate and trap parameters that are expected to hold in the TF regime, specifically $gn_0 = \mu$, $\xi = \hbar/(m\omega R)$ and $\mu = m\omega^2 R^2$. Using them we can show that

$$M_v \simeq 4mn_0\pi\xi^2 R_z \ln\left(\frac{R}{\xi}\right), \tag{4–77}$$

where m is the mass of each atom in the condensate, n_0 is some characteristic condensate density, ξ the vortex core radius, and R_z the length of the vortex line. The factor of $mn_0\pi\xi^2 R_z$ is then just the mass of the vortex core, where the fluid is in the normal phase.

Static vortex potential. The vortex part of S_3 in Eq. (4–68) after performing the spatial integral, corresponds to the vortex energy E_v obtained earlier from static energetic considerations in Eq. (4–44). This contribution to the action has the form of a particle in an external potential, $V_v(\mathbf{x}_v)$.

Effect of rotation. It is intuitively apparent from the structure of S_4 that the terms containing the angular frequency of rotation and it square correspond to the Coriolis and centrifugal forces acting on the vortex in the rotating frame.

We now decompose the phase into analytic and vortex parts, $\theta = \theta_a + \theta_v$, $\nabla \times \nabla\theta_a = 0$. We wish to integrate out the analytic part of the phase and derive an action solely in terms of the vortex coordinates. With this objective in mind, let us collect all terms in the action that depend on the analytic part of the phase and write it in the following suggestive form,

$$\begin{aligned} S_a = \int dtdz \int d^2x \quad \Bigg\{ & -\frac{\hbar^2}{2g}\Bigg[\left(\frac{\partial\theta_a}{\partial t}\right)^2 + 2\frac{\partial\theta_a}{\partial t}\frac{\partial\theta_v}{\partial t} \\ & + 2\Omega\left(\frac{\partial\theta_a}{\partial t}\frac{\partial\theta_a}{\partial\phi} + \frac{\partial\theta_a}{\partial t}\frac{\partial\theta_v}{\partial\phi} + \frac{\partial\theta_a}{\partial\phi}\frac{\partial\theta_v}{\partial t}\right) + \Omega^2\left(\left(\frac{\partial\theta_a}{\partial\phi}\right)^2 + 2\frac{\partial\theta_a}{\partial\phi}\frac{\partial\theta_v}{\partial\phi}\right)\Bigg] \\ & + \frac{\hbar^2}{2m}\rho_s(r)\Big[\left(\nabla\theta_a\right)^2 + 2\nabla\theta_a.\nabla\theta_v\Big]\Bigg\}. \end{aligned} \tag{4–78}$$

This leaves out some terms which just depend on θ_v which we will take into account later. For the time being we vary the action with respect to θ_a and write down the corresponding Euler-Lagrange equation,

$$\frac{\partial^2\theta_a}{\partial t^2} - \frac{g}{m}\nabla.\left(\rho_s\nabla\theta_a\right) + \Omega\frac{\partial^2\theta_a}{\partial t\partial\phi} + \Omega^2\frac{\partial^2\theta_a}{\partial\phi^2} = -\frac{\partial^2\theta_v}{\partial t^2} + \frac{g}{m}\nabla\rho_s(r).\nabla\theta_v - \Omega\frac{\partial^2\theta_v}{\partial t\partial\phi} - \Omega^2\frac{\partial^2\theta_v}{\partial\phi^2}, \tag{4–79}$$

The analytic part of the phase can in principle be solved from the Green's function of the generalized, inhomogeneous wave equation above: $\theta_a(\mathbf{x}, t) = \int dt' d^2x' G(\mathbf{x}, \mathbf{x}'; t, t')f(\mathbf{x}', t')$ where $f(\mathbf{x}, t)$ is the source function in terms of the vortex phase, on the right hand side of Eq. (4–79). This part of the action therefore has the structure,

$$S_a = \frac{\hbar^2 R_z}{2g}\int dt\, dt' \int d^2x\, d^2x'\, G(\mathbf{x}, \mathbf{x}'; t, t')f(\mathbf{x}, t)f(\mathbf{x}', t'). \tag{4–80}$$

Now reassembling all the pieces in the action, we have the form,

$$S = S_m + S_a - \int dt V_v(\mathbf{x}_v) + S_2^v + S_4^v, \tag{4–81}$$

Here S_m is the Magnus term [called S_1 in Eq. (4–68)], V_v is the vortex potential described in the previous section, and the other pieces are defined as

$$\begin{aligned} S_2^v &= \frac{\hbar^2}{2g}\int dt \int d^2x \left(\frac{\partial \theta_v}{\partial t}\right)^2, \\ S_4^v &= -\frac{\hbar^2}{2g}\int dt \int d\mathbf{x}\left[2\Omega \frac{\partial \theta_v}{\partial \phi}\frac{\partial \theta_v}{\partial t} + \Omega^2\left(\frac{\partial \theta_v}{\partial \phi}\right)^2\right]. \end{aligned} \tag{4–82}$$

Here S_2^v and S_4^v are the vortex part of the expressions S_2 and S_4 defined earlier in Eq. (4–68) and correspond to the static vortex mass and the noninertial terms respectively, as discussed in a pervious paragraph. S_a is the only nonlocal piece in the action of a vortex, the determination of which would require a solution of the Green's function.

Calculation of the Green's function for the rotating wave equation in the neighborhood of a vortex. We replace the superfluid density by its constant value at the vortex position i.e. $\rho_s(\mathbf{x}_v)$ in Eq. (4–79). The wave speed is thus determined by the density of the condensate at the vortex position. This homogenizing assumption is plausible because most of the contribution to the energy/action of the condensate comes from near the vortex as the superfluid velocity falls away as $1/r$ far from the vortex.

The computation of the Green's function for the solution of Eq. (4–79) is rendered nontrivial by the presence of the terms involving derivative with respect to the azimuthal angle. These arise because of the rotation of the trap. We propose to solve the problem through a separation of variables in a cylindrical system of coordinates in the real space. By Fourier transforming to frequency space in time and separating the radial and azimuthal coordinates, the Green's function can be written as

$$G(\mathbf{x}-\mathbf{x}') = \frac{1}{2\pi}\sum_{m=-\infty}^{\infty} g_m(\rho,\rho';\omega)e^{im(\phi-\phi')}, \tag{4–83}$$

where the m takes all integer values to preserve the periodic boundary condition in the azimuthal direction. Inserting this into the equation for the Green's function resulting

from Eq. (4–79), and which is written as

$$\left(-\omega^2 - c^2\nabla^2 + i\omega\Omega\frac{\partial}{\partial\phi} + \Omega^2\frac{\partial^2}{\partial\phi^2}\right) G(\mathbf{x}-\mathbf{x}') = -\frac{2\pi}{\rho}\delta(\rho-\rho')\delta(\phi-\phi'), \tag{4–84}$$

we obtain a differential equation for the radial part of the Green's function:

$$\frac{1}{\rho}\frac{\partial}{\partial\rho}\left(\rho\frac{\partial g_m}{\partial\rho}\right) - \left(\frac{\omega_m^2}{c^2}\frac{m^2}{\rho^2}\right) g_m = -\frac{2\pi}{\rho}\delta(\rho-\rho'). \tag{4–85}$$

Here $\omega_m \equiv \sqrt{\omega^2 + m\omega\Omega + m^2\Omega^2}$. When $\rho \neq \rho'$, the above corresponds to a modified Bessel's equation whose general solution is a linear combination of the modified Bessel's functions of the first and second kind. Now by integrating over the jump discontinuity in the derivative at $\rho \neq \rho'$ and ensuring the appropriate conditions for a well-behaved function (i.e. function decays to zero sufficiently far away and remains finite at the origin), we obtain an expression for the Green's function as

$$G(\mathbf{x}-\mathbf{x}';\omega) = \sum_{m=-\infty}^{\infty} I_m\left(\frac{\omega_m\rho_<}{c}\right) K_m\left(\frac{\omega_m\rho_>}{c}\right) e^{im(\phi-\phi')}. \tag{4–86}$$

This in principle would let us calculate the contribution of the phonon part to the hydrodynamic action, which after integrating out the phonons and the spatial coordinates, would give an action in terms of the vortex coordinates that is nonlocal in time.

Vortex dynamics in a nonrotating frame. The problem of vortex dynamics becomes tractable in the special case where the trap is not rotating, i.e. $\Omega = 0$. While this does not allow for the metastability of the vortex at the center of the trap, and therefore no possibility of the macroscopic quantum tunneling of the vortex, it reveals explicitly the nonlocal nature of the action of the vortex, and shows that the vortex mass is in fact frequency dependent. In the absence of rotation, the analytic part of the phase satisfies an inhomogeneous wave equation obtained by setting $\Omega = 0$ in Eq. (4–79):

$$\frac{\partial^2\theta_a}{\partial t^2} - c^2\nabla^2\theta_a = -\frac{\partial^2\theta_v}{\partial t^2}. \tag{4–87}$$

The Green's function for this wave operator has the familiar form

$$G(\mathbf{q},\omega) = \frac{1}{-\omega^2 + c^2 q^2}, \tag{4–88}$$

in frequency space, and the corresponding part of the action S_a [defined in Eq. (4–78)] can be expressed as

$$S_a = R_z \frac{\hbar^2}{2g} \int dt\, dt' \int d\mathbf{q} - \frac{\partial^2 G(\mathbf{q}; t-t')}{\partial t^2} \frac{\partial \theta_v(\mathbf{q}, t)}{\partial t} \frac{\partial \theta_v(-\mathbf{q}, t')}{\partial t'}, \tag{4–89}$$

where we have used integration by parts to transfer the two time derivatives to the Green's function from the source functions given in terms of the vortex phase. We have to be careful while integrating by parts as the vortex phase is a nonanlytic function. The spatial Fourier transform of the source function is given by

$$\frac{\partial \theta_v}{\partial t}(\mathbf{q}, t) = \frac{e_v h}{m} \epsilon_{ij} \frac{q_i}{q^2} (v_v)_j e^{-i\mathbf{q}.\mathbf{x}_v(t)}, \tag{4–90}$$

where ϵ_{ij} is the completely antisymmetric tensor in 2D. Inserting the above expression into Eq. (4–89) and using the Green's function from Eq. (4–88), we get

$$S_a = R_z \frac{\hbar^2}{2g} \int dt\, dt' \mathbf{v}_v(t) \cdot \mathbf{v}_v(t') F(\mathbf{x}_v(t) - \mathbf{x}_v(t'), t - t'), \tag{4–91}$$

where we have defined the kernel as an integral in frequency space as

$$F(\mathbf{x}, t) = \int \frac{d\mathbf{q}}{q^2} e^{-i\mathbf{q}.\mathbf{x}} \int \frac{d\omega}{2\pi} \frac{\omega^2}{-\omega^2 + c^2 q^2} e^{i\omega t}. \tag{4–92}$$

This integral can be easily evaluated after separating out a local piece using partial fractions

$$\begin{aligned} F(\mathbf{x}, t) &= \int \frac{d\mathbf{q}}{q^2} e^{-i\mathbf{q}.\mathbf{x}} \int \frac{d\omega}{2\pi} \left(-1 + \frac{q^2 c^2}{-\omega^2 + c^2 q^2} \right) \\ &= -F_0(\mathbf{x})\delta(t) + F_1(\mathbf{x}, t), \end{aligned} \tag{4–93}$$

where

$$F_1(\mathbf{x}, t) = \frac{\pi c\, \theta(ct - |\mathbf{x}|)}{\sqrt{c^2 t^2 - |\mathbf{x}|^2}} \tag{4–94}$$

is the usual retarded Green's function for a wave equation in 2D. The local piece of the action obtained from F_0 actually cancels the term S_2^v corresponding to static vortex mass, and defined in Eq. (4–82). The total action for a vortex moving in a nonrotating trap can then be written as

$$S = S_m - \int dt\, V_v(\mathbf{x}_v) + \frac{\pi\hbar^2\rho_s R_z e_v^2}{2m^2c} \int dt\, dt' \frac{\mathbf{v}_v(t).\mathbf{v}_v(t')\ \theta(c(t-t') - |\mathbf{x}-\mathbf{x}'|)}{\sqrt{c^2(t-t')^2 - |\mathbf{x}-\mathbf{x}'|^2}}. \quad (4\text{–}95)$$

It involves terms corresponding to the Magnus force or Berry's phase, the potential from the trap felt by the vortex, and interestingly, a nonlocal inertial term obtained by integrating out the phonon part of the phase. This is intuitively understood to be a coupling of the vortex with itself at some earlier time mediated by the phonons excited by the motion of the vortex.

The vortex mass can be calculated from this inertial term in the limit where the vortex moves very slowly relative to the sound speed such that $c(t-t') \gg |\mathbf{x}-\mathbf{x}'|$ is always satisfied. This gives the dynamic vortex mass as

$$M_v \sim \frac{\pi\hbar^2\rho_s R_z e_v^2}{2m^2c^2} \ln(\omega\tau), \quad (4\text{–}96)$$

where ω is some frequency characteristic of the vortex dynamics, and τ is some cutoff time scale introduced to regulate the divergence in the time integral. It can be identified with a small time scale in the system, $\tau \sim R/c$, where R is the size of the condensate and c, the speed of sound. This logarithmic behavior can also be reproduced from a local expansion of the general, real space Green's function obtained in Eq. (4–86). By setting $\Omega = 0$ and expanding for small ω, we see that the dominant contribution is from the $m = 0$ term in the sum. The asymptotic behavior for the modified Bessel's functions for small argument is $K_0(x) \sim -\ln(x)$ for small x and $I_0(0) = 1$. On making a low frequency approximation (which corresponds to the long time interval approximation used above), the inertial term is found to depend logarithmically on frequency.

This feature of a nonlocal inertial term which contributes a “mass’ that is logarithmically divergent in frequency is also expected to hold in a general, rotating trap. So we have derived the dynamics of the vortex from the underlying hydrodynamic theory and have identified the three main factors that determine its dynamics: the Magnus force, the vortex potential, and the nonlocal inertial term which can be identified with a mass on making a local approximation. This is sensible in the limit that the vortex velocity is small compared to the speed of sound in the system. In such a situation, therefore, it is possible to write down an equation of motion of the vortex as if it were a point particle obeying Newtonian mechanics. We have therefore started from a continuum theory, integrated out various modes, and obtained the Lagrangian of a single particle.

CHAPTER 5
MACROSCOPIC QUANTUM TUNNELING OF A VORTEX IN A ROTATING BOSE GAS

A superfluid vortex in a large condensate is a macroscopic object expected to behave classically. This is because the vortex core contains a large number of atoms when the condensate density is high, and so is described by a many-body wavefunction with many degrees of freedom. In Chapter 4, we derived the dynamics of a vortex using purely classical considerations. This is legitimate because Bose-Einstein condensation leads to a macroscopic quantum state that can be described by a classical field theory featuring a single scalar wavefunction, as is done in the Gross-Pitaevskii formalism for BEC at zero temperature. The classical dynamics of a single vortex in a rotating BEC have been worked out in Refs. [100, 101] as also in Chapter 4. Here we consider the possibility of quantum tunneling of a vortex.

The tunneling of microscopic particles through some classically forbidden region is a well-known quantum phenomenon. Additionally, the superposition of macroscopic states is key to the foundations of quantum mechanics. The direct experimental evidence of this would be the tunneling of a macroscopic object [116], such as a vortex. The search for such macroscopic quantum tunneling (MQT) has had some success in the context of strongly correlated systems, such as superconducting Josephson junctions [117], but has not been observed in a BEC. Previous authors have discussed the possibility of tunneling of a single vortex between pinning sites in BEC in a trap [118], or in general, two-dimensional, superfluids [119–121]. In this chapter, we will consider the yet-unexplored question of tunneling of a single vortex in a trapped BEC through the potential barrier created by the rotation of the trap [100, 103].

In the first section, we introduce the general theory of the classical dynamics of a vortex treated as a point particle, and establish an analogy with a charged particle traveling in a magnetic field. We then determine the probability of quantum tunneling of a vortex from semiclassical considerations in the second section. The quantum

mechanics of a slowly-moving vortex could be described by the Schrödinger equation of a charged particle in a magnetic field, and the tunneling event can then be described in a WKB framework. However, our derivation in Chapter 4 of the full action of a vortex, shows that there are nonlocal contributions to the vortex inertia from the couplings with the phonon modes it excites during its motion. In this case, simple WKB methods fail, and we have to resort to more sophisticated tools like the "instanton" method. We introduce this method and sketch out a possible tunneling calculation. Finally, we discuss the feasibility of setting up actual experiments in rotating traps of ultracold atoms, with observable rates of tunneling for a single vortex.

5.1 Classical Mechanics of a Vortex

A vortex can be thought of as a point mass in the 2D plane, whose motion is described by a Newton's law of the form

$$M_v \ddot{\mathbf{x}}_v(t) = \mathbf{F}_\perp + \mathbf{F}_{||} + \mathbf{F}_{ext} \tag{5–1}$$

where M_v is the "mass" associated with the vortex, $\mathbf{x}_v$ is the position coordinate of the vortex in the $x-y$ plane, and the terms on the right hand side correspond to various forces, whose exact forms and physical origins we now discuss in turn. The exact value of the vortex mass is controversial, and has been found to take values from zero to infinity by different authors! For the purposes of this chapter, we assume a finite value for the vortex mass.

The term $\mathbf{F}_\perp$ consists of forces which act transverse to the vortex velocity, and have a form akin to the Lorentz force acting on an electric charge moving in a magnetic field . The superfluid Magnus force (see derivation in Section 4.3.1), an exact analog of the Magnus force felt by rotating objects moving in classical fluids, is one such transverse force having the form

$$\mathbf{F}_M = \rho_s \kappa \times (\dot{\mathbf{x}}_v - \mathbf{v}_s). \tag{5–2}$$

The ρ_s above is the 2D superfluid density (the Magnus force in classical fluids depends exactly in the same way on the total fluid density). We call the quantized circulation of the superfluid velocity around a vortex, κ, and it is given by

$$\kappa = \frac{e_v h}{m}\hat{z}, \tag{5–3}$$

where e_v is the charge or winding number of the vortex, and m the mass of each constituent particle, which could be atoms in a trapped BEC, or helium atoms in strongly correlated liquid He. Another transverse force suggested by some authors (but disputed by others) is the Iordanskii force [122], which has the same form as the Magnus force above but arises from the motion of the vortex relative to the normal fraction of the fluid:

$$\mathbf{F}_l = \rho_n \kappa \times (\dot{\mathbf{x}}_v - \mathbf{v}_n). \tag{5–4}$$

The motion of the vortex relative to the normal fluid also subjects it to a longitudinal damping force written as

$$\mathbf{F}_{||} = -\gamma(\dot{\mathbf{x}}_v - \mathbf{v}_n). \tag{5–5}$$

The damping constant $\gamma(T)$ is strongly dependent on temperature. This arises from vortex interaction with the quasiparticles in the normal fraction. We confine the rest of our discussion to the zero temperature limit, where the Gross-Pitaevskii description is applicable. Here the entire system is in the condensed or superfluid phase, and we steer clear of the controversy surrounding the Iordanskii force. The damping force described above is also absent. Other forces on the vortex could arise from external sources, such as the effective potential $V_v(r)$ felt because of the trap, and pinning forces from impurities

$$\mathbf{F}_{ext} = -\nabla V_\mathrm{v} + \mathbf{F}_\mathrm{pinning}. \tag{5–6}$$

We are mostly interested in the effect of the trap and its rotation. The external force is then just the gradient of the potential experienced by the vortex in a rotating, isotropic trap (found in Chapter 4) . So at zero T, after ignoring the effects of dissipation and

pinning, the classical dynamics of the vortex treated as a single particle, is dictated by the Magnus force and the trap-dependent potential. This is summed up in a simple Newton's law, which essentially describes the classical dynamics of a charged particle in a plane with a non-uniform magnetic field[1] in the Magnus force acting perpendicular to it and in the presence of a central potential,

$$M_v \ddot{\mathbf{x}}_v(t) = \rho_s(\kappa \times \dot{\mathbf{x}}_v) - \nabla V_v. \tag{5–7}$$

The energy cost of creating a vortex at an arbitrary position in a rotating trap was found earlier to be

$$V_v(\mathbf{r}) = V_0\left[\left(1 - \frac{r^2}{R^2}\right)^{3/2} - \frac{\Omega}{\Omega_c}\left(1 - \frac{r^2}{R^2}\right)^{5/2}\right], \tag{5–8}$$

where the symbols have their pre-defined meanings.

For the sake of completeness, we now review the Lagrangian mechanics of the analogous problem of a charge traveling in a magnetic field and subject to a central potential. The Lagrangian for such a particle (free to move in the plane perpendicular to the magnetic field) in cylindrical coordinates is

$$\mathcal{L}(r, \phi; \dot{r}, \dot{\phi}) = \frac{1}{2}M(\dot{r}^2 + r^2\dot{\phi}^2) - V(r) + q\mathbf{A} \cdot \mathbf{v}, \tag{5–9}$$

where $\mathbf{A} \equiv Br\hat{\phi}/2$ is the magnetic vector potential in the symmetric gauge, $V(r)$ is a general central potential in 2D, and the rest of the symbols have their usual meanings. The symmetric gauge is a natural choice in a central potential where the x and y-directions are on equal footing.

[1] We will use the term "magnetic field" interchangeably with the "field" $\rho_s h/m$ corresponding to the Magnus force, throughout this chapter

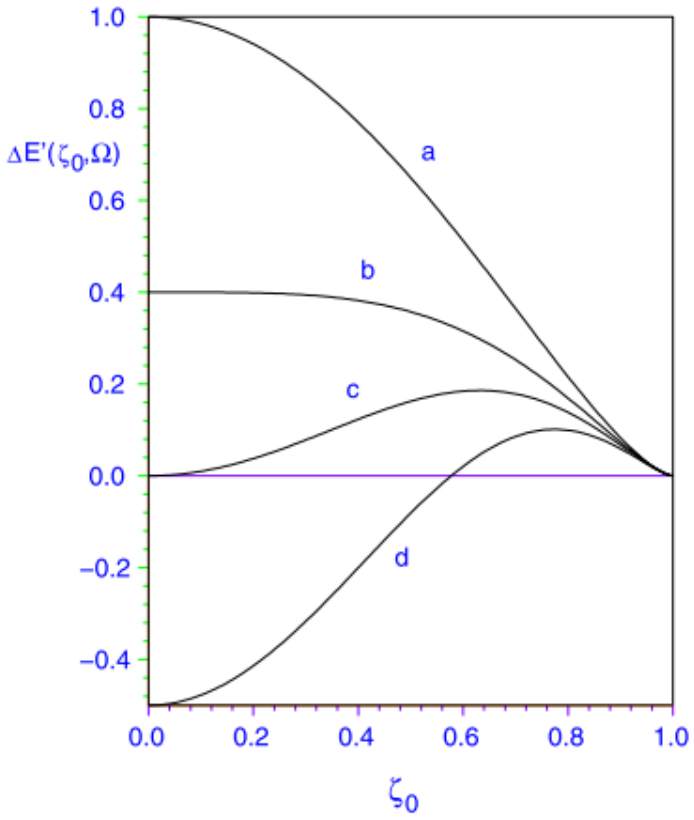

Figure 5-1. Energy cost (nondimensionalized) associated with a singly quantized straight vortex in a rotating asymmetric trap in the TF limit as a function of a fractional vortex displacement ζ_0 from the symmetry axis. Different curves represent different fixed values of the external angular velocity (a) $\Omega = 0$ (unstable); (b) $\Omega = \Omega_m$ (the onset of metastability at theorigin); (c) $\Omega = \Omega_c$ (the onset of stability at the origin); (d) $\Omega = \frac{3}{2}\Omega_c$. In the metastable regime, $\Omega_m < \Omega < \Omega_c$, there is a barrier through which the vortex can tunnel outwards from the central minimum. Reprinted with permission from Ref. [38] [A. L. Fetter, J. Phys.: Condens. Matter **13** R135 (2001)], ©IOP, 2001.

The azimuthal angle ϕ is a cyclic variable in the above Lagrangian, and Noether's theorem suggests the conservation of a corresponding angular momentum as

$$\frac{\partial \mathcal{L}}{\partial \dot{\phi}} = \text{constant} \quad \Rightarrow \quad Mr^2\dot{\phi} + \frac{1}{2}qBr^2 = L$$
$$\Rightarrow \quad \dot{\phi} = \frac{L}{Mr^2} - \frac{1}{2}\omega_c \ , \tag{5–10}$$

where the constant is an angular momentum called L, and $\omega_c \equiv qB/M$ is the cyclotron frequency in SI units.

We can then use this expression for the angular velocity to find another constant from the equations of motion, in terms of the radial coordinate alone, as

$$\frac{1}{2}M\dot{r}^2 + V(r) + \frac{1}{8}M\omega_c^2 r^2 + \frac{L^2}{2Mr^2} = \text{constant}, \tag{5–11}$$

which is basically the energy conservation equation for a particle traveling in 1D in an effective potential, $V_{eff}(r) = V(r) + M\omega_c^2 r^2/2 + L^2/2Mr^2$, that has contributions from the magnetic field and the centrifugal barrier. The exact trajectory of the particle could then be solved in principle by quadrature. This derivation further suggests that the problem in a central potential is still separable in radial and azimuthal coordinates, and can be reduced to an effectively 1D problem, even in the presence of a magnetic field. This has important implications for the tunneling calculation.

When the magnetic field is very low, the particle trajectory would be slightly perturbed by the small magnetic field from the usual elliptical orbit expected in a central potential. When the magnetic field is very high, the inertial term may be neglected in the equation of motion, and then the particle simply moves along the equipotential lines. These are just circles in the case of a central potential. For the vortex in a trapped BEC, this would mean a precession around the center of the trap at a frequency which is determined by balancing the gradient of the potential against the Magnus force,

$$\nabla V \simeq e_v \mathbf{v} \times \mathbf{B}. \tag{5–12}$$

If the magnetic field in the case being considered is perpendicular to the plane of the particle's motion, the above equation implies that the motion is perpendicular to the gradient of the potential, i.e., along equipotential lines. Let us now use this equation, and the expression for the "magnetic field" corresponding to the Magnus force on a vortex as found in Eq. (4–72), to predict the velocity of a vortex in the potential of a rotating harmonic trap given by Eq. (5–8). The vortex is then found to move in circles around the center of the trap. Its speed has a somewhat complicated dependence on the radial

position of the vortex in the trap :

$$\mathbf{v}_v = \frac{4e_v h}{MR^2} \ln\left(\frac{R}{|e_v|\xi}\right)\left[\sqrt{\frac{n(0)}{n(r_v)}} - \frac{\Omega}{\Omega_m}\sqrt{\frac{n(r_v)}{n(0)}}\right](\hat{z}\times\hat{r}), \tag{5–13}$$

where $n(r)$ is the Thomas-Fermi (TF) density profile of the condensate, Ω is the trap rotation frequency, Ω_m the metastable frequency found earlier, and the rest of the symbols having their predefined meanings. This result has been found in a different form by a more detailed analysis involving matched asymptotic solutions of the dynamic GP equation near and far away from the vortex, by Rubinstein and Pismen for general superfluids in 1994 [123], and by Fetter and Svidzinsky for similar trapped BECs in 2000 [101]. The latter authors also look at the general case of asymmetric traps and curved vortex lines, and reach essentially similar conclusions. The vortex is thus seen to precess around the center of the trap, with a precession frequency that depends on the radius of the vortex orbit. This frequency near the center of the trap is found to be

$$\omega_p \simeq \frac{4e_v h}{MR^2} \ln\left(\frac{R}{|e_v|\xi}\right)\left[1 - \frac{\Omega}{\Omega_m}\right]. \tag{5–14}$$

Thus, a positive vortex precesses in a counterclockwise direction when the trap is rotated at a frequency higher than the metastability ($\Omega > \Omega_m$), and clockwise when lower than it. There is no precession when rotated at metastability, and the vortex energy profile flattens. We have to remember that this is with respect to the rotating frame of the trap.

Further, it is useful to compare the precession frequency with other time scales in the system. We see that the precession frequency is approximately a factor of $(1 - \Omega/\Omega_m)$ times the metastable angular velocity. Therefore, if the trap is rotated near metastability, the precession is very slow (as pointed out earlier). The precession frequency depends directly on the potential gradient but inversely on the effective magnetic field. This is in some sense the reverse of the magnetic cyclotron frequency $\omega_c = qB/M$, which is directly proportional to the magnetic field. A small value of

precession frequency relative to the cyclotron frequency ($\omega_p \ll \omega_c$) then suggests a high magnetic field limit. The corresponding trajectory is a slow circular precession around the center of the trap, and rapid cyclotron oscillations in tight circles superimposed on it, which go away on averaging - leading to the equipotential circular orbits expected in the high field case. The ratio of the precession and the cyclotron frequencies is therefore a useful quantity that can be estimated from experimental parameters.

Also the precession frequency or velocity of the vortex seems to increase with increasing distance from the center of the trap as the gradient of the potential is sharper, and the Magnus force becomes weaker further out. Of course, beyond a certain distance the "high magnetic field" approximation above fails, and the vortex inertia begins to contribute to its trajectory. In our present analysis, we are interested in outward tunneling of the vortex from the metastable minimum at the center of the trap ... so we expect to remain in the high magnetic field limit discussed above as long as there is a high enough condensate density at the center of the trap.

5.2 Semiclassical Estimates of Vortex Tunneling

A vortex, though macroscopic, is a quantum object, especially at low T. Its quantum dynamics is rigorously described through the evolution of its density matrix [124] which in the classical limit yields a Newton's law of the form given in Eq. (5–7). When treated as a single particle as done so far in this chapter, we ought to be able describe it using a Schrödinger's equation, which then yields the quantum mechanics of a charged particle in a magnetic field.

5.2.1 Schrödinger Equation for a Charge in a Magnetic Field

The time-independent Schrödinger equation in 2D for a charged particle in a magnetic field $B\hat{\mathbf{z}}$ and potential $V(r)$ is

$$\left[\frac{1}{2M}\left(i\hbar\nabla - q\mathbf{A}\right)^2 + V(r)\right]\psi = E\psi. \tag{5–15}$$

In the symmetric gauge of the magnetic vector potential, $\mathbf{A} = \frac{1}{2}Br\hat{\phi}$, and the Schrödinger equation takes the form,

$$\left[-\frac{\hbar^2}{2M}\nabla^2 + \frac{\omega_c}{2}\mathbf{r}\times\left(i\hbar\nabla\right) + \frac{1}{8}M\omega_c^2 r^2 + V(r)\right]\psi = E\psi, \tag{5–16}$$

where $\omega_c = qB/M$ is the cyclotron frequency for particle in the magnetic field. As the potential is central, the wavefunction can be separated into radial and angular parts as

$$\psi(r,\phi) = f(r)e^{il\phi}, \tag{5–17}$$

where l is the angular momentum quantum number. The Schrödinger equation for the radial part looks like

$$\frac{\hbar^2}{2M}\left(\frac{d^2f}{dr^2} + \frac{1}{r}\frac{df}{dr}\right) = \left[E' - V_{eff}(r)\right]f(r), \tag{5–18}$$

where $E' = E + \frac{1}{2}l\hbar\omega_c$, and the trap potential is modified by the centrifugal barrier from angular momentum as well as the magnetic field as

$$V_{eff}(r) = V(r) + \frac{1}{8}M\omega_c^2 r^2 + \frac{l^2\hbar^2}{2Mr^2}. \tag{5–19}$$

This corresponds exactly to the Lagrangian mechanics of a charged particle in a magnetic field as derived in the previous section, as seen from Eq. (5–11).

5.2.2 WKB Analysis of Tunneling

The WKB [125] method is widely used to find semiclassical approximations of the quantum wave function in both the classically allowed and the forbidden regions of quantum mechanics problems in 1D[2] . Note that although our problem is in 2D, the potential is central which allows a separation of variables, and we end up with an effectively 1D problem in the radial direction. We carry out an expansion of the radial

[2] Generalizations to multidimensional problems is possible but is usually more involved.

wave function in terms of a small parameter related to the Planck's constant as [126]

$$\begin{aligned} \epsilon^2 &= \frac{\hbar^2}{2M}, \\ f(r) &\sim e^{S_0(r)/\epsilon + S_1(r) + \mathcal{O}(\epsilon)}, \\ \frac{df}{dr} &\sim \left(\frac{S_0'}{\epsilon} + S_1'\right) f(r), \\ \frac{d^2 f}{dr^2} &\sim \left[\frac{S_0''}{\epsilon} + S_1'' + \left(\frac{S_0'}{\epsilon} + S_1'\right)^2\right]. \end{aligned} \tag{5–20}$$

Substituting the perturbative expansion in Eq. (5–20) into the Schrödinger equation stated in Eq. (5–18), we get

$$\begin{aligned} \mathcal{O}(1): &\qquad \left(S_0'\right)^2 = V_{eff}(r) - E', \\ \mathcal{O}(\epsilon): &\qquad S_0'' + 2S_0' S_1' + \frac{S_1'}{r} = 0. \end{aligned} \tag{5–21}$$

The probability of tunneling into the classically forbidden region of the potential is then given by

$$\Gamma = Ae^{-B/\hbar}, \tag{5–22}$$

where the tunneling exponent B is identified with the leading order term S_0 in the WKB expansion above, and A is a prefactor to be determined separately. Therefore,

$$B = \int_{r_i}^{r_f} \sqrt{2M(V_{eff}(r) - E')}, \tag{5–23}$$

where r_i and r_f are the classical turning points. The most famous historical application of this expression was to the problem of alpha decay by tunneling in a nucleus worked out by Gamow.

The exact evaluation of the turning points and also the integral itself has to be carried out numerically because of the complicated form of the vortex potential (and the added centrifugal barrier term), but it is possible to analytically estimate this using an approximate form of the vortex potential. We begin by noticing that higher rates of tunneling are expected when the trap is being rotated close to metastability, because the

potential barrier height is lower (and also narrower) at such frequencies. Let us focus on this regime by defining a relevant small parameter, $\epsilon = \Omega/\Omega_m - 1$. This implies that the turning points, and the tunneling phenomenon itself, are situated near the center of the trap, and so it is instructive to expand the vortex potential in Eq. (5–8) in the radial coordinate as

$$\begin{aligned} V_v(r) &= V_0\left[\left(1-\frac{r^2}{R^2}\right)^{3/2} - \frac{3}{5}(1+\epsilon)\left(1-\frac{r^2}{R^2}\right)^{5/2}\right] \\ &\simeq V_0\left[1+\frac{3}{5}(1+\epsilon)+\frac{3}{2}\epsilon\frac{r^2}{R^2}-\frac{3}{4}\frac{r^4}{R^4}+\mathcal{O}\left(\frac{r^6}{R^6}\right)\right]. \end{aligned} \tag{5–24}$$

The magnetic field contributes a term quadratic in r to the effective potential in Eq. (5–19) and so for the zeroeth angular momentum state, the effective potential is still a quartic, written as $(ar^2 - br^4)$, where a and b are positive constants that depend on various trap parameters. The coefficient of the quadratic term, a, is renormalized by the cyclotron frequency or magnetic field, and dominates the contribution for higher magnetic fields. This form of the potential is valid for small radial distances, has the structure of a barrier through which tunneling can take place, and lets us calculate an approximate expression for the tunneling probability in a closed form quite simply, at least for the zero angular momentum ($l = 0$) channel.

In this simple tunneling calculation, we assume the initial energy of the vortex to be the same as its potential energy at the origin. The classical turning points are then the origin itself, $r_i = 0$, and the point determined by the trap parameters, $r_f = \sqrt{a/b}$. The tunneling exponent in Eq. (5–23) is then given by

$$B \simeq \int_0^{\sqrt{\frac{a}{b}}} dr\sqrt{2M(ar^2-br^4)} = \frac{\sqrt{M}(2a)^{3/2}}{3b}. \tag{5–25}$$

The dependence of this estimate for the tunneling probability exponent on the magnetic field is of particular interest to us. Recall from the form of the effective potential in Eq. (5–19), and the short distance expansion of the potential in Eq. (5–24), that the

exact forms of the coefficients a and b in our model potential, are given as

$$a = \frac{3}{2}\frac{\epsilon V_0}{R^2} + \frac{1}{8}M\omega_c^2, \quad b = \frac{3}{4}\frac{V_0}{R^4}. \tag{5–26}$$

Using these expressions, we find the approximate expressions for the tunneling probability exponent in various limiting cases from Eq. (5–25) as

$$B \simeq \frac{8}{9}\sqrt{2MV_0}R\epsilon^{\frac{3}{2}}\left[1 + \mathcal{O}\left(\frac{\omega_c^2}{\omega_t^2}\right)\right], \tag{5–27}$$

for "low" magnetic fields, and

$$B \simeq \frac{1}{12}\sqrt{2MV_0}R\left(\frac{m\omega_c^2R^2}{V_0}\right)^{\frac{3}{2}}\left[1 + \mathcal{O}\left(\frac{\omega_t^2}{\omega_c^2}\right)\right], \tag{5–28}$$

for the "high" field limit. Here, $\omega_t \simeq \sqrt{(\epsilon V_0/MR^2)}$ is some characteristic frequency that depends on trap parameters and is in fact similar to the precession frequency ω_m found in Eq. (5–14).

In this calculation, the field is said to be "low" ("high") if the cyclotron frequency ω_c is much smaller (bigger) than the characteristic frequency ω_t. These results suggest that the tunneling can be appreciable in lower magnetic fields, and is given by a "three-halves law" in ϵ, the shift in angular frequency of trap rotation from the onset of metastability; whereas the tunneling for high magnetic fields is exponentially suppressed as a power of the magnetic field. The high field result is consistent with our expectation that the particle moves in equipotential lines at high field and there is negligible tunneling in the radial direction. The low field, particularly the zero field, result is useful in that it establishes an upper bound on the tunneling probability. We should remark here that very high magnetic fields, would actually change the character of the potential barrier so that the small distance expansion as a quartic potential is no longer valid, and the above calculation breaks down.

So far we have addressed tunneling in the $l = 0$ angular momentum channel. This is where we expect maximum tunneling probability, as the centrifugal barrier suppresses

tunneling for higher angular momentum states. It is in fact possible to estimate a critical value of l at which the effective potential changes its shape and no longer possesses a metastable minimum to tunnel from. This is obtained using the model quartic effective potential and a criterion for the number of roots of a corresponding cubic equation. It is expressed in terms of the potential coefficients as

$$l_{critical} = \left[\sqrt{\frac{2}{27}} \frac{1}{\hbar} \sqrt{\frac{ma^3}{b}} \right], \tag{5–29}$$

where the square brackets above imply the 'greatest integer less than or equal to the quantity within the brackets. For typical values of the trap parameters, this actually does work out to $l = 0$ further confirming that this is the only channel which sees any tunneling of interest.

The WKB estimates help to establish an upper bound on the tunneling rate with a zero- or low- magnetic field estimate, and also confirm our expectation that tunneling is suppressed for higher magnetic fields. This is all there is to a problem of tunneling of a charged particle in a magnetic field and in the presence of an isotropic potential. However, so far we have not taken into account the nonlocal or "memory" effects in the action of the vortex, which result from the coupling of its motion to phonons. The problem of tunneling when the action has nonlocal terms in it will require tools beyond the WKB description, which we then describe in the next subsection.

5.2.3 The Method of "Instantons" or "Bounce" Trajectories

An oft-used approach to calculate the probability of a quantum tunneling event is to compute the action of the system along its classical path between the turning points. Quantum fluctuations around this classical path (found by a minimization of the action), computed in a saddle point approximation, then help determine the prefactor A in the expression for tunneling probability stated earlier in Eq. (5–22). The factor B in the exponent here is then just the action corresponding to the classical path. This method has been described by Coleman [127] and other workers in a field theoretic context,

who have applied it elegantly to solve the tunneling problem in double well potentials. The technique been called the “method of instantons”, after the classical solutions of field theories, which are localized in space-time like solitons in space. The classical path between the turning points in the tunneling problem is also sometimes called a “bounce” trajectory, as the particle is imagined to “bounce” back and forth between these points.

We introduce this method for a simple action for a particle in a 1D potential, where the Lagrangian can be written as $\mathcal{L} = m\dot{x}^2/2 - V(x)$. Let us now consider this action and the consequent equations of motion in imaginary or euclidean time. This effectively maps the problem to one with a negative or inverted potential, and the potential “barrier” (classically forbidden region) between the classical turning points becomes a potential “well” (classically accessible region). The Euclidean action between these two turning points (chosen to be x_i and x_f) is then computed as

$$S_E = \int_{-\infty}^{0} d\tau \Big[\frac{1}{2}M\Big(\frac{dx}{d\tau}\Big)^2 + V(x)\Big], \tag{5–30}$$

with the boundary conditions chosen as $x(-\infty) = x_i$, and $x(0) = x_f$. The Euler-Lagrange equations yield the total energy as an integral of motion

$$\frac{1}{2}M\Big(\frac{dx}{d\tau}\Big)^2 - V(x) = E, \tag{5–31}$$

where $E = V(x_i) = V(x_f)$. This reference energy level can be set to zero without any loss of generality, $E = 0$. This energy conservation relation can be used to derive a quadrature condition as

$$\frac{dx}{d\tau} = \sqrt{2MV(x)}, \tag{5–32}$$

which can then be used to re-express the action in Eq. (5–30) as an integral over space instead of time, as

$$S_E = \int_{x_i}^{x_f} dx \sqrt{2MV(x)}. \tag{5–33}$$

Thus for an action with this simple form, we obtain the same expression for the tunneling probability B as by the WKB method seen in Eq. (5–23) with energy set to zero.

The role of the magnetic field in tunneling becomes intuitively apparent from this instanton picture. The magnetic field tends to curve any classical path that might try to proceed in a radially outward direction, thus suppressing tunneling under an isotropic barrier. This effect becomes very pronounced in the high magnetic field limit, where the particle just moves along circular equipotential lines in a central potential. This suggests, discouragingly for us, that the semiclassical probability of tunneling tends to zero in the high magnetic field limit.

The full action for a vortex can however have nonlocal (in time) inertial terms as seen in Chapter 4. This action can then be written as

$$\begin{aligned} S &= \int_0^\infty d\tau \left[\frac{1}{2} M \dot{r}^2 + \frac{1}{2} M r^2 \dot{\phi}^2 + V(r) \right] \\ &+ \int_0^\infty d\tau \int_0^\infty d\tau' \eta(\tau - \tau') \dot{\mathbf{x}}(\tau) \cdot \dot{\mathbf{x}}(\tau'), \end{aligned} \tag{5–34}$$

where M is the mass obtained by a local expansion of the inertia, and the residual nonlocal effects are taken into account in the kernel $\eta(\tau - \tau')$. This action could in principle be calculated numerically, but it would be a computationally intensive procedure. One would first need to numerically solve the nonlocal Euler-Lagrange equation in 2D (the problem may not be separable once the nonlocal terms are included), and then integrate them to find the action. Our hope is that even in a high magnetic field, the nonlocal terms could serve to distort the perfectly circular classical paths to enhance tunneling.

It is possible to consider simpler limiting scenarios of the above, e.g. a sufficiently slowly moving vortex for which the nonlocal terms are small and can be treated perturbatively. One then just considers the classical path for a particle in a magnetic field, which is a separable problem. The angular variable is cyclic and can be integrated out as shown in ?. This path determined without the nonlocal effects is then used to

calculate the full action as

$$\begin{aligned} S_c &= \int_0^\infty d\tau \left[\frac{1}{2} M \dot{r_c}^2 + V(r_c) + \frac{1}{8} M \omega_c^2 r_c^2 + \frac{L^2}{2 M r_c^2} \right] \\ &+ \int_0^\infty d\tau \int_0^\infty d\tau' \eta(\tau - \tau') \dot{\mathbf{x}}_c(\tau) \cdot \dot{\mathbf{x}}_c(\tau'). \end{aligned} \tag{5–35}$$

5.3 Experimental Discussion

As mentioned earlier, there are two basic experimental approaches that have been used to create and study vortices in a BEC. The first, carried out in JILA in 1999 [36], uses a mixture of two hyperfine components of ^{87} Rb, spinning one up respect to the other by applying an external electromagnetic beam. The second was performed in ENS, Paris in 2000 [37]. We will use the latter as our prototype for our discussion on vortex dynamics and tunneling in this section. They trapped around a million atoms ($N \approx 10^6$), the trapping frequency in the direction transverse to the rotation is of the order of 100 Hz (which implies a harmonic oscillator quantum length of microns $a_{ho} \approx 10^{-6}$m , and the scattering length is usually tuned to a few nanometers, $a_s \approx 10^{-9}$ m. This suggests that the parameter $\lambda \equiv N a_s / a_{ho} \approx 10^3$ is quite high, and assures us that the typical condensate in which vortices are studied in the lab is indeed described by the Thomas-Fermi (TF) approximation. Some other quantities of interest that can be estimated based on these parameters are: size or radius of the condensate, $R \approx 10 a_{ho} \approx 10^{-5}$ m; healing length or core size of a vortex , $\xi \approx 100nm$; the "mass" of a vortex as the number of atoms in the core of the vortex, $M \approx 10^3 \times m \approx 10^{-22}$ kg; the critical velocity of trap rotation at which a vortex is first nucleated, $\Omega_c \approx 100Hz$; the "cyclotron frequency" corresponding to the Magnus force at the center of the trap $\omega_c \approx 10^6$ Hz.

These quantities can be used to reach several important conclusions. Most importantly, we can calculate an upper bound on the tunneling probability. We expect the highest rates of tunneling when there is little or no magnetic field, when the tunneling

exponent B is given by $\sqrt{2mV_0}R\epsilon^{\frac{3}{2}}$, V_0 being the vortex potential at the center of the trap, and ϵ the detuning of the trap rotation frequency from the metastable frequency. It turns out that for small enough detuning ($\epsilon \approx 10^{-4}$), the tunneling exponent can be of the order of Planck's constant, $B \sim \hbar$, which is necessary for appreciable tunneling (too high a magnitude of the exponent would mean suppressed tunneling). So if our prototypical trap is rotated very close to the metastable frequency of around 100 Hz, and extremely close to it, it is possible to attain estimated tunneling times of the order of seconds!

However this "low field" estimate is not realistic, because we are in fact always in a "high field" limit in the kind of condensates in the TF regime that we are considering, and also which are relevant to most experiments on BEC in the laboratory. Intuitively, this is because the Magnus force on a vortex depends on the condensate density, which is always high in the TF regime. It is also possible to see this from quantitative estimates, by comparing the two timescales involved in the motion of the vortex. The precession frequency is roughly given by $\omega_p \sim \Omega_m|(1 - \Omega/\Omega_m)|$, and we are interested in trap rotation frequencies in the metastable regime $\Omega_m < \Omega < \Omega_c$. This means that the precession frequency is very small compared to the metastable frequency when the trap is rotated near metastability as in the previous calculation for maximum tunneling, and is at most of the order of the metastable frequency, which is of the order of 100 Hz in our prototypical experiment. The cyclotron frequency for typical trap densities is on the other hand about 1 MHz. This means that the condition $\omega_p \ll \omega_c$ is always satisfied for our range of trap parameters, and we are effectively always in the high magnetic field limit! We already argued that there is vanishingly small tunneling in the high magnetic field situation, unless perhaps the nonlocal effects in the action are taken into account.

Our overall conclusion is that the tunneling rate through the metastable potential barrier experienced by a single vortex in a rotating trap is negligible in realistic experimental scenarios. However the effects of dissipation or coupling with the phonons can possibly enhance the inertia of a vortex and lead to enhanced tunneling rates.

Another interesting possibility is pinning centers for vortices in a BEC. A recent work treats the vortex potential resulting from two pinning centers as a model double well [118]. From a more general theoretical perspective, we have realized that the problem of macroscopic quantum tunneling for a single vortex in a BEC in the TF regime, is analogous to the tunneling of an electron in a high magnetic field. This has been elegantly solved for some model potentials [128], but no general prescription exists for such a calculation. Also the very notions of vortex mass and the exact nature of its dynamics are debated topics. We hope to have provided some theoretical insights into this longstanding problem.

CHAPTER 6
CONCLUSION

In this work, we have looked at two distinct realizations of the superfluid phase - in solid helium, and in a dilute Bose-Einstein condensate in a trap. In particular, we have tried to explain the apparently superfluid response (NCRI, as observed in a torsional oscillator experiment [23]) in solid helium as an effect of defects like dislocations and grain boundaries. In BECs, we look at the stability and dynamics of vortices in a rotating trap, and estimate their tunneling probability.

We have constructed a model for a supersolid based on superfluidity induced along a network of dislocations. Starting from a Landau theory for the bulk solid, we are able to systematically derive a one-dimensional equation describing superfluidity along a single dislocation. We then consider a network of dislocations and the effect of overlap of these strands of 1D superfluid, and show that it is possible to realize a bulk superfluid order along this network structure with an onset temperature that depends on the superfluid coupling between neighboring nodes in this network. This is analogous to an array of Josephson junctions or an XY model with random bonds. This effect should be observable in superconductors, where it should be possible to calculate the various constants in the Landau theory in terms of microscopic quantities (something we cannot do for solid ^{4}He). One of our more striking results is the sensitive dependence of the transition temperature for the dislocation network on the dislocation density (i.e., the sample quality). Grain boundaries as collections of dislocations are also similarly expected to enhance superfluidity locally. We derive a dependence of the critical temperature T_c of a grain boundary superfluid on the angle of the grain boundary in two opposite limits. We also analyze the Kosterlitz-Thouless properties of a grain boundary superfluid, and show that the inherent anisotropy in the grain boundary is irrelevant as far as the superfluidity is concerned.

The procedure for estimating the shift in superfluid critical temperature caused by an edge dislocation led us to the longstanding quantum problem of a two-dimensional dipole potential. The wave functions and the spectrum are obtained by numerically solving the Schrödinger equation with the 2D dipole potential, and also variationally in the case of the ground state. We find that the results obtained from the different methods are consistent and compare favorably with previous estimates in the literature. We also discover a simple pattern in the spectrum, where the quantum number of the state varies inversely as its energy ($n \sim \epsilon^{-1}$), which can be justified from semiclassical considerations. Certain features of the spectrum and wave functions are yet to be explained and might provide scope for future investigation. For example, the statistics of the level spacings could possibly be a signature of quantum chaos. The ground state of the quantum dipole problem is related to the binding energy of elastic impurities to edge dislocation lines. This is important in the context of helium for example, as the binding of ^{3}He impurities present in solid ^{4}He can have an effect on the stiffness and heat capacity of solid helium. This is for example the basis of the dislocation-pinning picture commonly suggested to explain the shear stiffening at low temperatures seen by Beamish *et al.* [28], and also for a Schottky anomaly in the specific heat. In the dislocation-based superfluid model we introduce, the linearized Landau equation is isomorphic to the Schrödinger equation [Eq. (2–32)]. The ground state energy and its wave function determined in this calculation provide an input to the calculation of the shift in the superfluid transition temperature, and the renormalized coefficient g [as defined in Eq. 2–14] of the nonlinear term in the 1D Landau model for superfluid along a single dislocation line , respectively.

We develop a “weakly nonlinear” analysis to obtain an approximate solution of the Landau equation in the presence of some defect potential. This is in terms of the solution of the linearized problem, which is nothing but a Schrödinger equation. This is expected to hold near the threshold of a transition when the order parameter is

small, and the extent of proximity to the threshold provides the small parameter needed for such a perturbative expansion. We demonstrate the efficacy of this method by calculating analytic corrections to the order parameter in the presence of a Coulomb potential. We also show how this perturbation can be done in a more controlled manner by a "stretched asymptotic" method that eliminates the secular terms from a naive perturbation theory. In essence, this formalism can be applied to any nonlinear Schrödinger equation where a small parameter that goes to zero at the bifurcation point can be identified. For example, this lets us calculate perturbatively the solution of the Gross Pitaevskii equation when the chemical potential is close to the ground state energy of the trapping potential. This corresponds to the threshold value required to load atoms into the trap. We show that this method predicts the condensate wave function in a BEC quite well for small condensates.

We consider the problem of a few vortices in a trapped BEC. We review the well known results for vortex energy and stability in a rotating trap in the Thomas-Fermi limit. Most extant theoretical work on vortices in BEC in fact uses the TF approximation, which is valid for typical experimental situations involving "large" condensates. We consider the problem of a vortex in a small condensate within our aforementioned "weakly nonlinear" approximation, and derive the critical angular velocity for vortex formation in such a system. This has been obtained previously by Linn and Fetter [105] through a formally different perturbation technqiue. We conclude that this rotation frequency is likely to make the trap unstable. A small condensate is thus not an experimentally feasible system for studying vortices, especially in their metastable regime.

We then derive the exact dynamics of a vortex in a BEC in the TF limit, by using the full hydrodynamical action in a rotating frame of reference, and integrating out the phonon (or "spin wave") modes in the superfluid. Some interesting conclusions we establish are:

- The vortex action has a term that is nonlocal in time. This can be physically interpreted as a consequence of vortex-phonon coupling, which causes a vortex to effectively interact with itself at some retarded/advanced time.
- This nonlocal inertial term can be approximated to a local form when the vortex moves slowly compared to the sound speed in the medium. This corresponds to the “mass” of a vortex which depends logarithmically on some frequency associated with the vortex dynamics
- For typical experimental parameters, the vortex motion is dominated by the Magnus dynamics, which is analogous to the motion of an electron in high magnetic field. This causes the vortex to precess along equipotential lines of the trap.

We next consider the problem of vortex tunneling from a metastable state at the center of the rotating trap. Our semiclassical estimates based on a local version of the action show that a high Magnus force tends to suppress the tunneling in typical condensates. We obtain an upper bound on the rate of tunneling by considering a situation without the Magnus force, and find that it would be barely observable for typical trap parameters. It is possible that the nonlocal effects from coupling to phonons, or dissipation from other sources, would enhance tunneling. This is work in progress. If found plausible, vortices in a BEC could be a candidates for observing macroscopic quantum tunneling (MQT) in addition to prototypical superconducting systems such as SQUIDs.

APPENDIX A
STRAIN FIELD FOR AN EDGE DISLOCATION

Let us consider a straight edge-dislocation in an isotropic solid, within linear elasticity theory. Let the dislocation be along the positive z-axis and the Burger's vector along the y-axis. If $\mathbf{b}$ is the Burger's vector and ν is the Poisson's ratio then the components of the displacement field (in polar coordinates) due to the dislocation are given by (see, for example, Refs. [43, 50])

$$\begin{aligned} u_r &= \frac{b}{2\pi}\left[(\pi/2-\theta)\sin\theta - \frac{1-2\nu}{2(1-\nu)}\cos\theta\ln(r/r_0)\right], \\ u_\theta &= -\frac{b}{2\pi}\left[(\pi/2-\theta)\cos\theta + \frac{\sin\theta+(1-2\nu)\sin\theta\ln(r/r_0)}{2(1-\nu)}\right], \end{aligned} \tag{A–1}$$

where r_0 is the size of the dislocation core.

The components of the strain tensor are obtained from the displacement field using,

$$\begin{aligned} u_{rr} = \frac{\partial u_r}{\partial r},\ u_{\theta\theta} &= \frac{1}{r}\frac{\partial u_\theta}{\partial\theta} + \frac{u_r}{r}, \\ 2u_{r\theta} &= \frac{\partial u_\theta}{\partial r} - \frac{u_\theta}{r} + \frac{1}{r}\frac{\partial u_r}{\partial\theta}. \end{aligned} \tag{A–2}$$

This trace of the strain tensor results in Eq. (2–3).

APPENDIX B
ANALYSIS OF A LANDAU MODEL WITH A $1/R$ POTENTIAL

In this Appendix we solve a simplified version of the dipole potential, replacing $\cos\theta/r$ by the attractive two-dimensional Coulomb potential $V(\mathbf{r}) = -1/r$. These two potentials share the same length scaling; however, the Coulomb potential is rotationally symmetric and the linear problem can be solved exactly. The details of the perturbation calculation follow the general scheme developed in Section 2.3. We compare the results of the perturbation theory with numerical solutions of the nonlinear field equation, and find close agreement for a wide range of ϵ.

The energy eigenvalues for the Hamiltonian $\hat{H} = -\nabla_\perp^2 - 1/r$ are given by [95, 96]

$$E_n = -\frac{1}{(2n+1)^2}, \quad n = 0, 1, 2, \ldots, \tag{B–1}$$

so $E_0 = -1$, with a ground state eigenfunction $\Psi_0(r) = \sqrt{2/\pi}e^{-r}$. The related linear operator [see Eq. (4–15)] is

$$\hat{L} = -\nabla_\perp^2 - \frac{1}{r} + 1. \tag{B–2}$$

Expanding ϕ as before,

$$\phi = \phi_0 + \epsilon\phi_1 + \epsilon^2\phi_2 + \ldots, \tag{B–3}$$

we have

$$\hat{L}\phi_0 = 0, \tag{B–4}$$

with the solution

$$\phi_0(r) = A_0\left(\frac{2}{\pi}\right)^{1/2} e^{-r} \tag{B–5}$$

(note that we will ignore the z-dependence in this Appendix). Substituting into the left hand side of the $\mathcal{O}(\epsilon)$ equation,

$$\begin{aligned} \hat{L}\phi_1 &= \phi_0 - |\phi_0|^2\phi_0 \\ &= A_0\left(\frac{2}{\pi}\right)^{1/2} e^{-r} - A_0^3\left(\frac{2}{\pi}\right)^{3/2} e^{-3r}. \end{aligned} \tag{B–6}$$

We left multiply this equation by $\sqrt{2/\pi}e^{-r}$ and integrate on d^2r to obtain $0 = A_0 - (1/2\pi)A_0^3$, so that $A_0 = \sqrt{2\pi}$. Substituting back into Eq. B–6, and assuming ϕ_1 has cylindrical symmetry, we obtain an inhomogeneous equation for ϕ_1:

$$-\frac{1}{r}\frac{d}{dr}\left(r\frac{d\phi_1}{dr}\right) - \frac{1}{r}\phi_1 + \phi_1 = 2e^{-r} - 8e^{-3r}. \tag{B–7}$$

The explicit solution of this equation (that decays to 0 for large r) is

$$\phi_1(r) = ce^{-r} + e^{-3r} + \frac{1}{2}e^{-r}\left[2r + \ln(2r) + \int_{2r}^{\infty}\frac{e^{-t}}{t}\right], \tag{B–8}$$

where c is an integration constant. We substitute $\phi_1(r)$ into the right hand side of the $\mathcal{O}(\epsilon^2)$ equation to obtain

$$\hat{L}\phi_2 = (1 - 3\phi_0^2)\phi_1. \tag{B–9}$$

We again left multiply by $\sqrt{2/\pi}e^{-r}$, integrate on d^2r and use the fact that $\hat{L}$ is Hermitian to obtain the solvability condition for the constant c, with the result

$$c = -\frac{11}{12} + \frac{\gamma}{2} + \ln(2) - \frac{3}{4}\ln(3) = -0.75887, \tag{B–10}$$

where $\gamma = 0.577210$ is the Euler-Mascheroni constant. We have now explicitly calculated two terms in the perturbation expansion; both terms are nonzero at the origin, with $\phi_0(0) = 2$ and $\phi_1(0) = \frac{1}{12} + \ln(2) - \frac{3}{4}\ln(3) = -0.047478$.

We have solved the nonlinear field equation for the $-1/r$ potential numerically for a wide range of values of $\epsilon = E - E_0 = E + 1$, using the shooting method [97]. The results for the order parameter are presented in Fig. B-1 for two different values of ϵ. The two-term perturbation theory gives an excellent approximation even a fairly large value of $\epsilon = 0.43$. To get a sense of the efficacy of the perturbation theory, we can calculate the amplitude of the order parameter at the origin:

$$\begin{aligned}\psi(0) &= \epsilon^{1/2}\phi_0(0) + \epsilon^{3/2}\phi_1(0) + \ldots \\ &= 2\epsilon^{1/2} - 0.047478\epsilon^{3/2} + \ldots\ .\end{aligned} \tag{B–11}$$

This result is plotted in Fig. B-2, along with our numerical results. Again, we see the excellent agreement between the two-term perturbation theory and the numerical results, even for relatively large values of ϵ.

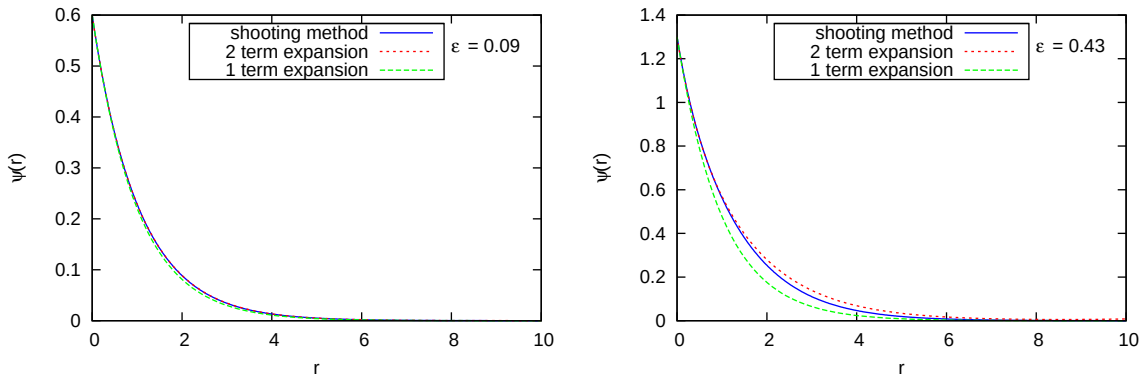

Figure B-1. Order parameter $\psi(r)$ versus r. The solid blue line is the numerical solution, the dashed green line is the one-term perturbative result, and the dotted red line is the two-term perturbative result. The upper panel compares the results for $\epsilon = 0.09$, and the lower panel for $\epsilon = 0.43$. The two term expansion provides an excellent approximation to the numerical result, even for $\epsilon = 0.43$. Reprinted with permission from Ref. [48] [D. Goswami, K. Dasbiswas, C.-D. Yoo and A. T. Dorsey, Phys. Rev. B **84**, 054523 (2011)], ©APS, 2011.

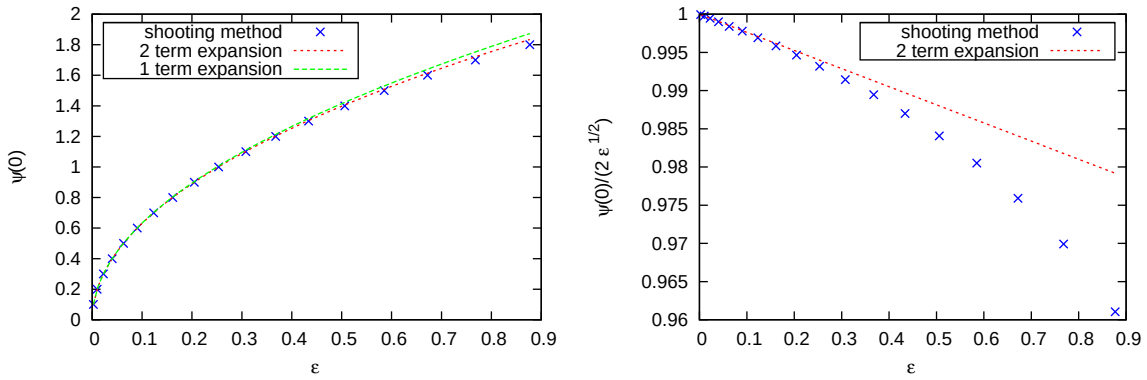

Figure B-2. Order parameter amplitude $\psi(0)$ as a function of ϵ. The crosses are the numerical results, the dashed green line is the one-term perturbative result, and the dotted red line is the two-term perturbative result. The upper plot compares the numerical results with the perturbation theory for a wide range of ϵ; the two-term perturbative result provides an excellent approximation even for values of ϵ as large as 0.8. The lower panel is a plot of $\psi(0)/2\epsilon^{1/2}$ as a function of ϵ, which highlights the role of the second order term in the expansion. Reprinted with permission from Ref. [48] [D. Goswami, K. Dasbiswas, C.-D. Yoo and A. T. Dorsey, Phys. Rev. B **84**, 054523 (2011)], ©APS, 2011.

APPENDIX C
ANALYSIS OF A TIME-DEPENDENT MODEL

In this Appendix we generalize the results of Section 2.3 to derive a one-dimensional dynamical model for the superfluid. For simplicity, we will assume that there are no conserved densities, so the dynamics are described by model A (often referred to as time-dependent Ginzburg-Landau theory) in the Hohenberg-Halperin classification [98, 99]. The relaxational equation of motion is

$$\frac{\partial \psi}{\partial t} = -\Gamma_0 \frac{\delta F}{\delta \psi^*} + \eta(\mathbf{x}, t), \tag{C–1}$$

where Γ_0 is a relaxation rate and η is the fluctuating noise term with Gaussian white noise correlations, i.e., $\langle \eta(\mathbf{x}, t) \rangle = 0$ and $\langle \eta(\mathbf{x}, t)^* \eta(\mathbf{x}', t') \rangle = 2 k_B T \Gamma_0 \delta(\mathbf{x} - \mathbf{x}') \delta(t - t')$. As before, to facilitate the reduction to a one-dimensional model we introduce dimensionless quantities, with a time scale $\tilde{t} = 2c/(\Gamma a_0^2 B^2) = 2l^2/(\Gamma c)$. In terms of the dimensionless variables,

$$\frac{\partial \psi}{\partial t} = \nabla^2 \psi - [V(\mathbf{r}) - E]\psi - |\psi|^2 \psi + \bar{\eta}(\mathbf{x}, t), \tag{C–2}$$

where the noise correlations are given by

$$\langle \bar{\eta}^{\xi}(\mathbf{x}, t) \bar{\eta}(\mathbf{x}', t') \rangle = 2(k_B T / F_0) \delta(\mathbf{x} - \mathbf{x}') \delta(t - t'). \tag{C–3}$$

As before, we introduce the small parameter $\epsilon = E - E_0$, and introduce $\psi = \epsilon^{1/2} \phi$, $z = \epsilon^{-1/2} \zeta$, $t = \epsilon^{-1} \tau$, and $\bar{\eta} = \epsilon^{3/2} \tilde{\eta}$, to obtain

$$\hat{L}\phi = \epsilon \left[-\partial_\tau \phi + \partial_\zeta^2 \phi + \phi - |\phi|^2 \phi + \tilde{\eta} \right]. \tag{C–4}$$

We again expand ϕ in powers of ϵ, and at $\mathcal{O}(1)$ we have $\hat{L}\phi_0 = 0$, the solution of which is

$$\phi_0 = A_0(\zeta, \tau) \Psi_0(\mathbf{r}). \tag{C–5}$$

Substituting this into the right hand side of the $\mathcal{O}(\epsilon)$ equation, left multiplying by ϕ_0, and then integrating on d^2r, the solvability condition yields

$$\partial_\tau A_0 = \partial_\zeta^2 A_0 + A_0 - g|A_0|^2 A_0 + \xi, \tag{C–6}$$

where ξ is the one-dimensional fluctuating noise term (the three-dimensional term with the transverse dimensions projected out),

$$\xi(\zeta,\tau) = \int d^2r \Psi_0(\mathbf{r})\tilde{\eta}(\mathbf{r},\zeta,\tau). \tag{C–7}$$

Using the fact that Ψ_0 is normalized to one, it is straightforward to show that ξ has Gaussian white noise correlations. Undoing the ϵ scalings, we obtain our final one-dimensional time-dependent Ginzburg-Landau theory,

$$\partial_t \varphi = \partial_z^2 \varphi + \epsilon\varphi - g|\varphi|^2\varphi + \xi. \tag{C–8}$$

APPENDIX D
VORTICES IN A TWO-DIMENSIONAL XY MODEL

In general, the phase in an XY model can be decomposed into an analytic, spin wave part and a singular, vortex part.

$$\theta(\mathbf{x}) = \theta_a(\mathbf{x}) + \theta_v(\mathbf{x}). \tag{D–1}$$

The corresponding phase gradients or "velocities" are longitudinal and transverse respectively, satisfying,

$$\mathbf{v}_s^{||} = \nabla\theta_a, \qquad \nabla \times \mathbf{v}_s^{||} = 0, \qquad \mathbf{v}_s^{\perp} = \nabla\theta_v, \qquad \nabla.\mathbf{v}_s^{\perp} = 0. \tag{D–2}$$

The curl of the gradient of a function will disappear everywhere except where it is not analytic, i.e. at the precise locations of the vortices. For a distribution of several line vortices at positions $\mathbf{x}_v^{\alpha}$ all pointing in the z-direction, we can define a vortex "source function", such that

$$\nabla \times \mathbf{v}_s^{\perp} = \mathbf{m}(\mathbf{x}) \equiv \sum^{\alpha} 2\pi e_v^{\alpha} \delta^2(\mathbf{x} - \mathbf{x}_v^{\alpha})\hat{z}. \tag{D–3}$$

A simple analogy can be established between the "velocity" field due to a vortex $\mathbf{v}_s^{\perp}$, and a magnetic field, and so the source function $\mathbf{m}(\mathbf{x})$ is like the current density that produces this magnetic field. After some further vector calculus,

$$\nabla \times (\nabla \times \mathbf{v}_s^{\perp}) = \nabla^2 \mathbf{v}_s^{\perp} = \nabla \times \mathbf{m}, \tag{D–4}$$

the transverse "velocity" field from a vortex can be derived as

$$\mathbf{v}_s^{\perp}(\mathbf{x}) = \nabla \times \int d^2x' G(\mathbf{x} - \mathbf{x}')\mathbf{m}(\mathbf{x}'), \tag{D–5}$$

where $G(\mathbf{x} - \mathbf{x}') = -2\pi \ln\left(|\mathbf{x} - \mathbf{x}'|/R\right)$ is the Green's function of the Laplace operator in 2D.

Now we are ready to use the explicit expression for the vortex-induced "velocity" obtained above to calculate the energy of a system of vortices. For a translationally invariant system it is useful to Fourier transform in space. We then obtain

$$\begin{aligned} E_{el} &= \frac{1}{2}\rho_s \int d^2x \int d^2x' \, \mathbf{m}(\mathbf{x}') G(\mathbf{x}-\mathbf{x}') \mathbf{m}(\mathbf{x}) \\ &= \frac{1}{2}\rho_s \int \frac{d^2q}{(2\pi)^2} \frac{\mathbf{m}(\mathbf{q}).\mathbf{m}(-\mathbf{q})}{q^2}. \end{aligned} \tag{D–6}$$

First we derive the energy for the particular (and simplest) case of a single vortex. For a vortex located at $\mathbf{x}_v$, the Fourier transform of the vortex source function is

$$\mathbf{m}(\mathbf{q}) = \int d^2x \quad e^{i\mathbf{q}.\mathbf{x}} 2\pi e_v \hat{z} \delta^2(\mathbf{x}-\mathbf{x}_v) = 2\pi e_v \hat{z} e^{i\mathbf{q}.\mathbf{x}_v}. \tag{D–7}$$

Inserting this into Eq.(D–6), we obtain,

$$E_{el} = \frac{1}{2}\rho_s \left(e_v\right)^2 \int \frac{d^2q}{q^2} = \pi (e_v)^2 \rho_s \ln(R/a), \tag{D–8}$$

where the ultraviolet and infrared cutoffs in frequency were chosen to correspond to the lattice spacing a and system size R respectively. Note that this expression for vortex energy was derived by a more direct method in Eq.(3–19) in Chapter 3. The total energy for a system of vortices will involve their energy of interaction in addition to the sum of their individual energies of creation.

$$\begin{aligned} \mathbf{m}(\mathbf{q}) &= \int d^2x \, e^{i\mathbf{q}.\mathbf{x}} \sum_\alpha 2\pi e_v^\alpha \hat{z} \delta^2(\mathbf{x}-\mathbf{x}_v^\alpha) = 2\pi \hat{z} \sum_\alpha e_v^\alpha e^{i\mathbf{q}.\mathbf{x}_v^\alpha}, \\ E_{el} &= \frac{1}{2}\rho_s \sum_{\alpha,\beta} e_v^\alpha e_v^\beta \int \frac{d^2q}{q^2} e^{i\mathbf{q}.(\mathbf{x}_v^\alpha - \mathbf{x}_v^\beta)} = \sum_\alpha E^\alpha + \sum_{\alpha,\beta} 2\pi \rho_s e_v^\alpha e_v^\beta \ln(R/r_{\alpha\beta}). \end{aligned} \tag{D–9}$$

The integral in frequency space above has been carried out by first integrating over the angle (which gives a Bessel function of zeroeth order) and subsequently over the radial coordinates, which gives a logarithm to leading order. The cutoffs imposed on the radial integration to take care of the logarithmic divergence, are inverses of the system size (IR or low frequency cutoff) and of the minimum distance r (UV or high frequency cutoff)

between neighboring vortices, i.e. the minimum value that the distance $r_{\alpha\beta}$ between a pair of vortices labeled by α and β can have. This is needed because two vortices at the same place will involve an infinite energy cost:

$$\int \frac{dq}{q} \int_0^{2\pi} d\phi e^{iqr_{\alpha\beta}cos(\phi)} = \int_{1/R}^{1/r} dq \frac{J_0(qr_{\alpha\beta})}{q} \simeq \ln\left(\frac{R}{r}\right). \tag{D–10}$$

The energy of interaction between two vortices goes as a logarithm of the distance between them, and the sign is determined by the product of their charges. The expression for vortex energy in Eq.(D–9) can be recast in the form

$$E_{el} = \pi\rho_s \left[\Big(\sum_\alpha e_v^\alpha \Big)^2 \ln(R/a) + 2 \Big(\sum_{\alpha,\beta} e_v^\alpha e_v^\beta \ln(a/r_{\alpha\beta}) \Big) \right]. \tag{D–11}$$

This expression is particularly suggestive as it shows that the long wavelength energy of a "non-neutral" system of free vortices, i.e one for which total charge is not zero, diverges with system size. This is why it is always energetically more favorable to excite vortices in pairs of equal and opposite charge. This also suggests the vortex-antivortex pair binding picture of the BKT transition. Based on the above, we can now write down the total Hamiltonian for a system of vortices by including the core contribution, as

$$\mathcal{H}_v/T = -\pi K \sum_{\alpha,\beta} e_v^\alpha e_v^\beta \ln(r_{\alpha\beta}/a) + E_c/T \Big(\sum_\alpha e_v^\alpha \Big)^2. \tag{D–12}$$

We can compute various statistical averages based on this Hamiltonian. Free energy calculations show that the renormalized phase stiffness in the presence of vortices is determined by the correlation function of transverse velocities. This can in turn be related to the vortex source functions through Eq.(D–5) as

$$\langle \mathbf{v}_s^\perp(\mathbf{x}) \cdot \mathbf{v}_s^\perp(0) \rangle = \int d^2x_1 d^2x_2 \, \langle \mathbf{m}(\mathbf{x}_1) \cdot \mathbf{m}(\mathbf{x}_2) \rangle \nabla G(\mathbf{x} - \mathbf{x}_1) \cdot \nabla G(\mathbf{x} - \mathbf{x}_2)|_{x=0}. \tag{D–13}$$

The two Green's functions above can be traced over and combined into a single Green's function through their completeness property, as

$$\int d^2x \nabla G(\mathbf{x}-\mathbf{x}_1)\cdot\nabla G(\mathbf{x}-\mathbf{x}_2)|_{x=0} = -G(\mathbf{x}_1-\mathbf{x}_2)|_{x_1=0}, \tag{D–14}$$

where we have integrated by parts, and used the property of the Green's function. Now we Fourier transform to frequency space, and use this identity of Green's function to show that

$$\int d^2x \,\langle \mathbf{v}_s^{\perp}(\mathbf{x}).\mathbf{v}_s^{\perp}(0)\rangle = \frac{\langle \mathbf{m}(\mathbf{q}).\mathbf{m}(-\mathbf{q})\rangle}{q^2}. \tag{D–15}$$

Let us now evaluate the correlation of source functions using their definition in frequency space, $\langle \mathbf{m}(\mathbf{q}).\mathbf{m}(-\mathbf{q})\rangle = \left(2\pi\right)^2 \sum_{\alpha\neq\beta}\langle e_v^{\alpha} e_v^{\beta} e^{i\mathbf{q}.(\mathbf{x}_v^{\alpha}-\mathbf{x}_v^{\beta})}\rangle$. In the long wavelength limit, we can expand in small q and ignore higher order terms in q. Also if we consider a vortex gas with low fugacity, the configuration that has the highest order contribution to the statistical average and satisfies the charge neutrality condition, is the one corresponding to a single pair of vortices with unit charge. So

$$\begin{aligned}\langle \mathbf{m}(\mathbf{q}).\mathbf{m}(-\mathbf{q})\rangle &= -\left(2\pi\right)^2 q^2 \sum_{\alpha\neq\beta}\langle e_v^{\alpha} e_v^{\beta}(\mathbf{x}_v^{\alpha}-\mathbf{x}_v^{\beta})^2\rangle + \mathcal{O}(q^4)\\ &\simeq -\left(2\pi\right)^2 q^2 \sum_{\alpha\neq\beta}(\mathbf{x}_v^{\alpha}-\mathbf{x}_v^{\beta})^2 e^{\left[-2E_c/T-\pi K \ln(|\mathbf{x}_v^{\alpha}-\mathbf{x}_v^{\beta}|/a)\right]}.\end{aligned} \tag{D–16}$$

Now we go to the continuum limit and sum over all possible positions of the two vortices to find that

$$\frac{\langle \mathbf{m}(\mathbf{q}).\mathbf{m}(-\mathbf{q})\rangle}{q^2} = 4\pi^3 e^{-2E_c/T}\int \frac{dr}{a}\left(\frac{r}{a}\right)^{3-2\pi K}. \tag{D–17}$$

This result describes the pair correlation for vortex source functions in the limit of long wavelength and low fugacity (valid for low temperatures where the vortex density is dilute), and is used for obtaining the renormalized stiffness in Eq. (3–27).

REFERENCES

[1] H. K. Onnes., Phys. Lab. Univ. Leiden No. B **120**, 3 (1911).

[2] J. F. Allen and H. Jones, Nature **141**, 75 (1938); J. F. Allen and A. D. Misener, Nature **141**, 243 (1938).

[3] P. Kapitza, Nature **141**, 74 (1938).

[4] L. Tisza, Nature(London) **141**, 913 (1938).

[5] L. D. Landau, J. Phys U.S.S.R. **5**, 71 (1941); **8**, 1 (1944); **11**, 91 (1947); Phys. Rev. **70**, 356 (1941); **75**, 884 (1949).

[6] J. L. Yarnell, G. P. Arnold, P. J. Bendt, and E. C. Kerr, Phys. Rev. **113**, 1379 (1959).

[7] R. P. Feynman, in *Progress in Low Temperature Physics, volume 1* edited by C. J. Gorter, (North-Holland, Amsterdam, 1955); Revs. Mod. Phys. **29**, 205 (1957).

[8] E. L. Andronikashvili, Zh. Eksp. Teor. Fiz. **16**, 780 (1946).

[9] F. London, Nature **141**, 643 (1938); Phys. Rev. **54**, 947 (1938).

[10] A. Einstein, *Prussian Academy of Sciences* (1924).

[11] S. N. Bose, Zeitschrift für Physik **26**, 178 (1924).

[12] M. H. Anderson, J. R. Ensher, M. R. Matthews, C. E. Wieman, and E. Cornell, Science **269**, 198 (1995).

[13] K. B. Davis, M. O. Mewes, M. R. Andrews, N. J. Vandruten, D. S. Durfee, D. M. Kurn, and W. Ketterle, Phys. Rev. Lett. **75**, 3969 (1995).

[14] M. Greiner, O. Mandel, T. Esslinger, T. W. Hänsch, and I. Bloch, Nature (London) **415**, 39 (2002).

[15] N. Prokof'ev, Advances in Physics **56**, 381 (2007).

[16] S. Balibar, J. Phys. Cond. Mat. **20**, 173201 (2008).

[17] V. L. Berezinskii, Sov. Phys. JETP **34**, 610 (1972).

[18] J. M. Kosterlitz and D. J. Thouless, J. Phys. C **6**, 1181 (1973).

[19] O. Penrose and L. Onsager, Phys. Rev. **104**, 576 (1956).

[20] A. F. Andreev and I. M. Lifshitz, Sov. Phys. JETP **29**, 1107 (1969).

[21] D. J. Thouless, Ann. Phys. **52**, 403 (1969).

[22] G. V. Chester, Phys. Rev. A **2**, 256 (1970).

[23] E. Kim and M. H. W Chan, Nature **427**, 225 (2004).

[24] E. Kim and M. H. W. Chan, Science **305**, 1941 (2004).

[25] A. S. C. Rittner and J. D. Reppy, Phys. Rev. Lett. **97**, 165301 (2006).

[26] A. S. C. Rittner and J. D. Reppy, Phys. Rev. Lett. **98**, 175302 (2007).

[27] X. Lin, A. C. Clark and M. H. W. Chan, Nature **449**, 1025 (2007)

[28] J. Day and J. Beamish, Nature **450**, 853 (2007).

[29] D. Aleinikava and A. B. Kuklov, Phys. Rev. Lett. **106**, 235302 (2011).

[30] M. Bonsigneni, Phys. Rev. Lett. **97**, 080401 (2006).

[31] S. Sasaki, R. Ishiguro, F. Caupin, H. J. Maris and S. Balibar, Science **313**, 1098 (2006).

[32] A. T. Dorsey, P. M. Goldbart, and J. Toner, Phys. Rev. Lett. **96**, 055301 (2006).

[33] J. Toner, Phys. Rev. Lett. **100**, 35302 (2008).

[34] J. T. West, O. Syshchenko, J. D. Beamish and M. H. W. Chan, Nature Phys. **5**, 598 (2009).

[35] R. J. Donnelly, Quantized Vortices in Helium II (Cambridge University Press, Cambridge, UK, 1991).

[36] M. R. Matthews, B. P. Anderson, P. C. Haljan, D. S. Hall, M. J. Holland, J. E. Williams, C. E. Wieman, and E. A. Cornell, Phys. Rev. Lett. **83**, 2498 (1999).

[37] K. W. Madison, F. Chevy, W. Wohlleben, and J. Dalibard, Phys. Rev. Lett. **84**, 806 (2000); K. W. Madison, F. Chevy, W. Wohlleben, and J. Dalibard, J. Mod. Opt. **47**, 2715 (2000).

[38] A. L. Fetter, J. Phys.: Condens. Matter **13**, R135 (2001).

[39] A. L. Fetter, Rev. Mod. Phys. **81**, 647 (2009).

[40] L. D. Landau and E. M. Lifshitz, *Statistical Physics, part 1* (Butterworth-Heinemann, Oxford, England, 1980).

[41] V. L. Ginzburg and L. D. Landau, Zh. Eksp. Teor. Fiz. **20**, 1064 (1950).

[42] V. L. Ginzburg and L. P. Pitaevskii, Zh. Eksp. Teor. Fiz. **34**, 1240(1958) [JETP **7**, 858 (1958)].

[43] G. F. Mazenko, *Fluctuations, Order, and Defects* (John Wiley and Sons, New York, 2003).

[44] M. Boninsegni, A. B. Kuklov, L. Pollet, N. V. Prokof'ev, B. V. Svistunov, and M. Troyer, Phys. Rev. Lett. **99**, 035301 (2007).

[45] V. M. Nabutovskii and V.Ya. Shapiro, Sov. Phys. JETP **48**, 480 (1978).

[46] A. Gurevich and E. A. Pashitskii, Phys. Rev. B **56**, 6213 (1997).

[47] K. Dasbiswas, D. Goswami, C.-D. Yoo and A. T. Dorsey, Phys. Rev. B **81**, 64516 (2010).

[48] D. Goswami, K. Dasbiswas, C.-D. Yoo and A. T. Dorsey, Phys. Rev. B **84**, 054523 (2011).

[49] L. D. Landau and E. M. Lifshitz, *Theory of Elasticity* (Pergamon, Oxford, England, 1986).

[50] J. P. Hirth and J. Lothe, *Theory of Dislocations* (John Wiley and Sons, New York, 1982).

[51] R. Landauer, Phys. Rev. **94**, 1386 (1954).

[52] P. R. Emtage, Phys. Rev. **163**, 865 (1967).

[53] V. M. Nabutovskii and B. Ya Shapiro, JETP Lett. **26**, 473 (1977).

[54] V. A. Slyusarev and K. A. Chishko, Fiz. Met. Metalloved. **58**, 877 (1984).

[55] I. M. Dubrovskii, Low Temp. Phys. **23**, 976 (1997).

[56] J.-L. Farvacque and P. Francois, Phys. Status. Solidi(b) **223**, 635 (2001).

[57] A. T. Dorsey and J. Toner (unpublished); details are discussed in Section 2.4.3 of this dissertation.

[58] P. Amore, Central European Journal of Physics **10**, 96 (2012).

[59] K. W. Morton and D. F. Mayers, *Numerical Solution of Partial Differential Equations, An Introduction* (Cambridge University Press, 2005).

[60] R. Fletcher, Conjugate gradient methods for indefinite systems, *Numerical Analysis* (Springer, 1976), p. 73.

[61] G. Sleijpen, H. A. van der Vorst, SIAM J. Matrix Anal. Appl. **17**, 401 (1996).

[62] C. Lanczos, J. Res. Nat. Bur. Standards **45**, 255 (1950).

[63] M. Bollhöfer, Y. Notay, JADAMILU: software package based on Jacobi-Davidson method, available via http://homepages.ulb.ac.be/∼jadamilu/, accessed on 4 July 2009.

[64] R. B. Lehoucq, D. C. Sorensen, C. Yang, ARPACK: software package based on implicitly restarted Arnoldi methods, available via http://www.caam.rice.edu/software/ARPACK/, accessed on 4 July 2009.

[65] M. Bollhöfer and Y. Notay, Comp. Phys. Comm. **177**, 951 (2007).

[66] R. B. Lehoucq, D. C. Sorensen, C. Yang, ARPACK Users Guide: Solution of Large-Scale Eigenvalue Problems with Implicitly Restarted Arnoldi Methods, SIAM, Philadelphia, PA, 1998.

[67] X. L. Yang, S. H. Guo, F. T. Chan, K. W. Wong, and W. Y. Ching, Phys. Rev. A **43**, 1186 (1991).

[68] I. M. Lifshitz and K. I. Pushkarov, JETP Lett. **11**, 310 (1970).

[69] M. C. Gutzwiller, *Chaos in Classical and Quantum Mechanics* (Springer-Verlag, New York, 1991).

[70] P. M. Chaikin and T. C. Lubensky, *Principles of condensed matter physics* (Cambridge Univeristy Press, Cambridge, 1995).

[71] F. R. N. Nabarro, *Dislocations in Solids* (North-Holland Publishing Company, Amsterdam, 1979).

[72] L. Pollet, M. Boninsegni, A. B. Kuklov, N. V. Prokofev, B. V. Svistunov, and M. Troyer, Phys. Rev. Lett. **98**, 135301 (2007).

[73] A. Gurevich and E. A. Pashitskii, Phys. Rev. B **56**, 6213 (1997).

[74] L. D. Landau and E. M. Lifshitz, *Theory of Elasticity* (Pergamon, Oxford, England, 1986).

[75] N. D. Mermin and H. Wagner, Phys. Rev. Lett. **17**, 1133 (1966).

[76] L. D. Landau and E. M. Lifshitz, *Classical Mechanics* (Pergamon, Oxford, England, 1976).

[77] J. V. Jos, L. P. Kadanoff, S. Kirkpatrick, and D. R. Nelson, Phys. Rev. B **16**, 1217 (1977); Phys. Rev. B **17**, 1477 (1978).

[78] J. Toner, Phys. Rev. Lett. **100**, 35302 (2008).

[79] K. Dasbiswas, D. Goswami, C.-D. Yoo and A. T. Dorsey, Phys. Rev. B **81**, 64516 (2010).

[80] S. I. Shevchenko, Sov. J. Low Temp. Phys. **13**, 115 (1987).

[81] S. I. Shevchenko, Sov. J. Low Temp. Phys. **14**, 1011 (1988).

[82] J.-P. Bouchaud and G. Biroli, C. R. Physique **9**, 1067 (2008).

[83] Note that due to the translational invariance along the z-axis, the wavefunction should also contain a factor of e^{ikz}, which contributes k^2 to the energy eigenvalues. However, the ground state is always obtained for $k = 0$, so we suppress the z-dependence in the wavefunctions.

[84] P. G. Drazin and W. H. Reid, *Hydrodynamic Stability, Second Edition* (Cambridge University Press, Cambridge, UK, 2004).

[85] J. K. Kevorkian and J. D. Cole, *Multiple Scale and Singular Perturbation Methods* (Springer-Verlag, New York, 1996).

[86] R. P. Feynman and A. R. Hibbs, *Quantum Mechanics and Path Integrals* (McGraw-Hill, New York, 1965).

[87] L. W. Gruenberg and L. Gunther, Phys. Letters **38A**, 463 (1972).

[88] D. J. Scalapino, M. Sears, and R. A. Ferrell, Phys. Rev. B **6**, 3409 (1972).

[89] J. R. Tucker and B. I. Halperin, Phys. Rev. B **3**, 3768 (1971).

[90] A. B. Harris, J. Phys. C **7**, 1671 (1974).

[91] I. Iwasa, K. Araki and H. Suzuki, J. Phys. Soc. Japan **46**, 1119 (1979).

[92] I. Iwasa and H. Suzuki, J. Phys. Soc. Japan **49**, 1722 (1980).

[93] M. W. Ray and R. B. Hallock, Phys. Rev. Lett. **100**, 235301 (2008).

[94] For instance, see R. Shankar, *Principles of Quantum Mechanics, Second Edition* (Springer, New York, 1994).

[95] B. Zaslow and M. E. Zandler, Am. J. Phys. **35**, 1118 (1967).

[96] X. L. Yang, S. H. Guo, F. T. Chan, K. W. Wong, and W. Y. Ching , Phys. Rev. A **43**, 1186 (1991).

[97] W. H. Press, S. A. Teukolsky, W. T. Vetterling, and B. P. Flannery, *Numerical Recipes 3rd Edition: The Art of Scientific Computing* (Cambridge University Press, Cambridge, UK, 2007).

[98] P. C. Hohenberg and B. I. Halperin, Rev. Mod. Phys. **49**, 435 (1977).

[99] While we concentrate on relaxational dynamics, the general method outlined in Appendix A can be applied to other dynamical models, e.g., the reversible Gross-Pitaevskii dynamics of a Bose condensate.

[100] A. A. Svidzinsky and A. L. Fetter, Phys. Rev. Lett. **84**, 5919 (2000).

[101] A. A. Svidzinsky, and A. L. Fetter, Phys. Rev. A **62**, 063617 (2000).

[102] E. P. Gross, Nuovo Cimento **20**, 454 (1961); L. P. Pitaevskii, Sov. Phys. JETP **12**, 155 (1961).

[103] C. J. Pethick and H. Smith, *Bose-Einstein Condensation in Dilute Gases* (Cambridge University Press, Cambridge, 2001).

[104] L. Pitaevskii and S. Stringari, *Bose-Einstein Condensation* (Oxford Science Publications, Oxford, 2003).

[105] M. Linn and A. Fetter, Phys. Rev. A **61**, 063603 (2000).

[106] H. Lamb, *Hydrodynamics* (Cambridge University Press, Cambridge, 1932); G. K. Batchelor, *An Introduction to Fluid Mechanics* (Cambridge University Press, Cambridge, 1967).

[107] E. Madelung, Zeitschrift für Physik A **40**, 322 (1927).

[108] Q. Niu, P. Ao, and D. J. Thouless, Phys. Rev. Lett. **72**, 1706 (1994).

[109] X.-M. Zhu, Y. Tan, and P. Ao, Phys. Rev. Lett. **77**, 562 (1996).

[110] G. E. Volovik, Pisma Zh. Eksp. Teor. Fiz. **15**, 116 (1972) [JETP Lett. **15**, 81 (1972)].

[111] C. M. Muirhead, W. F. Vinen, and R. J. Donnelly, Philos. Trans., R. Soc. London A **311**, 433 (1984).

[112] V. N. Popov., Sov. Phys. JETP **37**, 341, (1973).

[113] J. M. Duan and A. J. Leggett, Phys. Rev. Lett. **68**, 1216 (1992).

[114] E. Simanek, *Inhomogeneous Superconductors* (Oxford University Press, Oxford, 1994).

[115] D. J. Thouless and J. R. Anglin, Phys. Rev. Lett. **99**, 105301 (2007).

[116] A. Leggett, Prog. Theor. Phys. Suppl. **69**, 80 (1980).

[117] A. Wallraff *et al.*, Nature (London) **425**, 155 (2003).

[118] O. Fialko, A. S. Bradley, and J. Brand, Phys. Rev. Lett. **108**, 015301 (2012).

[119] P. Ao and D. J. Thouless, Phys. Rev. Lett. **72**, 132 (1994).

[120] A. Auerbach, D. P. Arovas, and S. Ghosh, Phys. Rev. B **74**, 064511 (2006).

[121] D. P. Arovas and A. Auerbach, Phys. Rev. B **78**, 094508 (2008).

[122] S. V. Iordanskii, Ann. Phys. **29**, 335 (1964).

[123] B. Y. Rubinstein and L. M. Pismen, Physica (Amsterdam) **78D**, 1 (1994).

[124] L. Thompson and P. C. E. Stamp, Phys. Rev. Lett. **108**, 184501 (2012)

[125] G. Wentzel, Zeitschrift für Physik **38** (67): 518 (1926); H. A. Kramer, Zeitschrift für Physik **39** (1011): 828 (1926); L. Brillouin Comptes Rendus de l'Academie des Sciences **183**, 24 (1926).

[126] C. Bender and S. Orszag, *Advanced Mathematical Methods for Scientists and Engineers* (McGraw-Hill, New York, 1978).

[127] S. Coleman, Phys. Rev. D **15**, 2929 (1977); **16**, 1248(E) (1977).

[128] J. K. Jain and S. Kivelson, Phys. Rev. A **36**, 3467 (1987); Phys. Rev. B **37**, 4111 (1988).

BIOGRAPHICAL SKETCH

Kinjal Dasbiswas was born in Kolkata (formerly Calcutta) in eastern India and was educated at the Indian Institute of Technology in Kanpur. He managed to survive a five year integrated masters' program in physics there and joined the Department of Physics at the University of Florida in the fall of 2007. The sunny climate and warm people of Florida helped him settle down to life here while he was pondering on the mysteries of matter at very low temperatures. He worked in the area of theoretical condensed matter physics with Prof. Alan T. Dorsey, having joined his group in 2008. He gratefully received his PhD degree from this institute in the summer of 2012.